



MARMARA UNIVERSITY
FACULTY OF ENGINEERING



**Influence of Different Fe Levels on Mechanical Properties of Aluminum
Casting**

Cansu KARABULUT, Gülce MALKOÇ

GRADUATION PROJECT REPORT
Department of Mechanical Engineering

Supervisor
Prof. Dr. Paşa YAYLA
ISTANBUL, 2022



MARMARA UNIVERSITY
FACULTY OF ENGINEERING



**Influence of Different Fe Levels on Mechanical Properties of Aluminum
Casting Alloys**

By

Cansu KARABULUT, Gülce MALKOÇ

June 15, 2022, Istanbul

**SUBMITTED TO THE DEPARTMENT OF MECHANICAL ENGINEERING IN
PARTIAL FULFILLMENT OF THE REQUIREMENTS FOR THE DEGREE
OF
BACHELOR OF SCIENCE
AT
MARMARA UNIVERSITY**

**The author(s) hereby grant(s) to Marmara University permission to reproduce and
to distribute publicly paper**

**and electronic copies of this document in whole or in part and declare that the
prepared document does not in anyway include copying of previous work on the
subject or the use of ideas, concepts, words, or structures regarding the subject
without appropriate acknowledgement of the source material.**

Signature of Author(s)

Department of Mechanical Engineering

Certified By

Project Supervisor, Department of Mechanical Engineering

Accepted By

Head of the Department of Mechanical Engineering

ACKNOWLEDGEMENT

First, we would like to thank our supervisor Prof. Dr. Paşa YAYLA, for the valuable guidance and advice on preparing this thesis and for giving us moral and material support.

We'd like to express our gratitude to CEVHER Wheel Industry A.Ş. as well for their contributions both as knowledge and financial support. We also would like to especially thank Onur ÖZAYDIN and Yiğit KAYA for their support throughout the project.

We would like to thank Marmara University – Engineering Faculty – Metallurgy and Materials Engineering Department - Head of department Prof. Dr. Recep ARTIR and the Metallurgy Laboratory technician Semih GÜVEN for their support and help. Also, we would like to thank Marmara University Faculty of Technology - Electrical And Electronics Engineering- Department Of Control Systems Lecturer Fatih Serdar SAYIN.

We'd also want to express our gratitude to TÜBİTAK for funding our project under 2209-A, which promotes Undergraduate Graduation Projects.

June, 2022

Cansu KARABULUT , Gülce MALKOÇ

CONTENTS

ACKNOWLEDGEMENT.....	3
CONTENTS	4
ÖZET.....	4
ABSTRACT.....	5
SYMBOLS	6
ABBREVIATIONS	7
LIST OF FIGURES	9
LIST OF TABLES	13
1 INTRODUCTION.....	14
1.1 Purpose of the Thesis.....	14
1.2 Literature Survey	15
1.2.1 Classification of Cast Aluminum Alloy.....	15
1.3 Mechanical Test Methods.....	16
1.3.1 Charpy Impact Testing	16
1.3.2 Instrumented Charpy Impact Testing	17
1.4 Tensile Testing	19
1.4.1 Ultimate Tensile Strength (UTS).....	20
1.4.2 Yield Strength (YS)	21
1.4.3 Elongation	21
1.5 Optical Microscope	22
1.6 Scanning Electron Microscope (SEM)	22
1.6.1 Using SEM and EDX Analysis Together	23
1.7 Green Deal.....	23
1.7.1 The Role of Aluminum in the Green Deal.....	24
2 MATERIAL AND METHOD.....	25
2.1 Measurement of Sample Qualification	25
2.2 Hardness	25
2.2.1 Density.....	27

2.3 Sample Production.....	28
2.4 Sample (Specimen) Preparation	29
2.4.1 Charpy V-notch Test Specimens	30
2.4.2 Tensile Test Specimens	30
3 TESTING AND DATA INTERPRETATION	31
3.1 Charpy V-notch TEST.....	31
3.1.1 Impact tests for 0.11 Fe content.....	31
3.1.2 Impact tests for 0.25 Fe content.....	33
3.1.3 Impact tests for 0.42 Fe content.....	35
3.1.4 Impact tests for 0.65 Fe content.....	37
3.1.5 Comparison between different Fe contents according to Charpy testing	39
3.2 Tensile Test	41
3.2.1 Tensile tests for 0.11 Fe content.....	41
3.2.2 Tensile tests for 0.25 Fe content	43
3.2.3 Tensile tests for 0.42 Fe content	44
3.2.4 Tensile tests for 0.65 Fe content	45
3.3 Comparison of the Different Fe contained samples.....	47
3.3.1 Yield Strength (YS)	47
3.3.2 Ultimate Yield Strength (UTS).....	48
3.3.3 Elongation	48
4 MACROSCOPIC and MICROSCOPIC EXAMINATION.....	49
4.1 Microscopic Examination of Sample.....	49
4.1.1 Sample Selection in Metallography	50
4.1.2 Sample Preparation.....	51
5 RESULTS and DISCUSSION.....	58
5.1.1 Optical Microscope Results.....	58
5.2 Optical Examination of Fracture Surface	63
5.2.1 Sampling.....	65
5.2.2 Optical Results.....	65
5.3 SEM and EDX Examination of Fracture Surface	69
5.3.1 SEM and EDX Results	70

6	CONCLUSIONS	93
6.1	Main Conclusions.....	93
6.2	Recommendation for Further Work.....	94
6.3	Evaluation of the Work from MUDEK Perspective	94
6.3.1	Economic Analysis	94
6.3.2	Real-Life Conditions	95
6.3.3	Productibility	95
6.3.4	Constraints.....	95
	REFERENCES	96
	APPENDICES	99

ÖZET

Demir Oranının Alüminyum Alaşımının Mekanik Özelliklerine Etkisi

Cansu KARABULUT, Gülce MALKOÇ

Bu tez çalışmasında, döküm ile üretilen AlSi7Mg3 (A346) alaşımının farklı Fe oranları ile İnstumente Charpy V-çentik darbe testi, çekme testi analizi yapılmıştır. Numuneler oran olarak 0.11, 0.25, 0.42 ve 0.65 Fe içermektedir. Belirlenen Charpy V-çentik Test numuneleri, TR ISO EN 148-3 standardına göre incelenmiş ve hazırlanmıştır. Charpy V-çentik testi ile darbe enerjisi, çarpma anında maksimum kuvvet yükü belirlenmiştir. Çekme Testi numuneleri TS EN ISO 6892-1:2020 standardına göre incelenip, hazırlanmıştır. Çekme testlerinden numunelerin YS, UTS ve uzama değerleri elde edilmiştir. Ayrıca numunelerin sertlik ve yoğunluk değerleri de ölçülmüştür.

Daha sonra Charpy V-çentik ve Çekme Testi numunelerinin kırılma yüzeyleri, numunelerin süneklik-gevreklik açısından incelenmiştir. Önce görsel ve optik mikroskop sonuçları ile incelemeler yapılmış. Örnekler birbirleriyle karşılaştırılmıştır. Fe oranı değişiminin etkilerini daha iyi anlamak için her malzeme için numunelerin mikro yapıları incelenmiştir.

Daha sonra numunelerin kırılma yüzeyleri taramalı elektron mikroskopunda incelenmiştir.

Test ve incelemelerimiz sonucunda Fe yüzdelerinin değiştiği seviyelerde gevrek ve sünek kırılmalar gözlenmektedir.

Sonuç olarak malzemenin Fe oranın artmasının kırılganlığı arttığını gözlemediğimiz. Ayrıca Fe oranı arttıkça malzemenin darbe dayanımı düşüğü gözlenmiştir. Ayrıca malzemenin mukavemetinde de azalma gözlemlenmiştir.

ABSTRACT

Influence of Different Fe Levels on Mechanical Properties of Aluminum Casting Alloys

Cansu KARABULUT, Gülce MALKOÇ

In this thesis, instrumented Charpy V-notch impact test, tensile test analysis of AlSi7Mg3 alloy (A346) produced by casting, with different Fe levels. The samples have contained 0.11, 0.25, 0.42 and 0.65 level of Fe. The Charpy V-notch Test samples prepared and examined with accordance to TR ISO EN 148-3 standard. From the Charpy V-notch determined impact energy, max force load at impact. The Tensile Test samples were prepared and examined in accordance to TS EN ISO 6892-1:2020 standard. From the tensile tests, we obtained YS, UTS and elongation values of the samples. Also, it is measured the hardness and density values of samples.

Then, fracture surfaces of Charpy V-notch and Tensile Test samples were investigated for ductility-brittleness of the samples. At first, it is investigated by visual and optical microscope results. Samples were compared with each other. For a better understanding the effects of the Fe level change, microstructures of the samples are examined for each material.

Then the fracture surfaces of samples are examined through a scanning electron microscope.

As result of our tests and investigations, brittle and ductile fractures are observed in levels with change of Fe percentages.

As a result, we observed as the Fe content of the material increases, the brittleness. Also, the impact resistance of the material decreases as the Fe percentage increases. Also, the strength of the material decrease.

SYMBOLS

d Diameter

α Alpha

μ Micro

ABBREVIATIONS

A356	AlSi7Mg0.3 alloy
AA	The Aluminum Association
Al	Aluminium
Al ₂ O ₃	Aluminum Oxide
AlSi7Mg	Aluminium Silicon Magnesium alloy
AW	Aluminum Wrought alloy
B	Boron
BSD	Backscatter Electron Detector
Ca	Calcium
CBN	Cubic Baron Nitride
Co	Cobalt
Cr	Chromium
Cr ₂ O ₃	Chromium (III) oxide
Cu	Copper
EDX	Energy Dispersive X-Ray Analysis
EN	European Normative
Fe	Iron
ISO	International Organization for Standardization
Mg	Magnesium
MgO	Magnesium oxide

Mn	Manganese
Na	Sodium
Ni	Nickel
OM	Optical microscopy
P	Phosphorus
Sb	Antimony
SEM	Scanning Electron Microscope
Si	Silicon
Sn	Tin
Sr	Strontium
Ti	Titanium
UTS	Ultimate Yield Strength
V	Vanadium
XRD	X-ray Powder Diffraction
YS	Yield Strength
Zn	Zinc
Zr	Zirconium

LIST OF FIGURES

Figure 1.3.1.1 Charpy impact testing machine [6].....	17
Figure 1.3.2.1 Instrumented Charpy device used in the experiments	18
Figure 1.3.2.1 Visualization of the mechanical changes while tensile testing [7]	19
Figure 1.3.2.2 Tensile test device used in the experiments.....	20
Figure 1.4.1.1 Basic schematic of stress-strain graph [8]	21
Figure 1.4.3.1 Basic schematic of stress-strain graph with elongation points [9]	21
Figure 1.4.3.1 SEM working schematic [10]	23
Figure 1.7.1.1 hardness measurement points (red dots).....	26
Figure 2.2.1.1 Density Measurement	27
Figure 2.2.1.1 Thermal Image Of The Casting Process	28
Figure 2.4.1.1 Charpy test specimens	30
Figure 2.4.2.1 Tensile Test Specimen.....	30
Figure 3.1.1.1 Charpy V-notch test Force vs. Time Graph for sample 1	31
Figure 3.1.1.2 Charpy V-notch test Energy vs. Time Graph for sample 1	32
Figure 3.1.2.1 Charpy V-notch test Force vs. Time Graph for sample 2.....	33
Figure 3.1.2.2 Charpy V-notch test Energy vs Time Graph for sample 2	34
Figure 3.1.3.1 Charpy V-notch test Force vs. Time Graph for sample 3.....	35
Figure 3.1.3.2 Charpy V-notch test Energy vs. Time Graph for sample 3	36
Figure 3.1.4.1 Charpy V-notch test Force vs. Time Graph for sample 4.....	37
Figure 3.1.4.2 Charpy V-notch test Energy vs. Time Graph for sample 4	38
Figure 3.1.5.1 Average force values at impact	39
Figure 3.1.5.2 Average energy values at impact.....	40
Figure 3.1.5.3 Maximum Load of the impact comparison graph	40
Figure 3.1.5.4 initiation impact energy and total energy comparison graph	41
Figure 3.2.1.1 Tensile test results of sample 1	42
Figure 3.2.2.1 Tensile test results of sample 2.....	43
Figure 3.2.3.1 Tensile test results of sample 3	44
Figure 3.2.4.1 Tensile test results of sample 4.....	46
Figure 3.3.1.1 YS comparison table.....	47
Figure 3.3.2.1 UTS comparison graph.....	48
Figure 3.3.3.1 elongation comparison graph.....	49
Figure 3.3.3.1 steps	50
Figure 4.1.1.1 microstructure examination sample with directions	51

Figure 4.1.2.1 Struers Discotom-5 Abrasive Cutter.....	54
Figure 4.1.2.2 Struers Prontopress 10 molding device	55
Figure 4.1.2.3 Struers LaboPro-21 grinding device.....	56
Figure 4.1.2.4 Struers LaboPol-6 polishing device.....	57
Figure 5.1.1.1 0.11 Fe level microstructure microscope results (a)x10, (b)x10 with porosity, (c)x20 (d)x20 with porosity; magnification at horizontal surface	59
Figure 5.1.1.2 0.11 Fe level microstructure microscope results (a)x10, (b)x10 with porosity, (c)x20 (d)x20 with porosity; magnification at vertical surface	59
Figure 5.1.1.3 0.25 Fe level microstructure microscope results (a)x10, (b)x10 with porosity, (c)x20 (d)x20 with porosity; magnification at horizontal surface	60
Figure 5.1.1.4 0.25 Fe level microstructure microscope results (a)x10, (b)x10 with porosity, (c)x20 (d)x20 with porosity; magnification at vertical surface	60
Figure 5.1.1.5 0.42 Fe level microstructure microscope results (a)x10, (b)x10 with porosity, (c)x20 (d)x20 with porosity; magnification at horizontal surface	61
Figure 5.1.1.6 0.42 Fe level microstructure microscope results (a)x10, (b)x10 with porosity, (c)x20 (d)x20 with porosity; magnification at vertical surface	61
Figure 5.1.1.7 0.65 Fe level microstructure microscope results (a)x10, (b)x10 with porosity, (c)x20 (d)x20 with porosity; magnification at horizontal surface	62
Figure 5.1.1.8 0.65 Fe level microstructure microscope results (a)x10, (b)x10 with porosity, (c)x20 (d)x20 with porosity; magnification at vertical surface	62
Figure 5.2.1.1 classification of mechanical test	63
Figure 5.2.1.2 Charpy fracture surface visual comparison between samples with different Fe level	64
Figure 5.2.2.1 0.11 Fe level Charpy test fracture surface optical microscope results (a)x10, (b)x80, (c)x10; magnification of fracture surface	65
Figure 5.2.2.2 0.25 Fe level Charpy test fracture surface optical microscope results (a)x10, (b)x50, (c)x10; magnification of fracture surface	66
Figure 5.2.2.3 0.42 Fe level Charpy test fracture surface optical microscope results (a)x10, (b)x30, (c)x10; magnification of fracture surface	66
Figure 5.2.2.4 0.65 Fe level Charpy test fracture surface optical microscope results (a)x10, (b)x50, (c)x10; magnification of fracture surface	66
Figure 5.2.2.5 0.11 Fe level tensile test fracture surface optical microscope results (a)x15, (b)x30, (c)x10; magnification of fracture surface	67
Figure 5.2.2.6 0.25 Fe level tensile test fracture surface optical microscope results (a)x15, (b)x30, (c)x10; magnification of fracture surface	67

Figure 5.2.2.7 0.42 Fe level tensile test fracture surface optical microscope results (a)x15, (b)x30, (c)x10; magnification of fracture surface	67
Figure 5.2.2.8 0.65 Fe level tensile test fracture surface optical microscope results (a)x15, (b)x30, (c)x10; magnification of fracture surface	68
Figure 5.2.2.9 Iron Aluminum Phase Diagram	68
Figure 5.2.2.1 SEM - ZEISS Evo MA10	69
Figure 5.2.2.2 Placement of samples into SEM	70
Figure 5.3.1.1 Charpy Impact Test SEM Micrographs at 500X magneficaton (A) 0.11 Fe, (B) 0.25 Fe, (C) 0.42 Fe, (D) 0.65 Fe.	72
Figure 5.3.1.2 Charpy Impact Test SEM Micrographs with 0.11 Fe level (A)150X magnification, (B) 500X magnification, (C) 1.0kX magnification (D) 3.0kX magnification	73
Figure 5.3.1.3 Charpy Impact Test SEM Micrographs with 0.25 Fe level (A)150X magnification, (B) 500X magnification, (C) 1.0kX magnification (D) 3.0kX magnification	74
Figure 5.3.1.4 Charpy Impact Test SEM Micrographs with 0.42 Fe level (A)150X magnification, (B) 500X magnification, (C) 1.0kX magnification (D) 3.0kX magnification	75
Figure 5.3.1.5 Charpy Impact Test SEM Micrographs with 0.65 Fe level (A)150X magnification, (B) 500X magnification, (C) 1.0kX magnification (D) 3.0kX magnification	76
Figure 5.3.1.6 Charpy Impact Test SEM micrographs in BSD mode (A) 0.11 Fe, (B) 0.25 Fe, (C) 0.42 Fe, (D) 0.65 Fe.....	77
Figure 5.3.1.7 Tensile Test SEM Micrographs with 0.11 Fe level (A)150X magnification, (B) 500X magnification, (C) 1.0kX magnification (D) 3.0kX magnification	78
Figure 5.3.1.8 Tensile Test SEM Micrographs with 0.25 Fe level (A)150X magnification, (B) 500X magnification, (C) 1.0kX magnification (D) 3.0kX magnification	79
Figure 5.3.1.9 Tensile Test SEM Micrographs with 0.42 Fe level (A)150X magnification, (B) 500X magnification, (C) 1.0kX magnification (D) 3.0kX magnification	80
Figure 5.3.1.10 Tensile Test SEM Micrographs with 0.65 Fe level (A)150X magnification, (B) 500X magnification, (C) 1.0kX magnification (D) 3.0kX magnification	81

Figure 5.3.1.11 Tensile Test SEM micrographs in BSD mode (A) 0.11 Fe, (B) 0.25 Fe, (C) 0.42 Fe, (D) 0.65 Fe.....	82
Figure 5.3.1.12 XRD Mapping of 0.65 Fe level 4th specimen	83
Figure 5.3.1.13 Charpy Impact Test sample with 0.11 Fe level, fracture surface EDX analysis at general area	85
Figure 5.3.1.14 Charpy Impact Test sample with 0.11 Fe level, fracture surface EDX analysis at point 2.....	86
Figure 5.3.1.15 Charpy Impact Test sample with 0.25 Fe level, fracture surface EDX analysis at general area	87
Figure 5.3.1.16 Charpy Impact Test sample with 0.25 Fe level, fracture surface EDX analysis at point 2.....	88
Figure 5.3.1.17 Charpy Impact Test sample with 0.42 Fe level, fracture surface EDX analysis at general area	89
Figure 5.3.1.18 Charpy Impact Test sample with 0.42 Fe level, fracture surface EDX analysis at point 4.....	90
Figure 5.3.1.19 Charpy Impact Test sample with 0.65 Fe level, fracture surface EDX analysis at general area	91
Figure 5.3.1.20 Charpy Impact Test sample with 0.65 Fe level, fracture surface EDX analysis at point 2.....	92
Figure. A 0.11 Fe level sample point EDX analysis point 1.....	99
Figure. B 0.11 Fe level sample point EDX analysis point 3.....	100
Figure. C 0.25 Fe level sample point EDX analysis point 1.....	101
Figure. D 0.25 Fe level sample point EDX analysis point 3.....	102
Figure. E 0.42 Fe level sample point EDX analysis point 1.....	103
Figure. F 0.42 Fe level sample point EDX analysis point 2.....	104
Figure. G 0.65 Fe level sample point EDX analysis point 1	105
Figure. H 0.65 Fe level sample point EDX analysis point 3	106

LIST OF TABLES

Table 1.2.1.1 Aluminum alloy designation system – Aluminum Association [3].....	15
Table 1.7.1.1 Hardness test results.....	26
Table 2.2.1.1 Density measurement results	27
Table 2.2.1.1 Chemical compositions of A356 alloy samples.....	29
Table 3.1.1.1 Charpy test results of samples with 0.11 Fe level.....	32
Table 3.1.2.1 Charpy test results of samples with 0.25 Fe level.....	34
Table 3.1.3.1 Charpy test results of samples with 0.42 Fe level.....	36
Table 3.1.4.1 Charpy test results of samples with 0.65 Fe level.....	38
Table 3.2.1.1 Tensile test results of 0.11 Fe level sample	42
Table 3.2.2.1 Tensile test results of 0.25 Fe level sample	43
Table 3.2.3.1 Tensile test results of 0.42 Fe level sample	45
Table 3.2.4.1 Tensile test results of 0.65 Fe level sample	46

1 INTRODUCTION

After oxygen and silicon, aluminum is the third most plentiful element on the planet. It's present in metal compounds like iron, lead, and tin, which are all common in nature. Aluminum is one of the most commonly utilized metals due to its lightweight and simplicity of casting. This may now be seen in a variety of industries, including construction, defense, and automotive.

Aluminum is classified into two types based on its application: primary (primary) and secondary (secondary) (recycled). In terms of the energy required to obtain it and thus carbon emissions, primary aluminum is more unfavorable than secondary aluminum. Primary aluminum requires ten times more energy than secondary (recycled) aluminum, according to studies. [1] The usage of secondary aluminum in the industry becomes even more important since the Green Deal aims to reduce carbon footprint and hence carbon dioxide emissions. However, because the iron (Fe) ratio in secondary aluminum increases as a result of recycling, and because this increase has a negative impact on the mechanical properties of aluminum and its alloys, it is necessary to better understand the negative consequences of this negative impact on the material's structure and mechanical properties. Cast aluminum with various iron ratios was investigated in this study. The aluminum alloy's other components were kept constant and put through tests.

1.1 Purpose of the Thesis

The purpose of this study is to look at how varying Fe ratios affect the mechanical properties of aluminum alloy. In accordance with the experiments and researches to be done, Charpy, Tensile, SEM, and Optical Microscope tests will be undertaken in order to collect data on the mechanical properties that alter based on the amount of iron, how and how it will be used in the business. It is intended to gather and implement the relevant information in this area.

1.2 Literature Survey

It is crucial to comprehend how mechanical properties change as a result of composition percentages, as well as to comprehend measurement results in a healthy manner.

1.2.1 Classification of Cast Aluminum Alloy

Classifications are made to identify and communicate the alloys easily. Most countries have decided to use the four-digit classification for wrought alloy composition designation as a significant step toward international alignment of aluminum and aluminum alloy compositions. The Aluminum Association (AA) in Washington, USA, manages this system and compiles the data as “Registration record of International Alloy Designations and Chemical Composition Limits for Wrought Aluminum Alloys”. The alloys that are European referenced can be recognized by the prefix EN and AW, which stand for “European Normative Aluminum Wrought” alloys. The alloy numbers and composition restrictions are identical to those registered by the Aluminum Association in all other respects. [2]

Table 1.2.1.1 Aluminum alloy designation system – Aluminum Association [3]

Alloy Series	Alloying element (principal)	In some places, it is used and properties
1XX.X	Pure aluminum	Electric and chemical industry
2XX.X	AL-Cu alloys	The high strength of the material, aerospace industry
3XX.X	Al-Mn alloys	Pipe liquid tanks, architectural applications
4XX.X	Al-Si alloys	Welded structures, slab making, automotive parts manufacturing
5XX.X	Al-Mg alloys	Hardness and strength of material, brittle. Applications in sea.
6XX.X	Al-Mg-Si alloys	High formability, extrusion
7XX.X:	Al-Zn alloys	The high strength of the material, aerospace, and high strength applications
8XX.X	Al-Li alloys	good fatigue resistance, aerospace applications.
9XX.X	Various elements	Not commonly used

AL-Si-Cu Alloys

The addition of copper to an Al-Si alloy boosts the alloy's strength. It also promotes age hardening and machinability. Castability and ductility, on the other hand, are reduced. Aluminum alloys typically have a silicon content of 3 to 10.5 percent and a copper content of 1.5 to 4.5 percent. In pressure die casting, alloys with a higher silicon concentration (e.g., Al-10Si-2Cu) are employed. In permanent mold castings and sand castings, copper-rich alloys (e.g., Al-3Si-4Cu) are used [4]

Al-Si-Mg Alloys

Because of the features like as low density, strong corrosion resistance, and good castability, Al-Si alloys are used in a number of engineering applications. The absence of heat treatment capabilities is, however, the most significant disadvantage of these alloys. As a result, Mg is added to the alloy in order to improve its heat treatment capabilities and offer a better engineering alloy [5]. Because of the features of the aluminum alloys 6XXX Al-Si-Mg have been frequently used as structural components [6]

1.3 Mechanical Test Methods

1.3.1 Charpy Impact Testing

The Charpy impact test, also known as the Charpy V-notch test, is a classic high-strain rate test used in materials science to assess how much energy is absorbed by a material during fracture. The amount of energy absorbed indicates the material's notch toughness. It is widely utilized in the industry since it is simple to prepare and apply, with quick and inexpensive effects.

Impact testing examines the mechanics of a specimen when it is subjected to a shock loading those results in rapid deformation, fracture, or complete rupture. The specimen is placed in a holding device with the geometry and orientation indicated by the type of test, and then a known weight, commonly pendulum-shaped, is released from a known height to perform this test. The weight then slams against the sample with a powerful impact. The sample is frequently destroyed as a result of the impact between the weight and the sample.

However, the energy transfer between the two is used to calculate the material's fracture

mechanics. An impact test measures a material's ability to absorb energy in the event of a collision.

Depending on the test and the property to be assessed, this energy can be used to determine the material's toughness, impact strength, impact resistance, or fracture resistance. These figures are crucial for choosing materials for applications that require the material to withstand extremely rapid loading processes, such as automobile crashes.

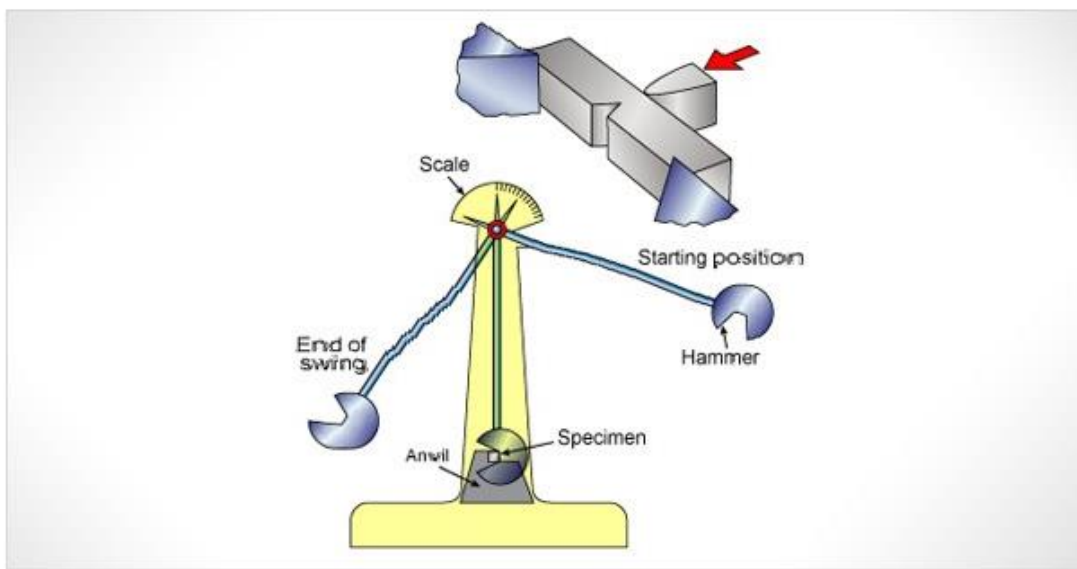


Figure 1.3.1.1 Charpy impact testing machine [7]

1.3.2 Instrumented Charpy Impact Testing

Because flexibility is the material's fragility value, flexibility is a critical attribute for businesses in the metal industry. The Charpy impact test, also known as the robustness test, involves a pendulum machine shattering a notched reference sample and measuring the impact energy. Businesses have their raw materials analyzed using Charpy reference samples on a pendulum impact machine.

Raw material selection, processing, homogeneity, and stability are important factors to consider while creating Charpy reference samples. Notch impact tests are a mechanical method for determining the sample's impact strength or notch toughness. The energy level required to break another piece of steel is determined using the energy level required to break a test specimen in this testing method. In the steel, aerospace, and automotive industries, these tests are often used.

In a nutshell, the notch impact test measures a material's dynamic toughness under conditions that cause it to behave brittle. When pressed at low temperatures or when a force is applied rapidly, such as an impact, ductile materials typically do not deform plastically and show brittle behavior. To determine this scenario, the Charpy or Izod test is used. A mass with specific potential energy is impinged on the V-notched test sample in these experiments, and the impact energy required to break the sample is computed.

Strength, crystalline structure, temperature, and chemical composition are the key factors that influence impact energy. The dynamic toughness of material against impact is measured by its strength. The material's crystal structure reveals its ductility and toughness, brittle structure, and brittle or tough behavior depending on the conditions. The material may lose its toughness and exhibit brittle behavior at certain temperatures. This is known as the ductile-brittle transition temperature. The chemical composition of the material influences this temperature.



Figure 1.3.2.1 Instrumented Charpy device used in the experiments

1.4 Tensile Testing

Tensile Testing, also known as tensile testing, is a destructive engineering and materials science test that determines the behavior of a sample by applying a force to a sample with controlled tension under an evidential load up to a certain level or until the material ruptures completely.

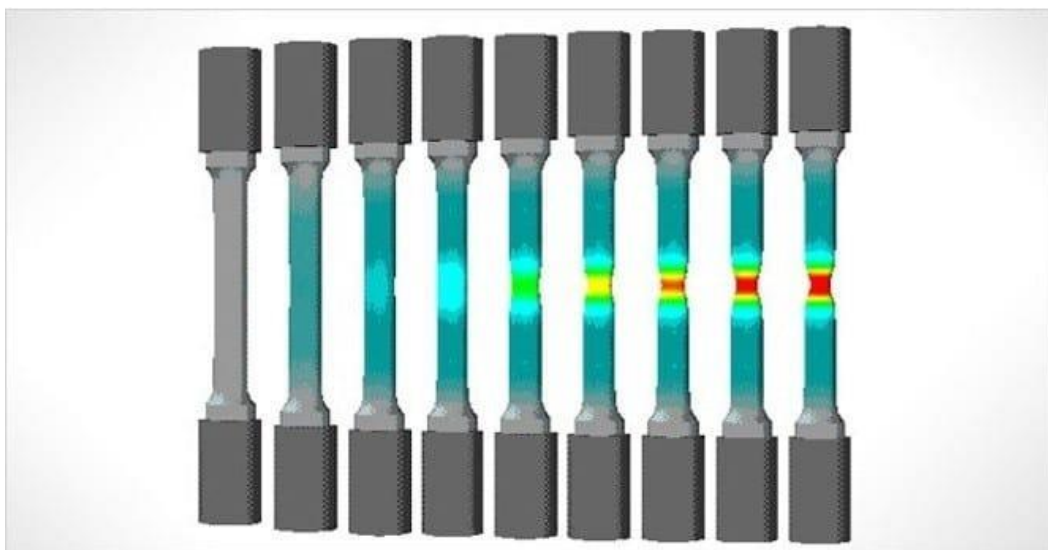


Figure 1.3.2.1 Visualization of the mechanical changes while tensile testing [8]

This is one of the most widely used mechanical testing methods. It is used to determine the strength of a material and how far it can be stretched before breaking. The yield strength, ultimate tensile strength, ductility, strain hardening characteristics, Young's modulus, and Poisson's ratio are all determined using this test method.

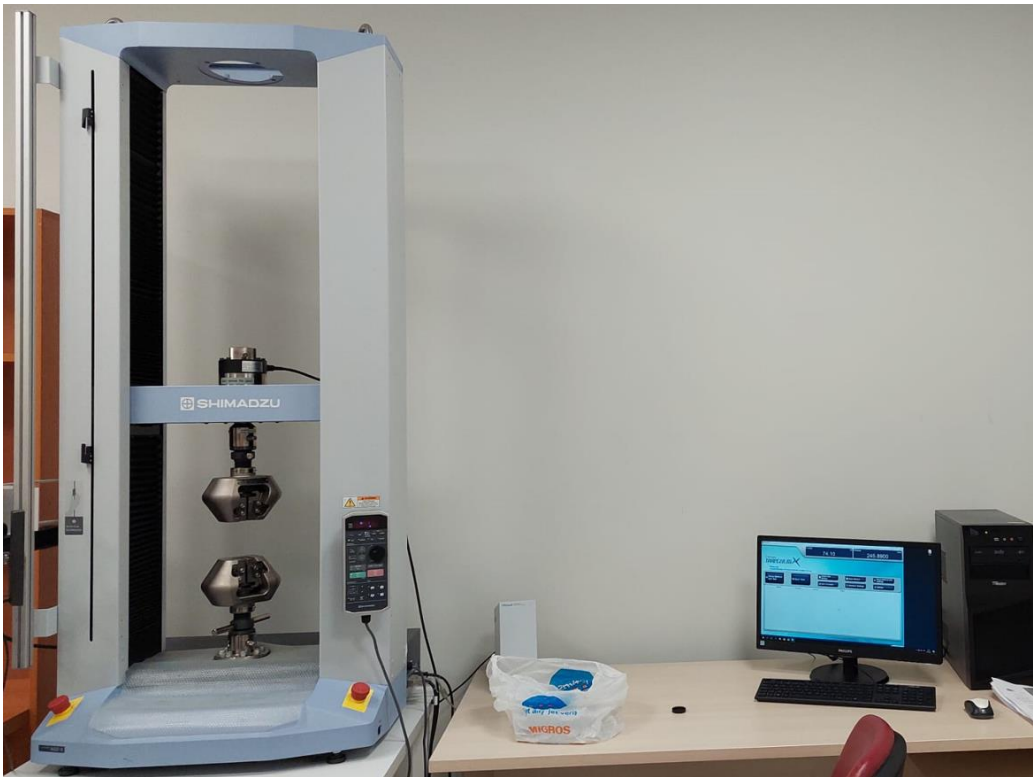


Figure 1.3.2.2 Tensile test device used in the experiments

1.4.1 Ultimate Tensile Strength (UTS)

This is the maximum amount of stress that a sample can withstand during testing. In other words, it is the sample's maximum tensile strength. This may differ from the specimen's break strength depending on whether it is brittle, ductile, or both. These material properties can change depending on the environment, such as when it is extremely hot or cold. This test is applicable to metals, plastics, elastomers, paper, composites, rubbers, fabrics, adhesives, films, and other materials.

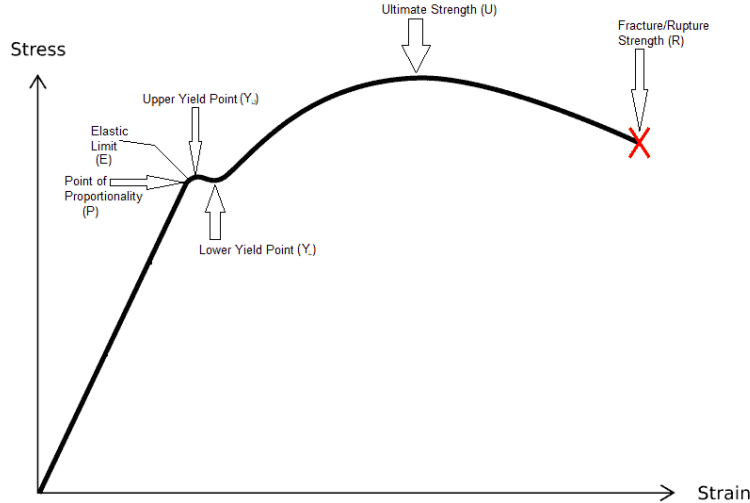


Figure 1.4.1.1 Basic schematic of stress-strain graph [9]

1.4.2 Yield Strength (YS)

The point at which plastic deformation begins under stress is known as yield strength. This is determined during the usage of extensometers to measure the gauge length.

1.4.3 Elongation

When a material is subjected to a tensile load, elongation is a measure of distortion that happens before it eventually breaks.

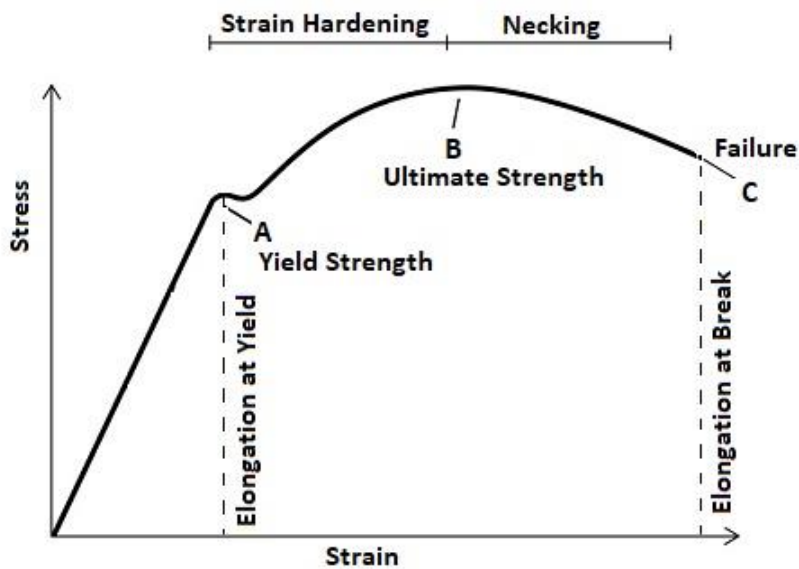


Figure 1.4.3.1 Basic schematic of stress-strain graph with elongation points [10]

1.5 Optical Microscope

Optical Microscopy Analysis magnifies a sample image using a lens system and visible light. Optical Microscopy (OM) is frequently used as the first technique to examine or compare products or to prepare small samples before further analysis. It is frequently used to record sampling sites or phenomena observed during other types of testing. Magnifications ranging from 10x to slightly more than 100x reveal numerous details and features of the specimens.

We can typically magnify a sample by 10-100x using OM. If a higher magnification is required, the Scanning Electron Microscope (SEM) can provide up to 500,000x magnification.

1.6 Scanning Electron Microscope (SEM)

Scanning Electron Microscopy (SEM analysis) delivers high-resolution images that can be used to check for surface cracks, flaws, impurities, or corrosion in a range of materials. Metallurgical professionals can study material qualities in depth using SEM and EDX investigations. SEM analysis is a strong research method that produces complex, greatly magnified images of a sample's surface topography using a focused stream of electrons [11].

After a region of interest on the sample has been located and examined using SEM, the material's features can be investigated using energy dispersive x-ray spectroscopy, or EDX analysis. Using a scanning electron microscope to perform a visual inspection of a surface can help identify impurities or unknown particles, the source of a malfunction, and material interactions.

SEM analysis is used for particle characterization, such as wear residues produced during mechanical wear testing, in addition to surface assessment. Our SEM analysis high magnification, high resolution imaging aids in the determination of the number, size, and morphology of small particles, allowing customers to understand the wear characteristics of their materials.

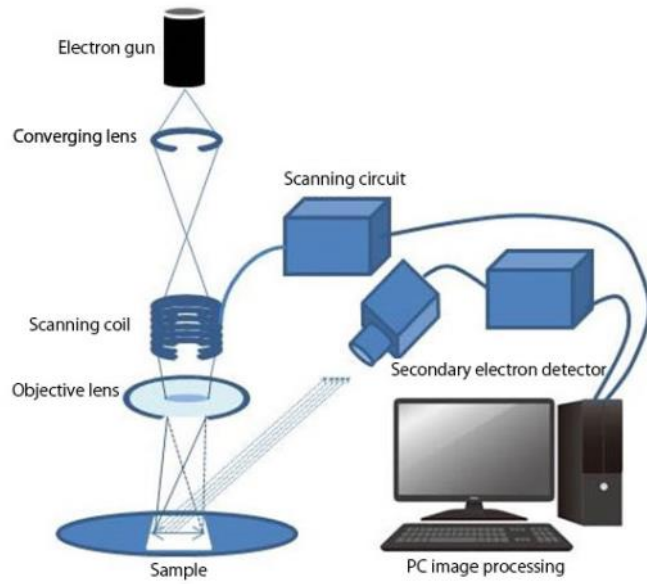


Figure 1.4.3.1 SEM working schematic [11]

1.6.1 Using SEM and EDX Analysis Together

During the SEM analysis process, energy dispersive x-ray spectroscopy, also known as EDX, EDS, or EDAX, provides a better understanding of the surface material. EDX analysis is used to determine the elemental composition of a sample and yields a more quantitative result than SEM analysis alone. The combination of SEM and EDX analysis provides chemical composition and fundamental research, as well as a thorough metallurgical evaluation.

1.7 Green Deal

Carbon emissions have become one of the most pressing environmental challenges in recent decades. Since the industrial revolution, increasing carbon emissions in our atmosphere, along with other greenhouse gases, has been the major cause of global warming and environmental disasters. Changes in the climate caused by carbon emissions are the primary cause of natural occurrences and disasters that are not commonly witnessed in our own geography and in different regions of the world. It is the goal of the EU green agreement action plan to use natural resources responsibly and reduce emissions that contribute to the climate catastrophe. In this regard, one of the most important policies is to reduce pollution levels in the environment.

1.7.1 The Role of Aluminum in the Green Deal

Lower carbon dioxide emissions are now required in business, owing to rising environmental concerns, particularly in recent years. The considerable energy required in the manufacturing of aluminum, which is one of the alloys used in many industries, adds to these concerns. Aluminum, as is well known, is employed in both primary and secondary applications (secondary). Primary Aluminum requires more energy to create than secondary Aluminum. When compared to primary aluminum production, secondary aluminum requires 95 percent less energy [12]. Carbon monoxide and carbon dioxide emissions rise as a result of this demand.

The usage of secondary (recycled) aluminum is critical in order to limit this emission. The use of secondary materials to reduce carbon dioxide emissions is preferred and encouraged, which increases the iron (Fe) content of the material. To observe the change in the mechanical properties of the material and to determine at what rate it will pose a risk, the material should be subjected to mechanical tests in order to minimize the risks that will arise, and an average / appropriate value should be obtained based on the results obtained.

This project aims to determine the allowable iron ratio of aluminum alloy, which is widely used in the automotive industry, and to investigate the mechanical and metallurgical properties of the material if this limit is exceeded, with the goal of reducing carbon dioxide emissions, which is one of the world's biggest problems.

Aluminum is utilized in manufacturing in two different forms: primary and secondary. It is well known that primary aluminum requires ten times the energy of secondary (recycled) aluminum [13]. As a result, a proposal to utilize secondary (recycled) aluminum in wheel manufacture is being developed. The iron ratio in primary ingot is known to range between 0.07 percent and 0.11 percent.

The mechanical properties will be examined in relation to the increase in iron content that will occur as a result of the usage of more secondary aluminum. It will be used in parts such as the swing part, clutch housing, electric bicycle rim, solar vehicle rim, engine cylinder head, engine bay, and engine blocks to assure the project's continuance. The Fe rate limit that can be determined here will be useful for aluminum alloy parts utilized in the automobile industry.

Cevher Wheels, which will be backed up during the testing period. Based on conversations with experts and a review of the literature, it has been found that producing products with a high percentage of primary ingots increases carbon emissions. The considerable energy consumed during primary aluminum production from ore using the Hall–Héroult method [14] is the cause of this increase in emissions. Because secondary aluminum production uses far less energy than primary aluminum production, the carbon footprint of secondary aluminum ingot manufacture is reduced. Despite the increased energy savings, the usage of secondary ingots is limited because the amount of Fe in the ingot has an unfavorable effect on the mechanical qualities. It will be demonstrated in this study which quantities of iron are necessary, as well as the maximum secondary aluminum consumption that can be used throughout manufacture. It is planned to advance and contribute to the automobile business as future mechanical engineers who aim to solve the sector's high emission problem.

2 MATERIAL AND METHOD

2.1 Measurement of Sample Qualification

We wanted to know about several characteristics of our sample before testing, so we took measurements. Our AlSi7Mg alloy samples with four different iron ratios were measured and the results are listed below.

2.2 Hardness

The Procep Equotip 550 Leeb portable measurement gadget was utilized to obtain the hardness levels before analyzing our samples. The 4 hardness's for each condition were checked from the red highlighted regions of the cut pieces to produce Brinell values.

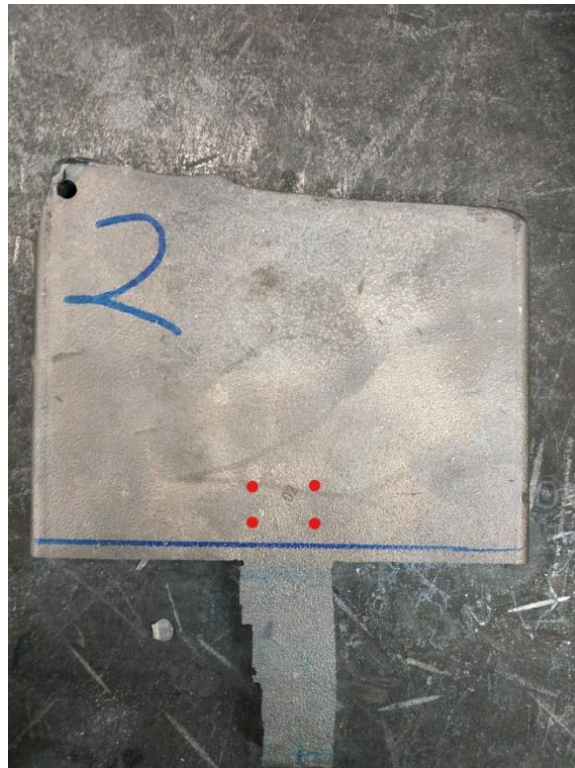


Figure 1.7.1.1 hardness measurement points (red dots)

The values recorded for various iron ratios are listed in the table below. As you can see in the table below.

Table 1.7.1.1 Hardness test results

Fe content	0,11	0,25	0,42	0,65
1st measurement	71,3	77,9	64	71,3
2nd measurement	64,8	67,9	68	69,6
3rd measurement	63,1	68,9	76,3	70,5
4th measurement	73,2	69,3	78,8	65,8
Average	68,1	70,975	71,775	69,3

When we look at the table, we can see that the hardness increases first, then lowers as the iron ratio rises. The reason for this is because iron is not the only factor that influences hardness; the ratio of other elements in the composition also has an impact.

2.2.1 Density

Prior to testing, we double-checked the density of our samples. Mettler AJ100 equipment was used for this measurement. The substance utilized is ethyl alcohol with a density of 0.8050. It took roughly 2 hours to complete the test. A simplified version of the measurement approach we employed is shown below.



Figure 2.2.1.1 Density Measurement

In the table below, the recorded values for the various iron ratios are listed. You can go back and review everything if you want to.

Table 2.2.1.1 Results from density measurement

Sample Number	Density (g/cm ³)
Sample 1	2,652
Sample 2	2,654
Sample 3	2,655
Sample 4	2,665

Before measuring the density, we sliced and filed the samples and finished the density test. When we looked at the measurements, the intensity levels did not vary considerably. As the iron ratio varied, the density did not alter appreciably.

2.3 Sample Production

For this project as we are examining the effects of the Fe content in mechanical properties, 4 different Fe level containing alloy had been made. These samples had been made from cast aluminum which was melted at 729C in a crucible furnace. The casting had been made in 750kg capacity crucible furnace; the casting made with about 300kg metal using book mold, as shown in the figure 2.2.1.1, with post casting thermal image.

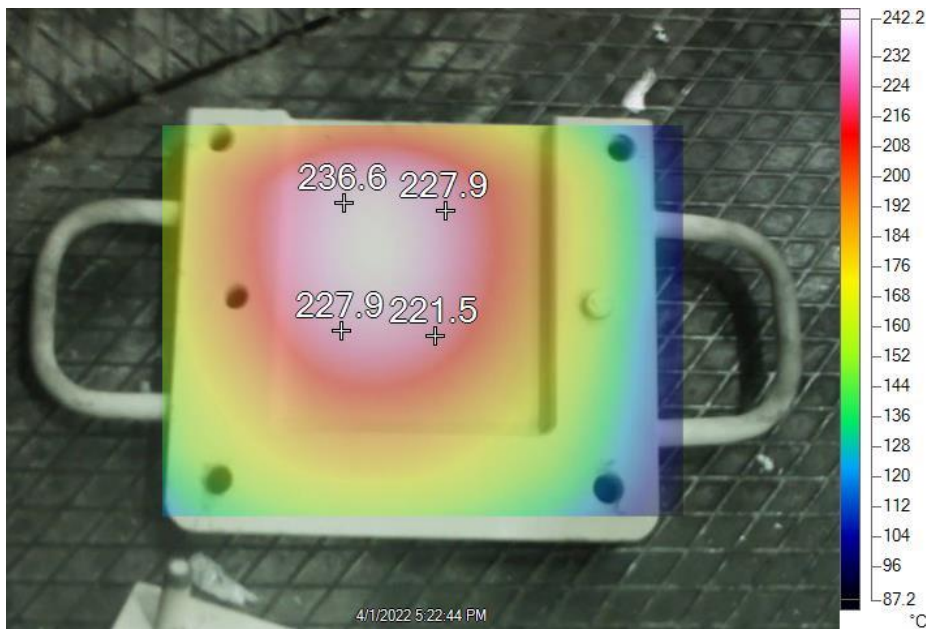


Figure 2.2.1.1 Thermal Image Of The Casting Process

From the mixing different content aluminum, 0.11, 0.025, 0.42 and 0.65 level of Fe contained samples were made. All the of metals are as shown in table 2.2.1.1, with percentage values.

Table 2.2.1.2 Chemical compositions of A356 alloy samples

Sample 1		Sample 2		Sample 3		Sample 4	
	Wt.		Wt.		Wt.		Wt.
Al	92.0235	Al	92.0526	Al	91.7269	Al	91.5483
Fe	0.11587	Fe	0.25264	Fe	0.42482	Fe	0.65121
Si	7.42442	Si	7.26952	Si	7.32596	Si	7.3782
Mg	0.28156	Mg	0.27143	Mg	0.26867	Mg	0.27032
Ti	0.11632	Ti	0.11608	Ti	0.11422	Ti	0.11188
Sr	0.01356	Sr	0.01178	Sr	0.01281	Sr	0.01178
Mn	0.00234	Mn	0.00251	Mn	0.00281	Mn	0.00325
Cu	0.0008	Cu	0.00088	Cu	0.00106	Cu	0.00127
Zn	0.00215	Zn	0.00241	Zn	0.00425	Zn	0.00264
Cr	0.00071	Cr	0.00075	Cr	0.00081	Cr	0.00093
Ni	0.00453	Ni	0.0046	Ni	0.00474	Ni	0.00486
Sn	0.00032	Sn	0.00034	Sn	0.00039	Sn	0.00047
Na	0.00036	Na	0.00034	Na	0.00021	Na	0.00021
Ca	0.00154	Ca	0.00137	Ca	0.0013	Ca	0.00148
Zr	0.00445	Zr	0.00434	Zr	0.00425	Zr	0.00428
V	0.01167	V	0.01149	V	0.01129	V	0.01137
Co	0.00003	Co	0.00003	Co	0.00005	Co	0.00006
Sb	0.00032	Sb	0	Sb	0	Sb	0
P	0	P	0	P	0	P	0
B	0	B	0	B	0.00001	B	0
Others	0.00514	Others	0.00503	Others	0.00487	Others	0.00497

2.4 Sample (Specimen) Preparation

After the preparation of book mold casting, the samples are prepared for each test.

2.4.1 Charpy V-notch Test Specimens

TS_EN_ISO_148_3 is the standard for Charpy V-notched tests, and according to this standard and our device requirements, our specimens are prepared to have 5mmx10mmx55mm dimensions. To minimize error due to the use of experimental methods, five specimens were made for each sample. Total of 20 Charpy V-notched specimen has been made. As can be seen from figure 2.4.1.1.

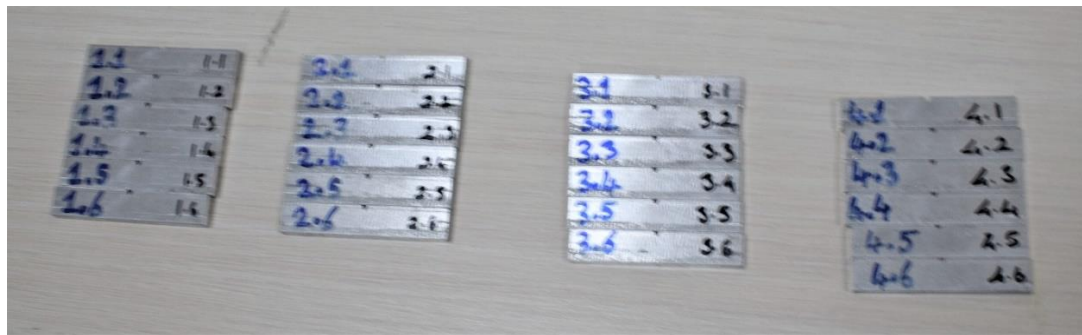


Figure 2.4.1.1 Charpy test specimens

2.4.2 Tensile Test Specimens

TS_EN_ISO_6892_1:2020, the standard is followed for the specimen preparation. For this test, sample prepared with $d = 5\text{ mm}$. As it was made for the Charpy Testing, for Tensile Testing also five specimens were prepared for each sample. A total of 20 Circular-diameter Tensile Test specimen was made as given in the figure 2.4.2.1



Figure 2.4.2.1 Tensile Test Specimen

3 TESTING AND DATA INTERPRETATION

3.1 Charpy V-notch TEST

3.1.1 Impact tests for 0.11 Fe content

Samples made with 0.11 Fe contents were placed into the Instron CEAST 9050 at the 20°C.

After breaking each sample, the software of the Instron CEAST 9050 impact pendulum machine was used to obtain time-dependent force and energy data of fracture.

For energy calculation, we divided the energy values to our cross-section of the fracture surface as; $(0.10 - 0.02) \times 0.005 = 0.0004 \text{ m}^2$.

With OriginPro8.5, the resulting Force-Time and Energy-Time data are visually organized.

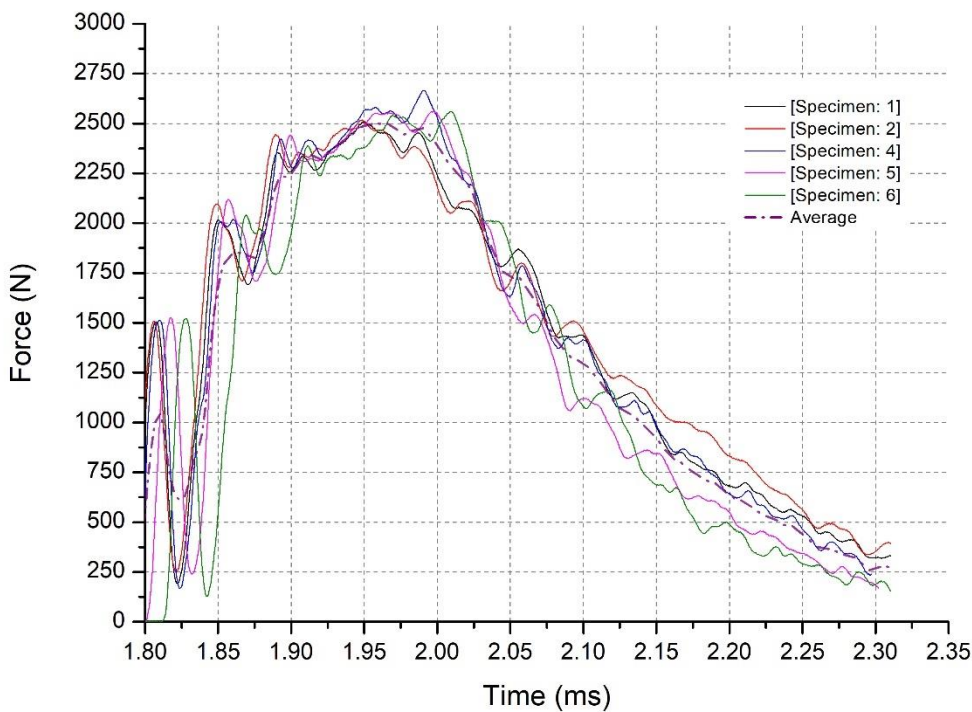


Figure 3.1.1.1 Charpy V-notch test Force vs. Time Graph for sample 1

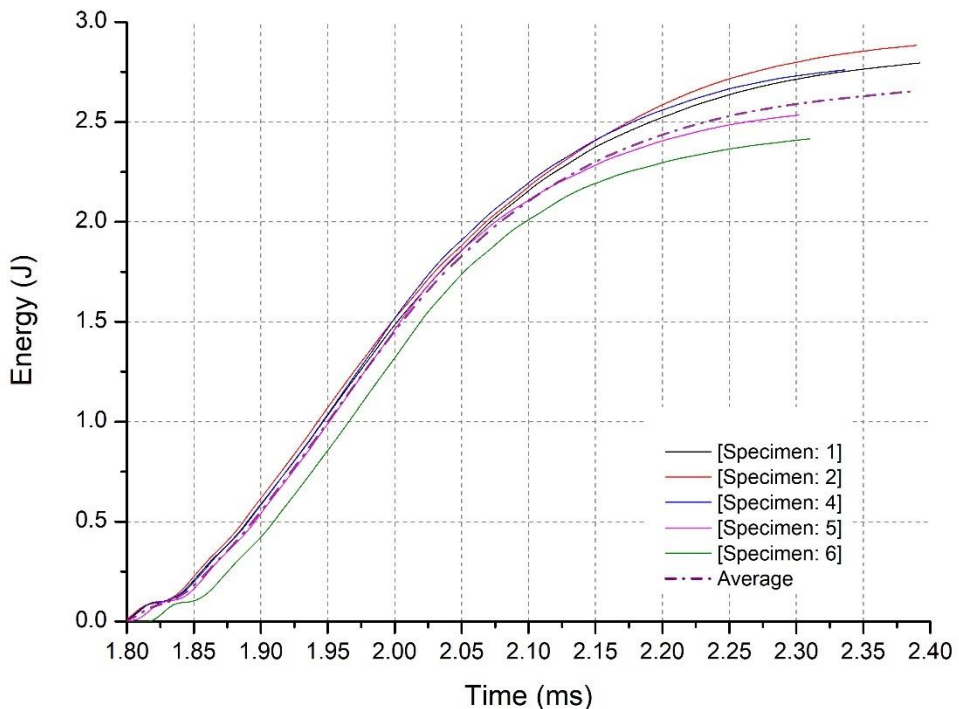


Figure 3.1.1.2 Charpy V-notch test Energy vs. Time Graph for sample 1

Table 3.1.1.1 Charpy test results of samples with 0.11 Fe level

	specimen 1	specimen 2	specimen 3	specimen 4	specimen 5	Average
Max Load (N)	2509.957005	2517.708571	2664.47155	2561.63411	2559.050255	2562.564298
Initiation Impact Energy (J/m^2)	2578.365	2638.3975	3576.385	3594.9925	3511.0225	3179.8325
Total Energy (J/m^2)	6988.555	7208.9075	7208.9075	6335.2425	6039.3475	6756.192
Propagation Impact Energy (J/m^2)	4410.19	4570.51	3632.5225	2740.25	2528.325	3576.3595

From the results and corresponding graphs, we can see that the max load is 2562.56 N, average initiation impact energy is $3179.83 \frac{J}{m^2}$; average propagation impact energy is $3576.36 \frac{J}{m^2}$, total average energy is $6756.192 \frac{J}{m^2}$,

Also, we can say the results for each specimen are closer to each other. It means that our results are possibly correct.

3.1.2 Impact tests for 0.25 Fe content

Samples that are made with 0.25 Fe contents had been placed into the Instron CEAST 9050 at the 20°C.

After breaking each sample, the software of the Instron CEAST 9050 impact pendulum machine was used to obtain time-dependent force and energy data of fracture.

For energy calculation, we divided the energy values to our cross-section of the fracture surface as; $(0.10 - 0.02) \times 0.005 = 0.0004 m^2$.

With OriginPro8.5, the resulting Force-Time and Energy-Time data are visually organized.

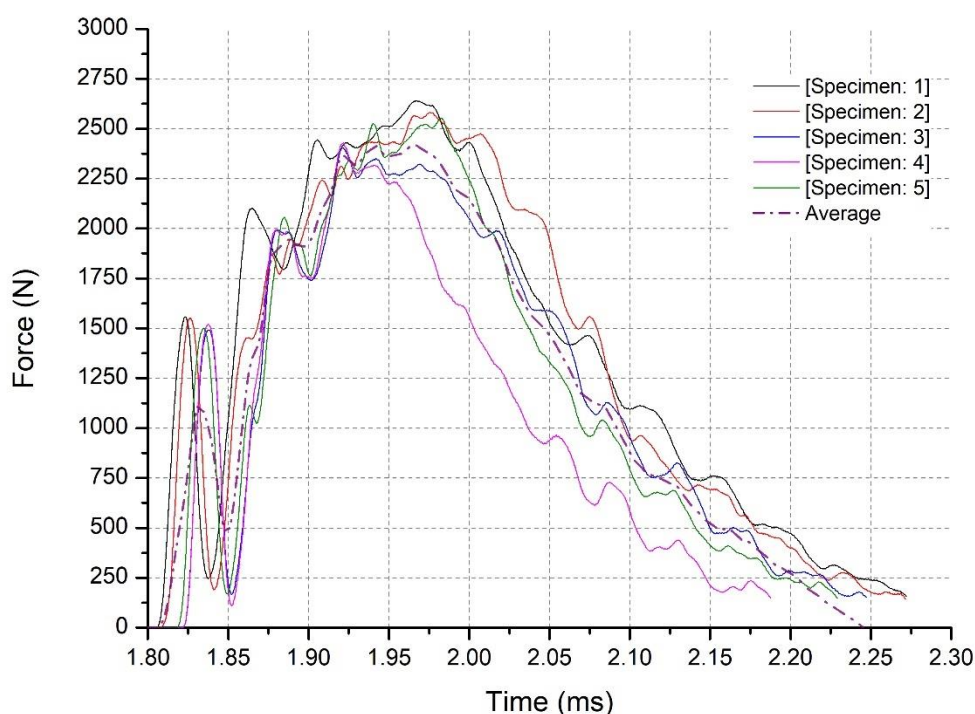


Figure 3.1.2.1 Charpy V-notch test Force vs. Time Graph for sample 2

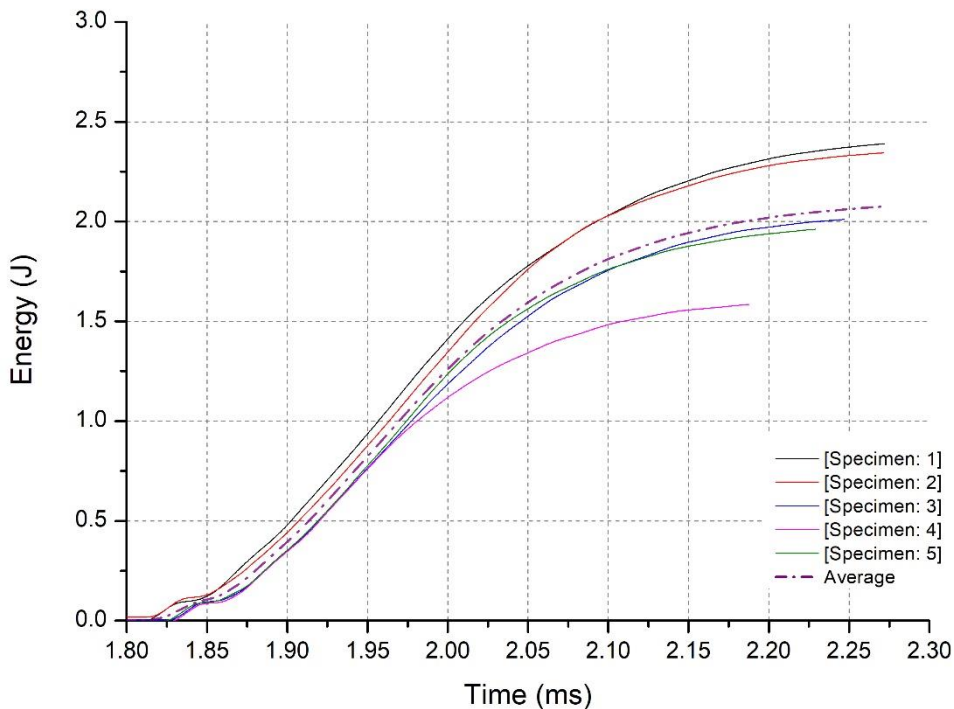


Figure 3.1.2.2 Charpy V-notch test Energy vs Time Graph for sample 2

Table 3.1.2.1 Charpy test results of samples with 0.25 Fe level

	specimen 1	specimen 2	specimen 3	specimen 4	specimen 5	Average
Max Load (N)	2640.7001	2581.27141	2405.569252	2427.7904	2553.8825	2521.843
Initiation Impact Energy (J/m^2)	2763.12	2790.935	1275.25	1279.9175	2707.67	2163.379
Total Energy (J/m^2)	5973.63	5860.3725	5025.8425	3960.715	4902.7	5144.652
Propagation Impact Energy (J/m^2)	3210.51	3069.4375	3750.5925	2680.7975	2195.03	2981.274

From the results and corresponding graphs, we can see that max load is $2521.843 N$, average initiation impact energy is $2163.379 \frac{J}{m^2}$; average propagation impact energy is $2981.274 \frac{J}{m^2}$, total average energy is $5144.652 \frac{J}{m^2}$,

Also, we can say the results for each specimen are closer to each other. It means that our results are possibly correct.

3.1.3 Impact tests for 0.42 Fe content

Samples made with 0.42 Fe contents were placed into the Instron CEAST 9050 at the 20°C.

After breaking each sample, the software of the Instron CEAST 9050 impact pendulum machine was used to obtain time-dependent force and energy data of fracture.

For energy calculation, we divided the energy values to our cross-section of the fracture surface as; $(0.10 - 0.02) \times 0.005 = 0.0004 \text{ m}^2$.

With OriginPro8.5, the resulting Force-Time and Energy-Time data are visually organized.

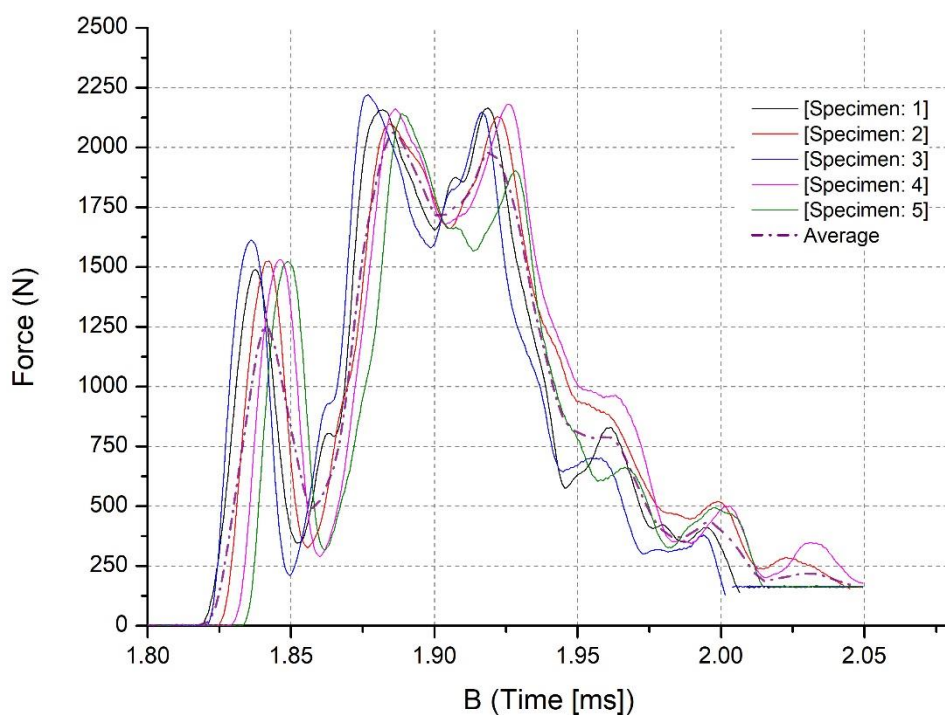


Figure 3.1.3.1 Charpy V-notch test Force vs. Time Graph for sample 3

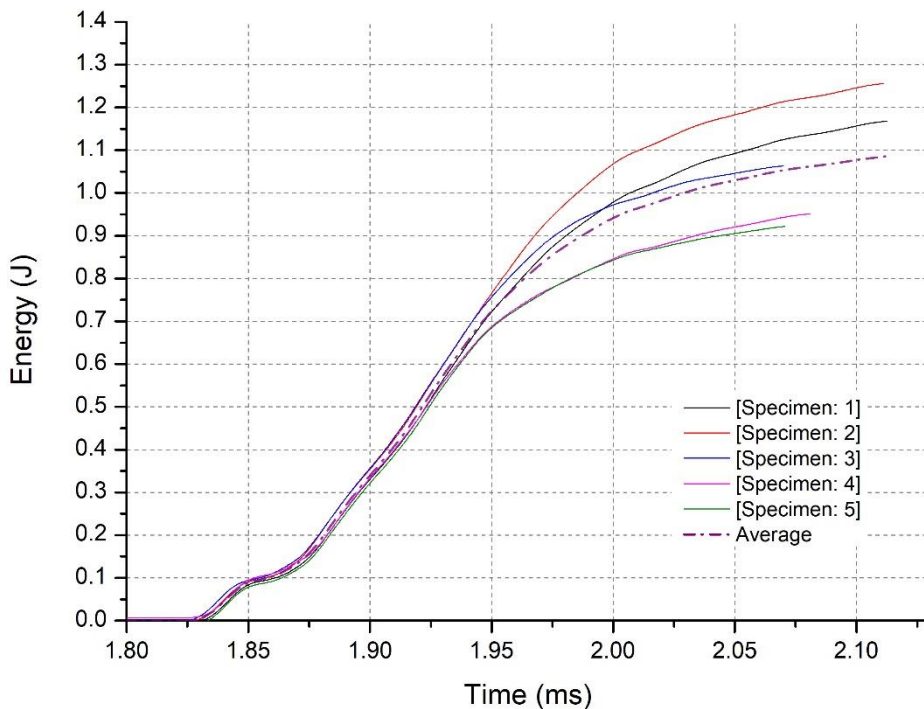


Figure 3.1.3.2 Charpy V-notch test Energy vs. Time Graph for sample 3

Table 3.1.3.1 Charpy test results of samples with 0.42 Fe level

	specimen 1	specimen 2	specimen 3	specimen 4	specimen 5	Average
Max Load (N)	2408.669878	2436.575515	2359.57663	2265.00753	2331.67099	2360.3
Initiation Impact Energy (J/m ²)	1285.0225	1316.04	1269.2475	1267.7475	1220.9125	1271.79
Total Energy (J/m ²)	2920.4075	3139.815	2658.4075	2378.495	2304.7825	2680.38
Propagation Impact Energy (J/m ²)	1635.385	1823.775	1389.16	1110.7475	1083.87	1408.59

From the results and corresponding graphs we can see that max load is $2360.33N$, average initiation impact energy is $1271.79 \frac{J}{m^2}$; average propagation impact energy is $1408.59 \frac{J}{m^2}$, total average energy is $2680.38 \frac{J}{m^2}$,

Also, we can say the results for each specimen are closer to each other. It means that our results are possibly correct.

3.1.4 Impact tests for 0.65 Fe content

Samples made with 0.65 Fe contents were placed into the Instron CEAST 9050 at the 20°C.

After breaking each sample, the software of the Instron CEAST 9050 impact pendulum machine was used to obtain time-dependent force and energy data of fracture.

For energy calculation, we divided the energy values to our cross--section of the fracture surface as; $(0.10 - 0.02) \times 0.005 = 0.0004 \text{ m}^2$.

With OriginPro8.5, the resulting Force-Time and Energy-Time data are visually organized.

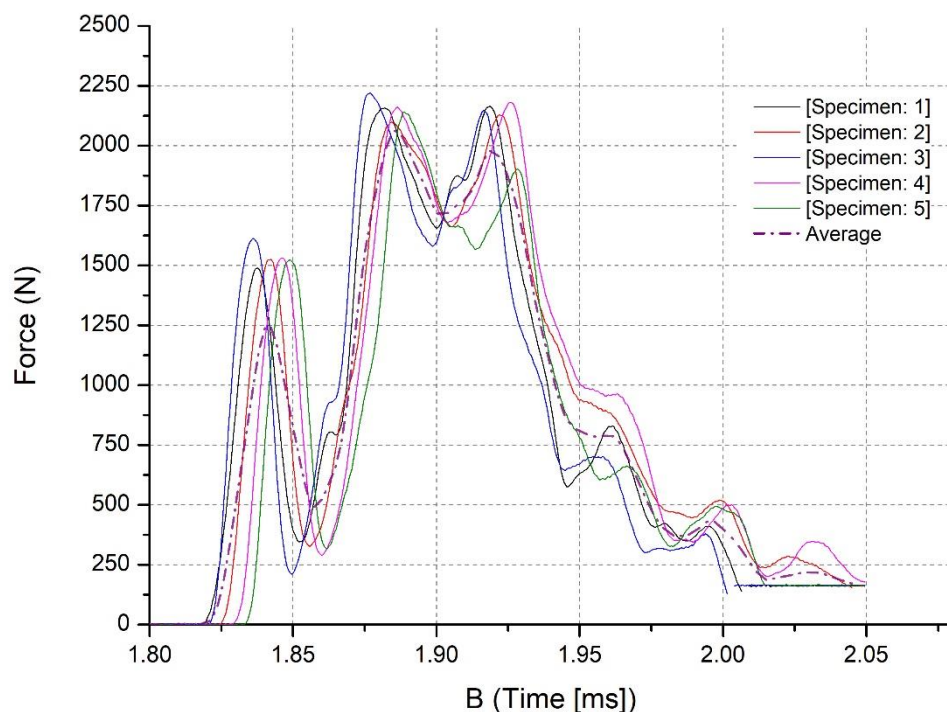


Figure 3.1.4.1 Charpy V-notch test Force vs. Time Graph for sample 4

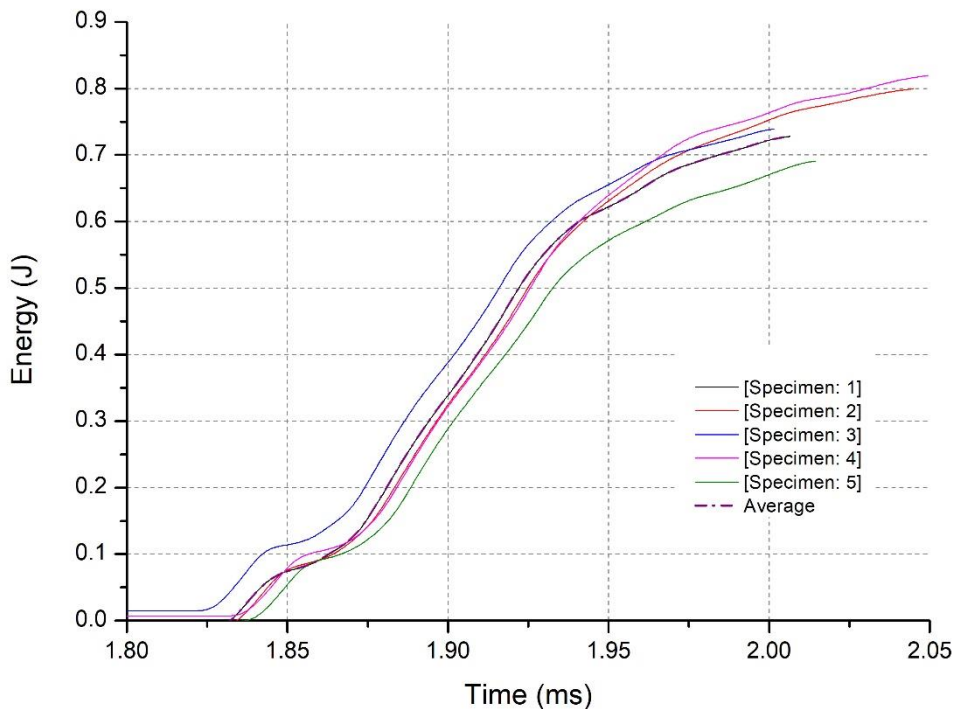


Figure 3.1.4.2 Charpy V-notch test Energy vs. Time Graph for sample 4

Table 3.1.4.1 Charpy test results of samples with 0.65 Fe level

	specimen 1	specimen 2	specimen 3	specimen 4	specimen 5	Average
Max Load (N)	2328.8288	2292.654777	2381.5394	2343.8151	2305.0573	2330.379
Initiation Impact Energy (J/m²)	1178.985	1193.925	561.2025	1248.73	502.8225	937.133
Total Energy (J/m²)	1819.8025	1999	1847.1525	2048.465	1727.03	1888.29
Propagation Impact Energy (J/m²)	640.8175	805.075	1285.95	799.735	1224.2075	951.157

From the results and corresponding graphs, we can see that max load is $2330.379N$, average initiation impact energy is $937.133 \frac{J}{m^2}$; average propagation impact energy is $951.157 \frac{J}{m^2}$, total average energy is $1888.29 \frac{J}{m^2}$,

Also, we can say the results for each specimen are closer to each other. It means that our results are possibly correct.

3.1.5 Comparison between different Fe contents according to Charpy testing

From figure 3.1.5.1, we can see the average forces vs time graph as the Fe content increases. In comparison of the data sets we can say impact force does decrease as the Fe content increases. We can say that time of the impact also decreases. From figure 3.1.5.2, we can see the average energies vs. time from this graph we can say total energy of the impact for each sample does decrease as the Fe content increases. Also, we can observe from the graph time of impact also decreases like the force curve. As a result of calculations from the impact test, as the Fe increased, the max impact load force decreased (figure 3.1.5.3). Also, from figure 3.1.5.4, we can see that as the Fe level increases also the total energy and crack initiation impact energy does also decreases. From these comparisons, we can say the impact resistance of an aluminum alloy decreases as the Fe content increases in the alloy.

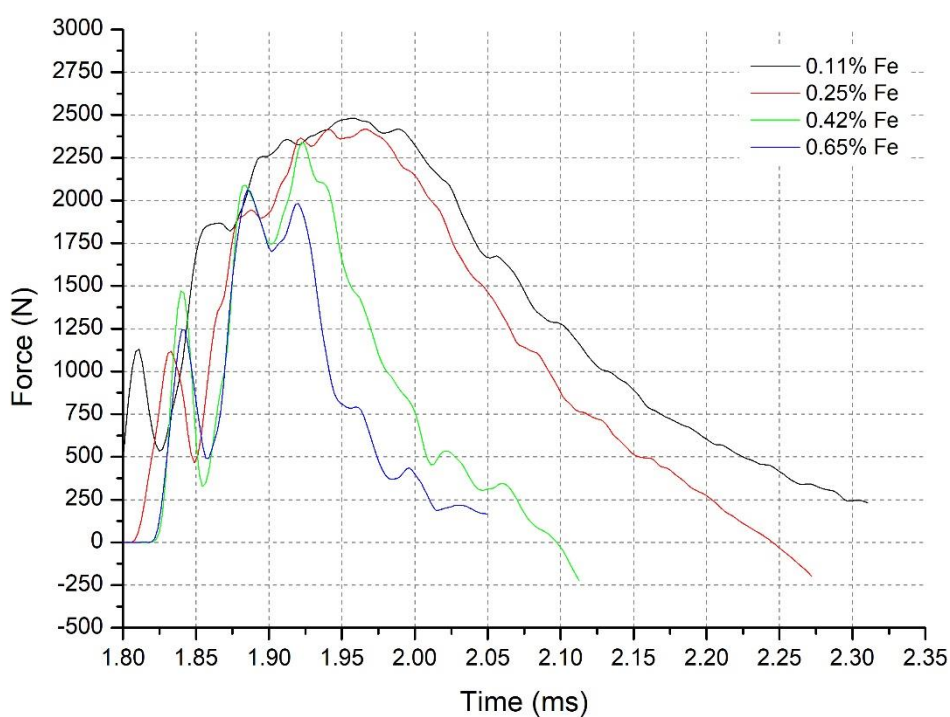


Figure 3.1.5.1 Average force values at impact

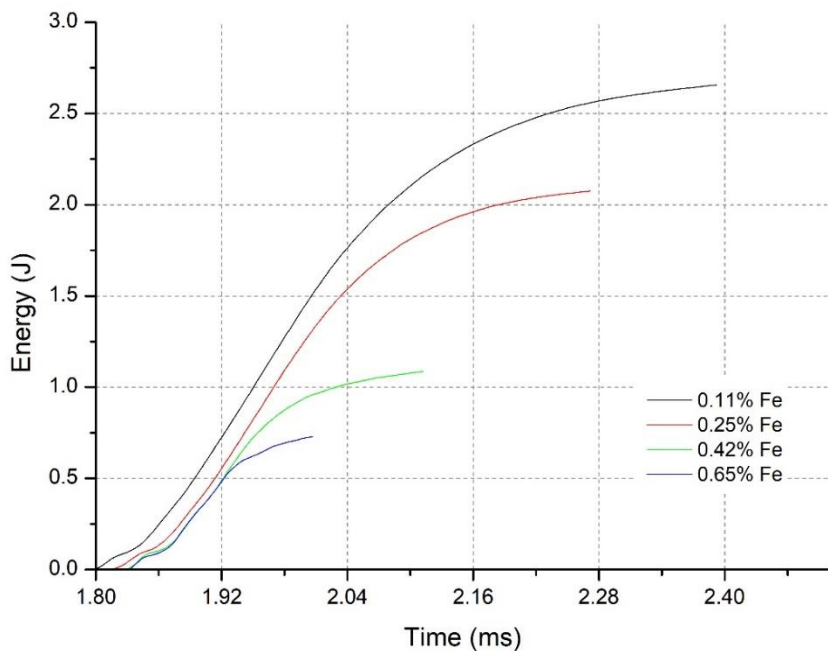


Figure 3.1.5.2 Average energy values at impact

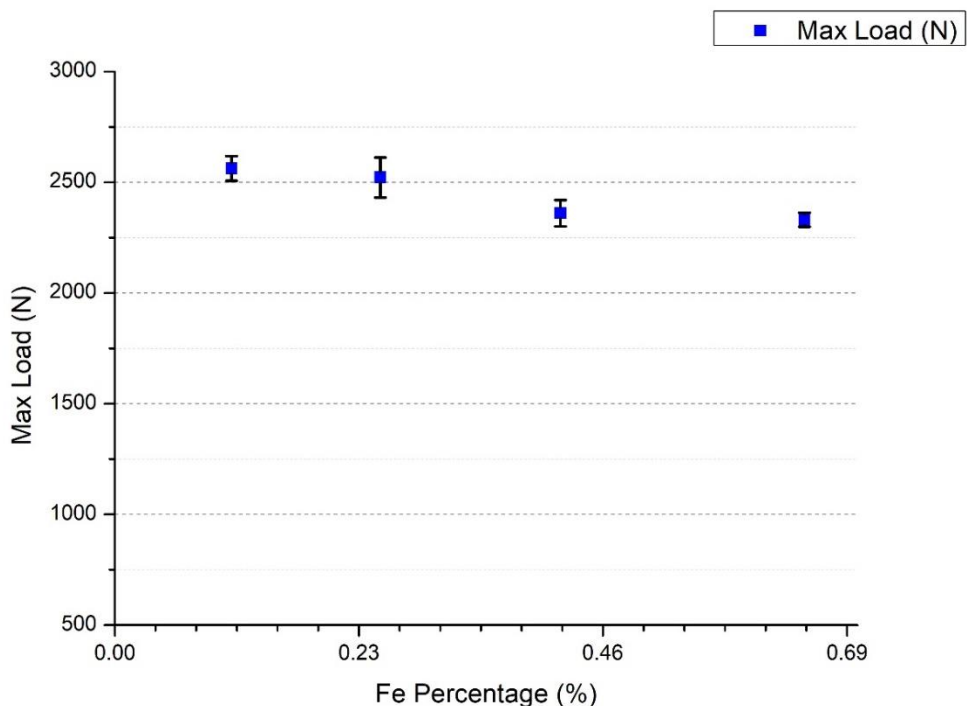


Figure 3.1.5.3 Maximum Load of the impact comparison graph

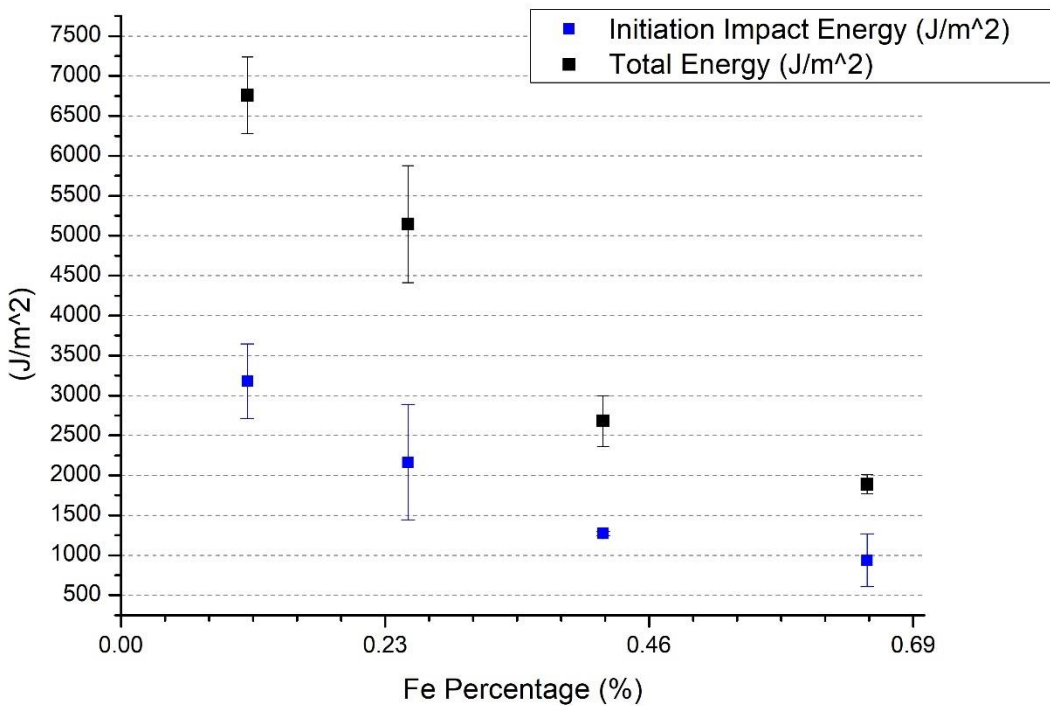


Figure 3.1.5.4 initiation impact energy and total energy comparison graph

3.2 Tensile Test

3.2.1 Tensile tests for 0.11 Fe content

Aluminum specimen with 0.11 Fe content at room temperature is placed into the Zwick Z100 testing machine.

The data from the machine has been processed using the OriginLab8.5.

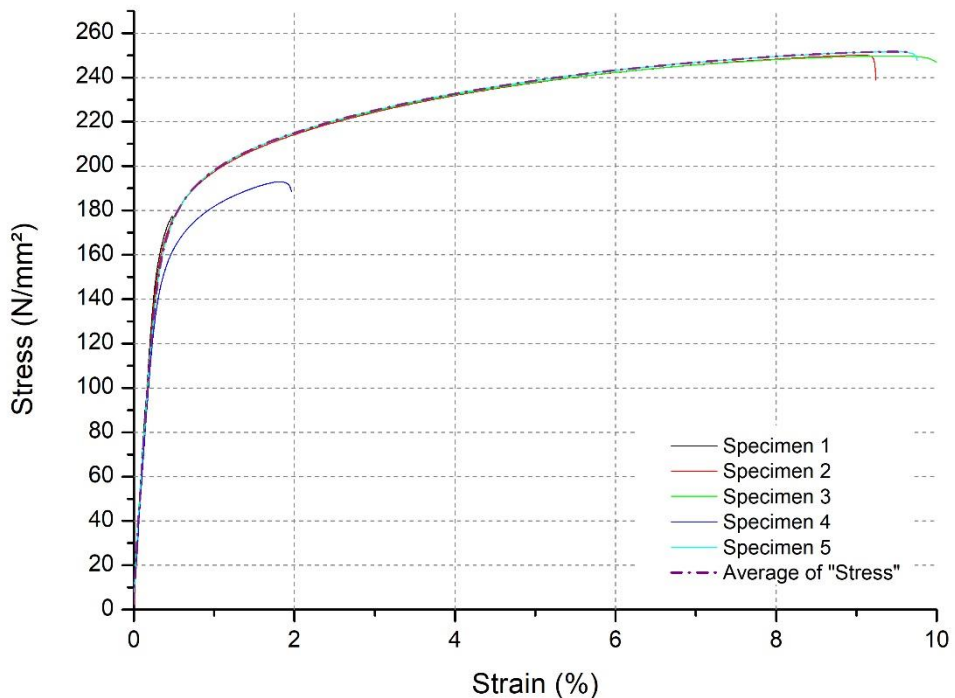


Figure 3.2.1.1 Tensile test results of sample 1

Table 3.2.1.1 Tensile test results of 0.11 Fe level sample

	d ₀	L ₀	R _{p0.2}	R _m	A ₂₅
n = 5	mm	mm	N/mm ²	N/mm ²	%
x	4.998	25	174.041479	224.3318671	5.972852581
s	0.004472136	0	6.397125645	36.17283907	4.551919493
n [%]	0.089478511	0	3.675632776	16.12469933	76.21014299

From the results from table 3.2.1.1, we can see that the average Yield Strength (YS) is 174.041479 N/mm², the average Ultimate Tensile Stress (UTS) is 224.3318671 N/mm², and the average elongation is 5.972852581%.

3.2.2 Tensile tests for 0.25 Fe content

Aluminum specimen with 0.25 Fe content at room temperature is placed into the Zwick Z100 testing machine.

The data from machine has been processed using the OriginLab8.5.

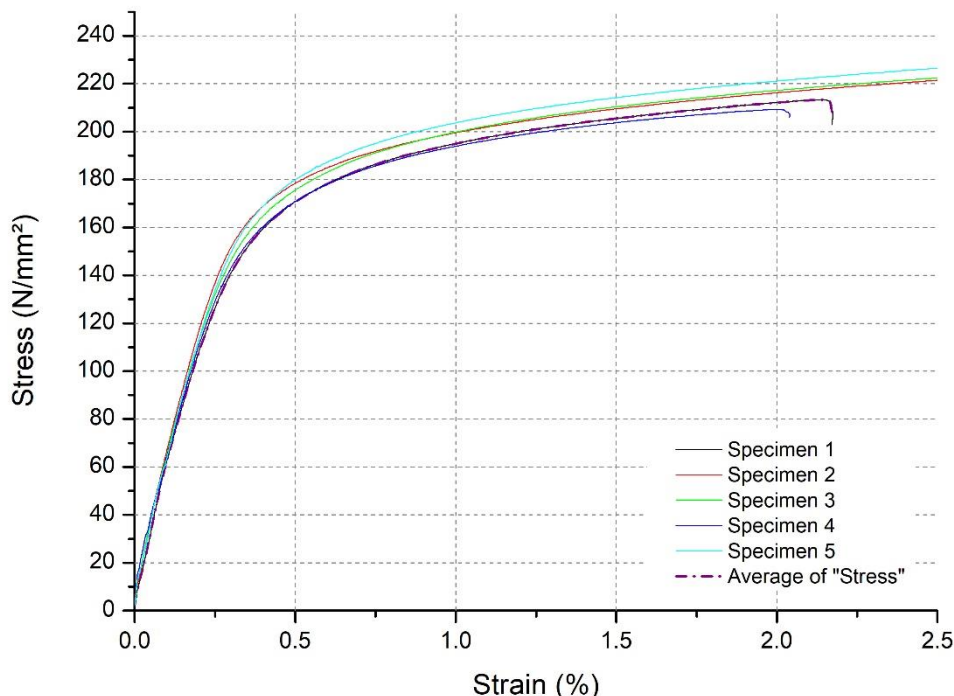


Figure 3.2.2.1 Tensile test results of sample 2

Table 3.2.2.1 Tensile test results of 0.25 Fe level sample

	d ₀	L ₀	R _{p0.2}	R _m	A ₂₅
n = 5	mm	mm	N/mm ²	N/mm ²	%
x	4.998	25	176.0799	225.0739	3.109254
s	0.004472136	0	4.208439	14.48672	1.502748
n [%]	0.089478511	0	2.390073	6.436426	48.33146

From the results from table 3.2.2.1, we can see that the average Yield Strength (YS) is 176.0799 N/mm², the average Ultimate Tensile Stress (UTS) is 225.0739 N/mm², and the average elongation is 3.109254%.

3.2.3 Tensile tests for 0.42 Fe content

Aluminum specimen with 0.42 Fe content at room temperature is placed into the Zwick Z100 testing machine.

The data from machine has been processed using the OriginLab8.5.

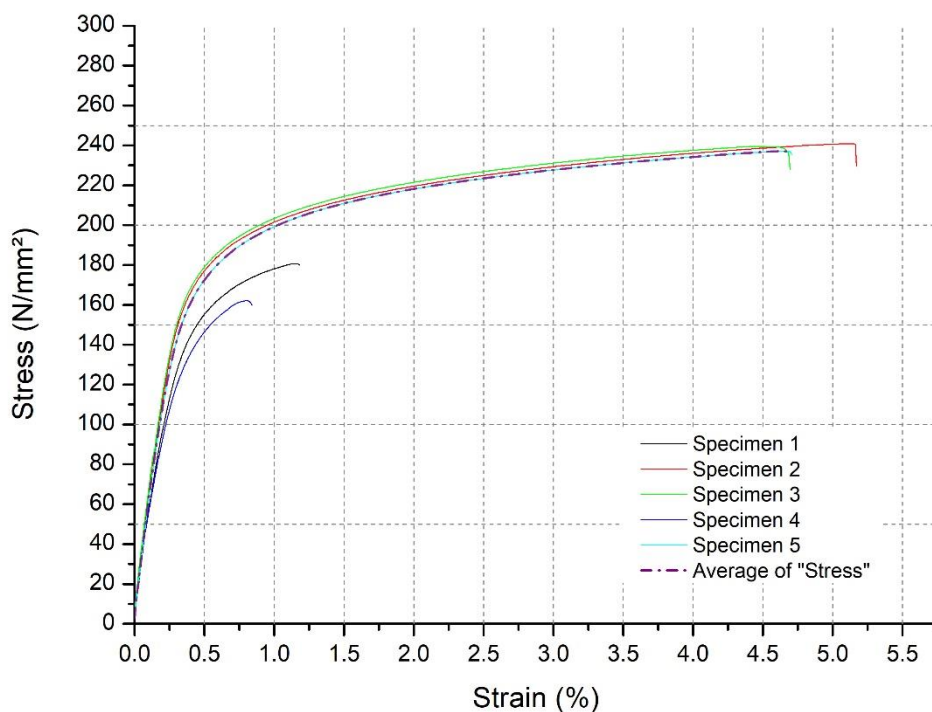


Figure 3.2.3.1 Tensile test results of sample 3

Table 3.2.3.1 Tensile test results of 0.42 Fe level sample

	d ₀	L ₀	R _{p0.2}	R _m	A ₂₅
n = 5	mm	mm	N/mm ²	N/mm ²	%
x	4.99	25	167.7767	212.0526	2.923206
s	0	0	13.45484	37.721	2.097381
n [%]	0	0	8.019492	17.78851	71.74933

From the results from table 3.2.3.1, we can see that the average Yield Strength (YS) is 167.7767 N/mm², the average Ultimate Tensile Stress (UTS) is 212.0526 N/mm², and the average elongation is 2.923206%.

3.2.4 Tensile tests for 0.65 Fe content

Aluminum specimen with 0.65 Fe content at room temperature is placed into the Zwick Z100 testing machine.

The data from machine has been processed using the OriginLab8.5.

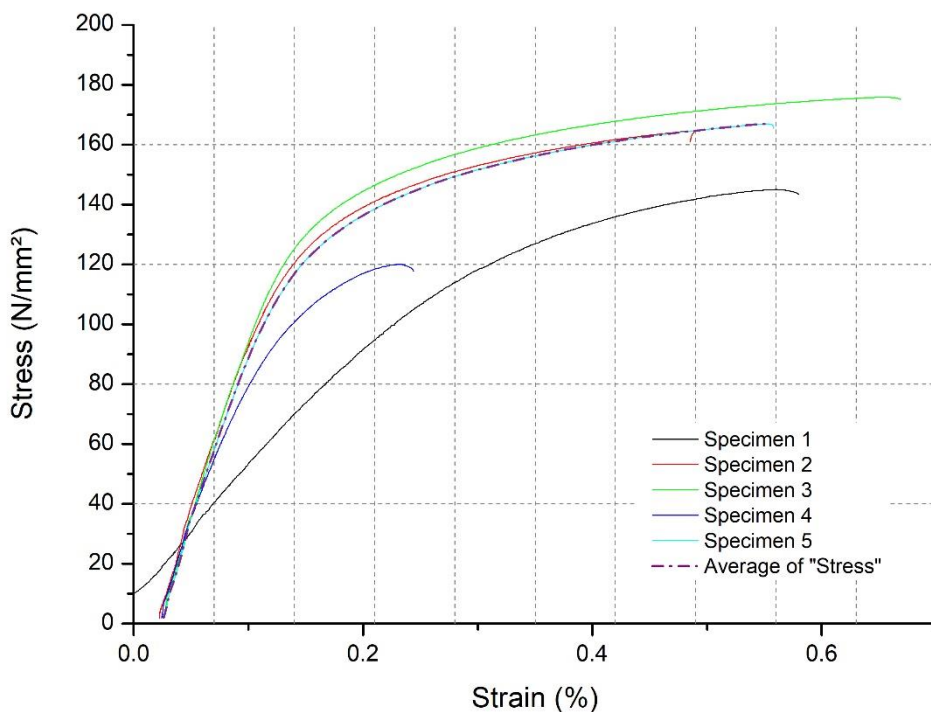


Figure 3.2.4.1 Tensile test results of sample 4

Table 3.2.4.1 Tensile test results of 0.65 Fe level sample

	d ₀	L ₀	R _{p0.2}	R _m	A ₂₅
n = 5	mm	mm	N/mm ²	N/mm ²	%
x	4.998	25	164.5899	185.8375	0.815708
s	0.004472	0	17.72004	35.40782	0.520859
n [%]	0.089479	0	10.76618	19.05311	63.8536

From the results from table 3.2.4.1, we can see that the average Yield Strength (YS) is 164.5899 N/mm², the average Ultimate Tensile Stress (UTS) is 185.8375 N/mm², and the average elongation is 0.815708%.

3.3 Comparison of the Different Fe contained samples

3.3.1 Yield Strength (YS)

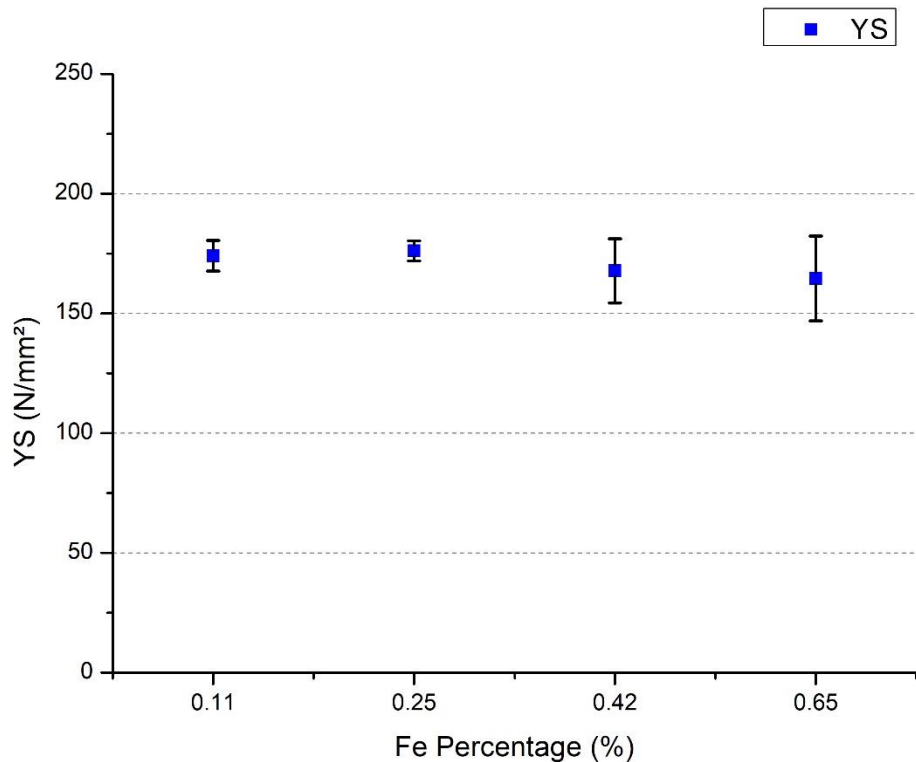


Figure 3.3.1.1 YS comparison table

As it can be seen from the figure 3.3.1.1, there is a slight increase in the YS values between sample 1 and sample 2. Starting from the 2nd sample, the YS values show a decreasing behavior.

3.3.2 Ultimate Yield Strength (UTS)

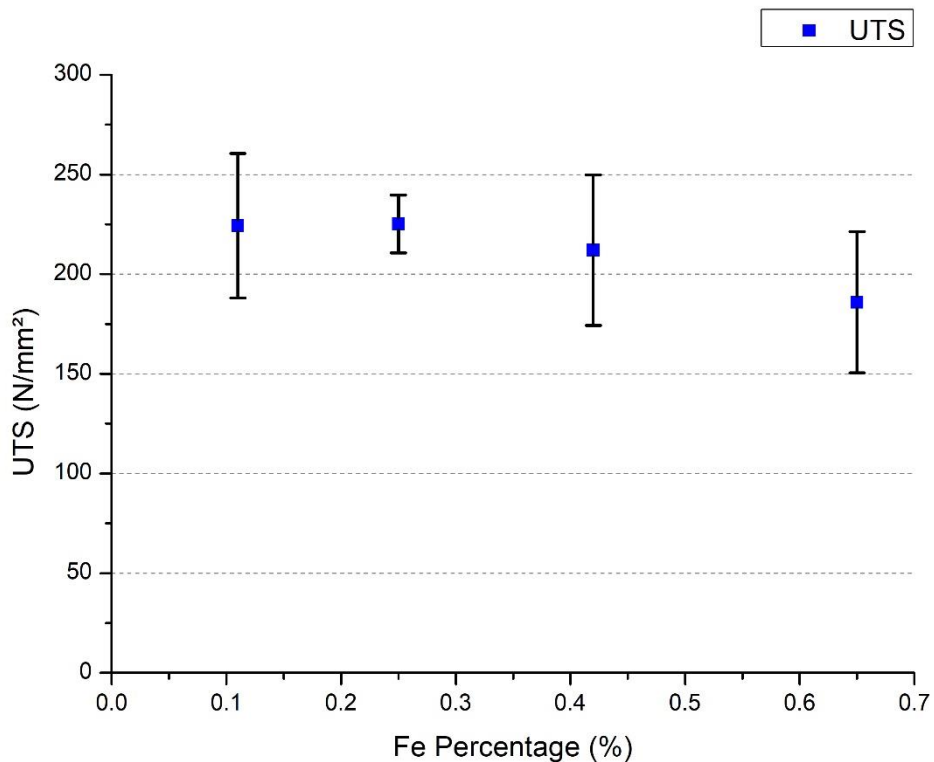


Figure 3.3.2.1 UTS comparison graph

As it can be seen in the figure 3.3.2.1, UTS value also shows a slight increase between sample 1 and sample 2. Then decreasing behavior can be seen from starting 2nd sample. At the samples 3 and 4 there is more deviation in the batch results.

3.3.3 Elongation

It can be observed in figure 3.3.3.1, as the Fe content in the aluminum, alloy's elongation value decreases.

As a result of our tensile tests, we can say the YS and UTS as well as the elongation values decrease as the Fe content increases. From this we can say as the mechanical strength of the aluminum alloy increases as the Fe content of it decreases.

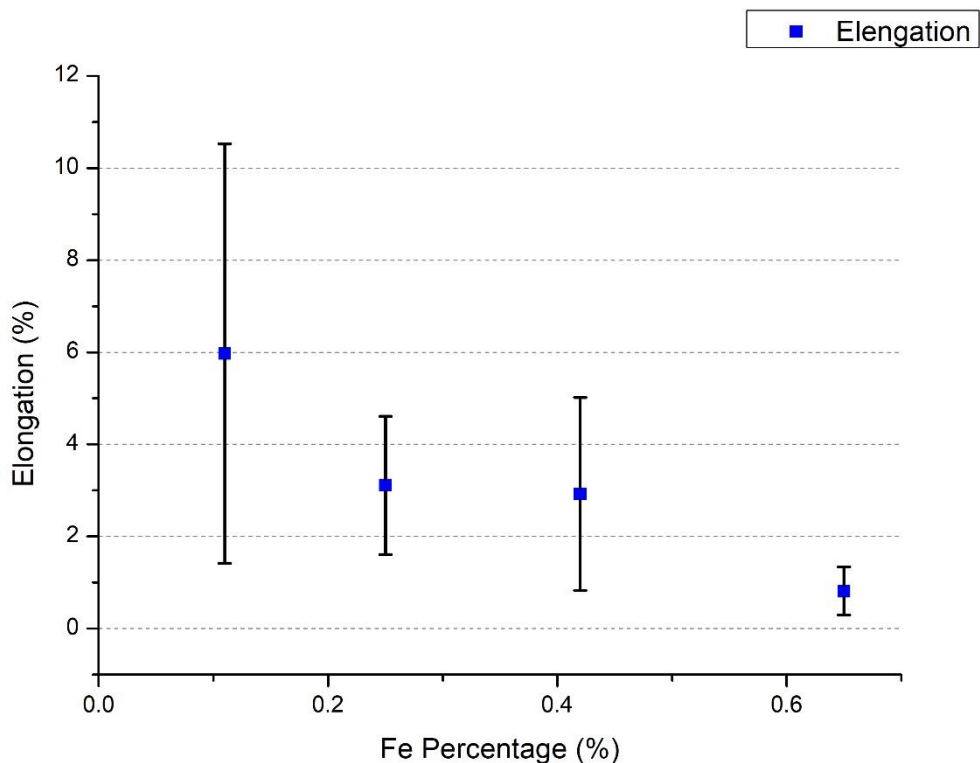


Figure 3.3.3.1 elongation comparison graph

4 MACROSCOPIC and MICROSCOPIC EXAMINATION

4.1 Microscopic Examination of Sample

Some treatments are applied to the material before it is examined using a microscope. These processes are required so that we may have a better view of the material and conduct a thorough microstructure study. These phases include molding, grinding, polishing, and etching.

Following these treatments, a better microstructure is expected. The scratches and look of the sample are verified with the naked eye when these steps are done, and the sample is dried and prepared for examination with a microscope.

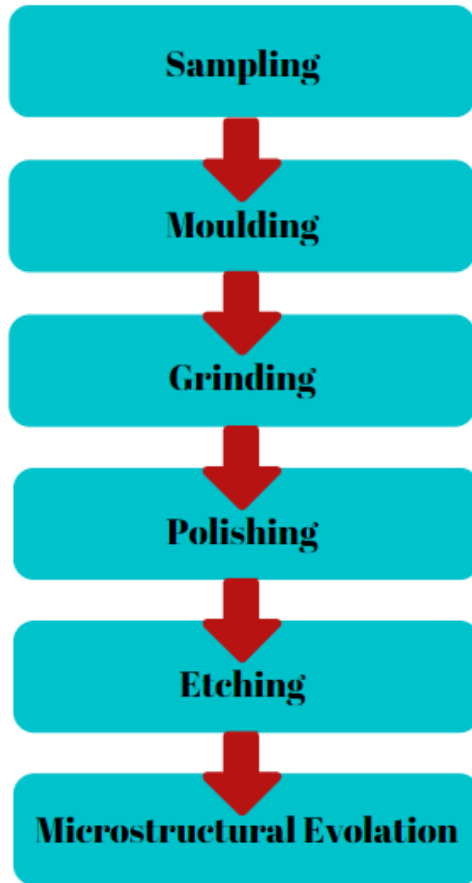


Figure 3.3.3.1 steps

Sections of the sample should be obtained in order to apply these methods. Longitudinal and transverse sections are collected, and some of the sample's important attributes are determined based on these two sections.

4.1.1 Sample Selection in Metallography

If it is desired to examine the subjects listed below, a cross section should be taken.

- Depth of carburization and internal structure of this region
- Depth of corrosion and internal structure of this region
- Decarbonisation depth and internal structure of this region
- Coating thickness and internal structure of this region
- Depth of surface defects,
- The distribution of the residues in the cross-sectional area,
- Internal structure changes from surface to center,

In longitudinal sections, the following topics are generally examined:

- Changes in the internal structure of the heat treatment,
- Grain shape changes resulting from plastic deformation,
- Changes in residues as a result of plastic deformation,
- Whether a texture is formed in the internal structure.

You can see below, our two sections on the sample in Figure 4.1.1.1.

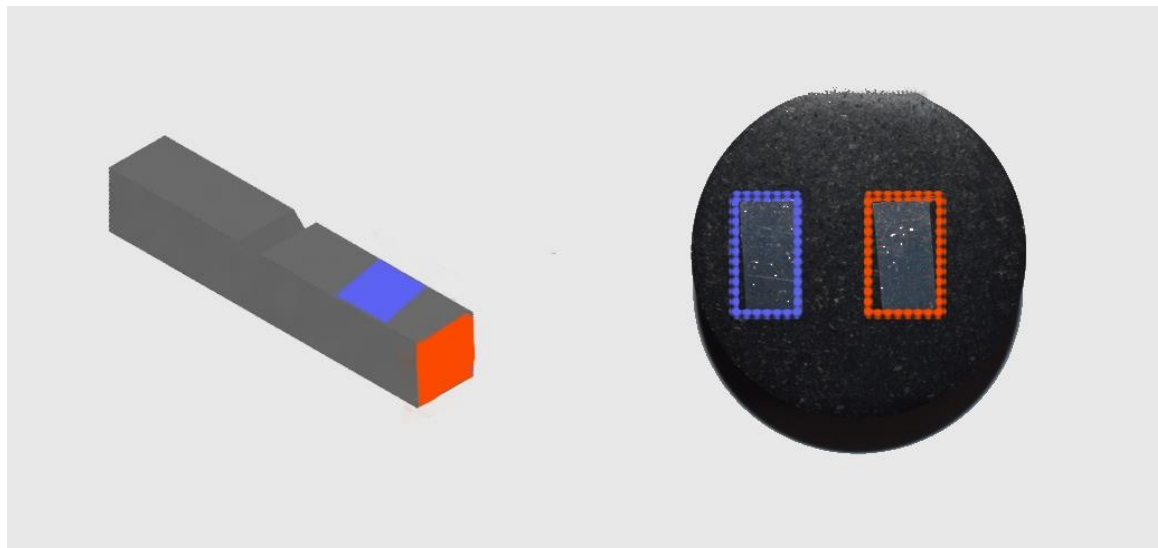


Figure 4.1.1.1 microstructure examination sample with directions

4.1.2 Sample Preparation

The goal of metallographic sample preparation, whether it's metal, ceramic, sintered carbide, or another solid substance, is to show the actual structure of the sample. The most straightforward way to accomplish this is to use a systematic approach. Because it will be desirable to analyze the same material in the same condition all of the time, sample preparation outcomes should be repeatable. For the most part, sample preparation adheres to the tight guidelines necessary for most materials. Different materials with similar qualities (hardness and ductility) react similarly and require the same sample preparation consumables.

Once a sample preparation process has been created and fine-tuned, it should yield consistent results for the same material every time it is used. This necessitates consumables of high quality and consistency. Controlling sample preparation parameters is another crucial factor.

Parameters:

- Speed and direction of rotation
- The load applied to the sample
- Type and amount of abrasive and lubricant
- Sample Preparation Time

These elements have a direct and considerable impact on the result of the Sample Preparation procedure. With automated equipment, many variables may be controlled and altered. The right structure is only required in a few rare circumstances. Light scratches and modest edge rounding are unimportant for most checks. In this scenario, we need to attain acceptable results. The final surface must only be as excellent as is required for analysis. Apart from this, any additional preparation step will only increase the cost of sample preparation.

Our goal is to look at a sample surface that, in principle, will show us the entire image of the structure we'll be looking at. We anticipate the following outcomes as a result of meticulous preparation:

- Deformation-free surface
- Scratch-free surface
- Surface without rupture gaps
- The Surface that does not contain foreign elements
- Contamination-free surface
- Surface without ridges or rounding of edges
- Surface without heat damage

When using the mechanical preparation approach, however, achieving the requirements mentioned above is nearly difficult. There will always be minor damage that an optical microscope cannot detect. The inspection results are unaffected by this minor damage.

This is described as a nearly perfect surface with just minor damage and the correct microstructure in general. The right structure is only required in a few rare circumstances. Light scratches and modest edge rounding are unimportant for most checks. This is defined as an almost perfect surface with only minimal damage and generally the correct microstructure.

4.1.2.1 Sampling

Our tensile and Charpy-tested samples will be examined under a microscope to determine their brittleness following these treatments.

4.1.2.1.1 Cutting

Cutting should result in the least heating and deformation of the specimen, as well as the least amount of material loss, particularly in small areas. During cutting procedures, the sample should always be chilled using a specified liquid. This fluid shields the sample from corrosion, reduces material-to-cutting-tool friction, and, most significantly, keeps the sample from overheating.

Cut-off wheels are utilized in different ways depending on the material- the cutting disc also varies depending on the sample to be cut's composition. The hardness and ductility of the material influence the cutting disc selection. Bakelite binder contains aluminum oxide (Al_2O_3), which is extensively utilized in abrasive, iron-based products. For tougher iron-based materials, CBN (cubic baron nitride) is becoming increasingly common.

Diamond cut-off wheels are classified as metal bonded cut-off wheels or Bakelite bonded cut-off wheels based on the type of binder they include. Both of these tools are used to cut materials that are exceptionally difficult to cut. CBN cut-off wheels are built completely of Bakelite and are designed to cut exceptionally hard ferrous materials like white cast iron. These discs' cutting properties vary based on the binder properties.

While editing our sample, we used the Struers Discotom-5 gadget. A cutter for abrasive discs. We estimate that cutting each sample takes about 2 minutes on average.



Figure 4.1.2.1 Struers Discotom-5 Abrasive Cutter

Binders are categorized based on their "hardness," or ability to hold or remove abrasive from the disc. "Hard" cut-off wheels hold abrasive grains in place better than "soft" discs. Hard, brittle materials are cut with "soft" cut-off wheels, which provide new, sharp abrasive grains when the soft binder breaks down. Cutting soft and ductile materials should be done with hard bond cutting discs.

4.1.2.2 Moulding

In practice, molding is referred to as "mounting." Hot molding, also known as mounting, and cold molding are both part of the molding process [15]. Molding is crucial because it facilitates the preparation process, provides a completely flat surface for microscopic observation, and protects the hand from chemicals to some extent.

If the size and geometry are appropriate, some specimens can be made without molding and inspected under a microscope.

We added the chopped samples and two scales of molding powder while we were molding. It took 12 minutes for each sample to be molded using the Struers ProntiPress-10 equipment. The Struers Prontopress 10 is a high-tech assembly press with a multi-program memory and programmed cycle options for optimizing metallurgical assembly process parameters. [15]



Figure 4.1.2.2 Struers Prontopress 10 molding device

4.1.2.3 Grinding

Grinding is the removal of metal using abrasives joined together to form a revolving wheel. When moving abrasive particles make contact with the work piece, they operate as tiny cutting tools, each removing a little chip. Because of the low hardness of aluminum, it is well known that the sanding and cutting processes both take a short time. However, when we examine our samples with four different iron ratios, we see that the fourth sample was sanded longer than the others, despite the fact that the iron ratio is gradually increasing.

Since its iron concentration is larger than that of the other samples, and an increase in the iron ratio enhances the material's hardness.

As a result, the material becomes more resistant, and the time lengthens. 220, 600, 800, and 1000 grit sandpapers were employed in this process, which was carried out with the Struers LaboPro-21 apparatus.



Figure 4.1.2.3 Struers LaboPro-21 grinding device

4.1.2.4 Polishing

First and foremost, before continuing from the sanding to the polishing procedure, it is critical to thoroughly clean the samples. To ensure that no particles remain in the sample, it should be thoroughly cleaned with plenty of water.

Mechanically, automatically, electrolytically, or chemically, it can be done. The mechanical polishing procedure was used in this investigation. Lint-free materials, such as canvas, are dressed on a spinning disc for rough polishing that revolves at a speed of 150-600 rpm.

Fabrics like hairy, broadcloth, velvet, and others are treated for fine polishing. The abrasive size used in rough polishing is 15-1 m. It is 0.5-0.05 m in fine polishing.

Polishing is done with abrasives such as Al₂O₃, Cr₂O₃, MgO, and diamond powder poured on cloth-covered discs. Only diamond dust is utilized in paste form among these abrasives. Others are generally sprayed or poured in suspension. Polishing suspension should be sprinkled intermittently, but not excessively, while polishing. In this project Al₂O₃ was used. Struers LaboPol-6 is the name of our device, and velvet is preferred as a fabric.

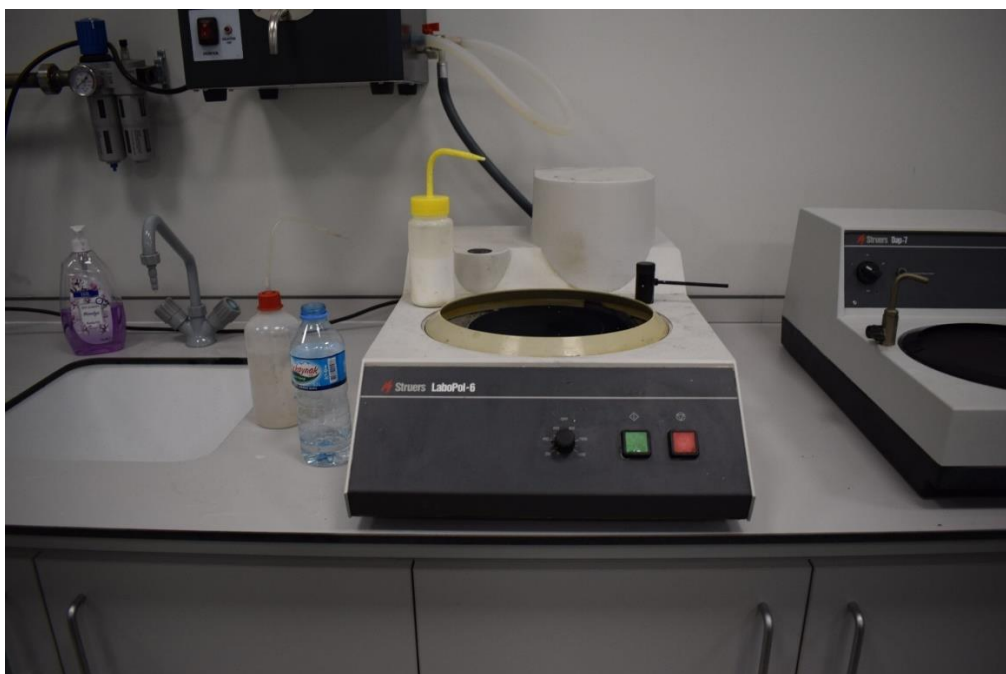


Figure 4.1.2.4 Struers LaboPol-6 polishing device

The sample should be rotated a quarter turn against the direction of rotation on the disc from time to time. It is checked visually and under a 100X magnification optical microscope to see if the polishing is satisfactory. When observed with the naked eye, it should have a mirror shine, and when studied via a microscope, no scratches should be visible. After polishing, the sample should be rinsed and dried with a drying equipment. The sample will be scratched if you use napkins or similar materials to dry it, so air drying is preferable, and then you can study it with a microscope.

4.1.2.5 Etching

While examining our sample, we didn't need to do any etching. Normally, prepared, finished samples are immersed in an acid bath called as abrasion or rinsed with acid to disclose bare metal by creating a line visible on our finished samples. [15]

The acid and the metal undergo a redox reaction. The waxed drawing is left to a depth on the plate, producing the desired smoothness and preparing the image, depending on time and acid strength. However, we were able to take great photographs under the microscope without having to dip it in acid.

5 RESULTS and DISCUSSION

5.1.1 Optical Microscope Results

You can see porous and non-porous shots of our samples when you look at the pictures. Porosity reduces as the iron concentration rises. This demonstrates that the quality of the casting is not consistent.

As a result, gas started to fill the sample structure. We may conclude, based on this tiny sample, that casting is most likely to result in a drop in casting quality.

The horizontal and vertical photographs of our Charpy samples collected during microscopic analysis are shown below. Photos were captured at various magnifications in our microscope while taking images.

The places with and without the porosities that catch our attention have been shot by zooming in even more in our overall photos. The following are the dimensions of the photographs that were taken.

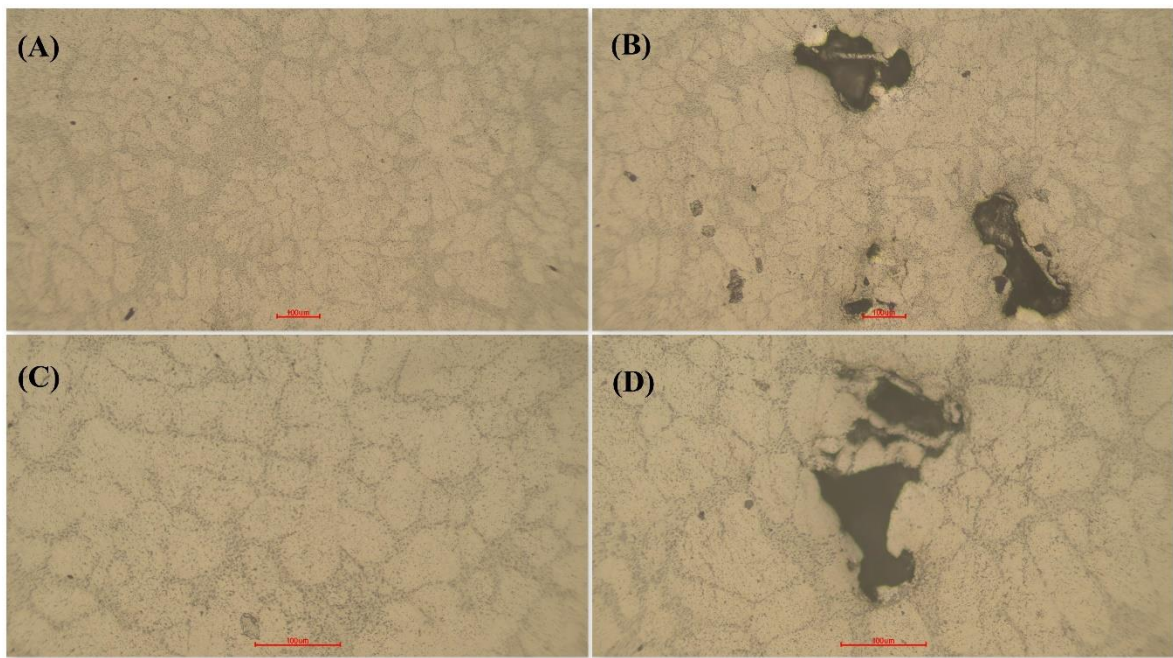


Figure 5.1.1.1 0.11 Fe level microstructure microscope results (a)x10, (b)x10 with porosity, (c)x20 (d)x20 with porosity; magnification at horizontal surface

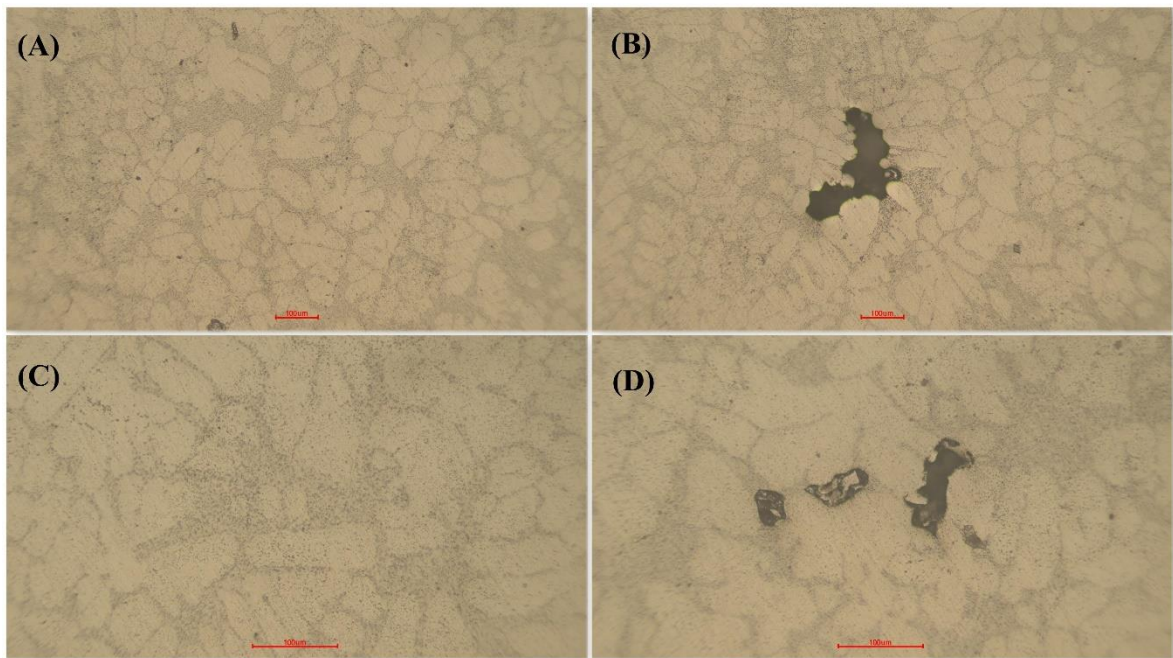


Figure 5.1.1.2 0.11 Fe level microstructure microscope results (a)x10, (b)x10 with porosity, (c)x20 (d)x20 with porosity; magnification at vertical surface

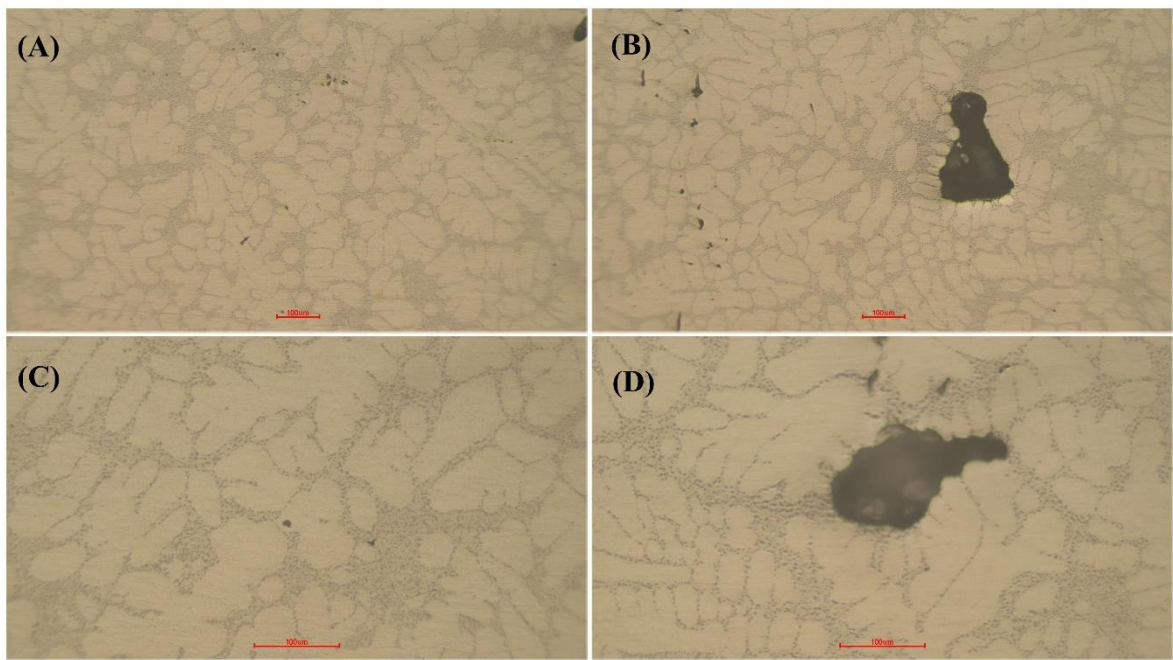


Figure 5.1.1.3 0.25 Fe level microstructure microscope results (a)x10, (b)x10 with porosity, (c)x20 (d)x20 with porosity; magnification at horizontal surface

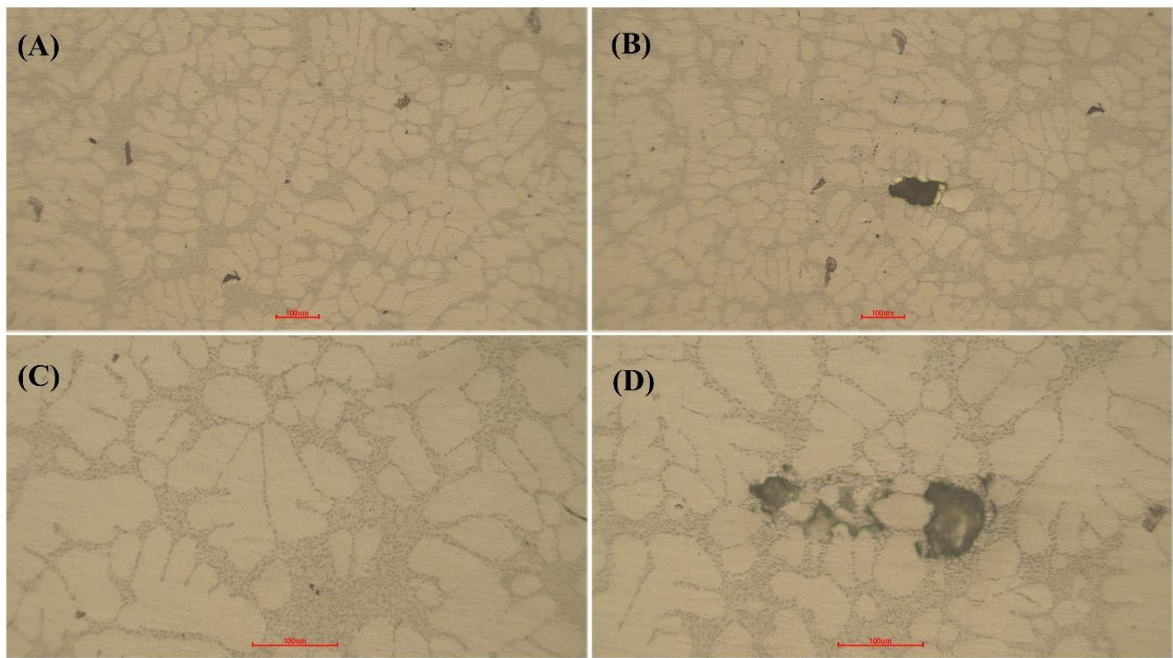


Figure 5.1.1.4 0.25 Fe level microstructure microscope results (a)x10, (b)x10 with porosity, (c)x20 (d)x20 with porosity; magnification at vertical surface

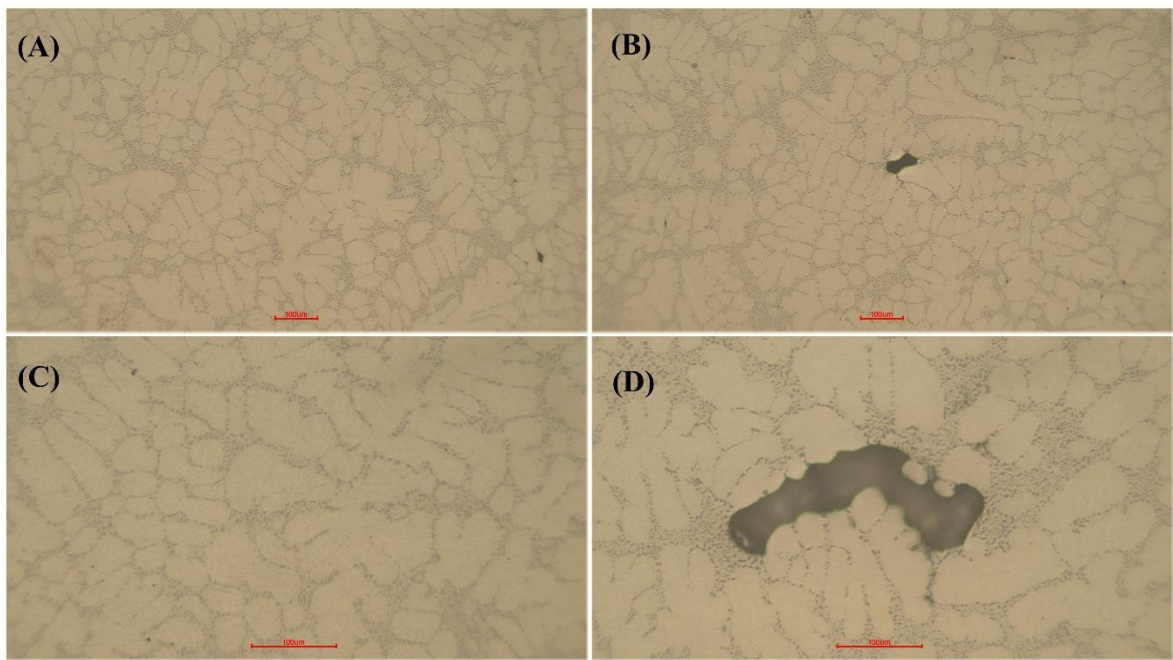


Figure 5.1.1.5 0.42 Fe level microstructure microscope results (a)x10, (b)x10 with porosity, (c)x20 (d)x20 with porosity; magnification at horizontal surface

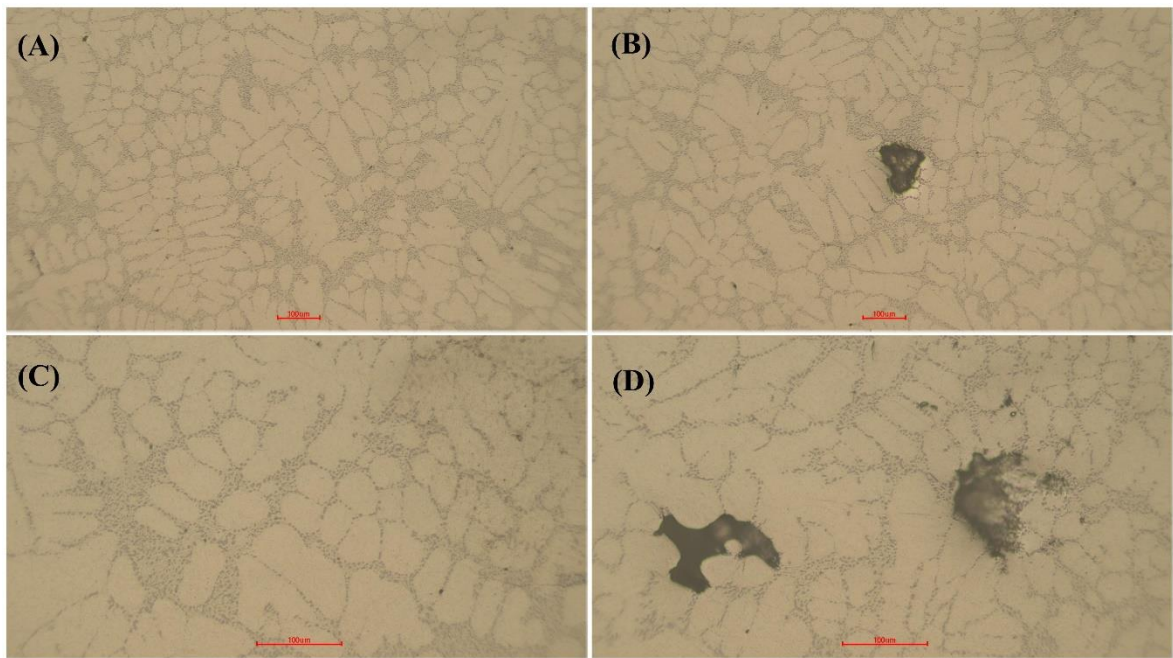


Figure 5.1.1.6 0.42 Fe level microstructure microscope results (a)x10, (b)x10 with porosity, (c)x20 (d)x20 with porosity; magnification at vertical surface

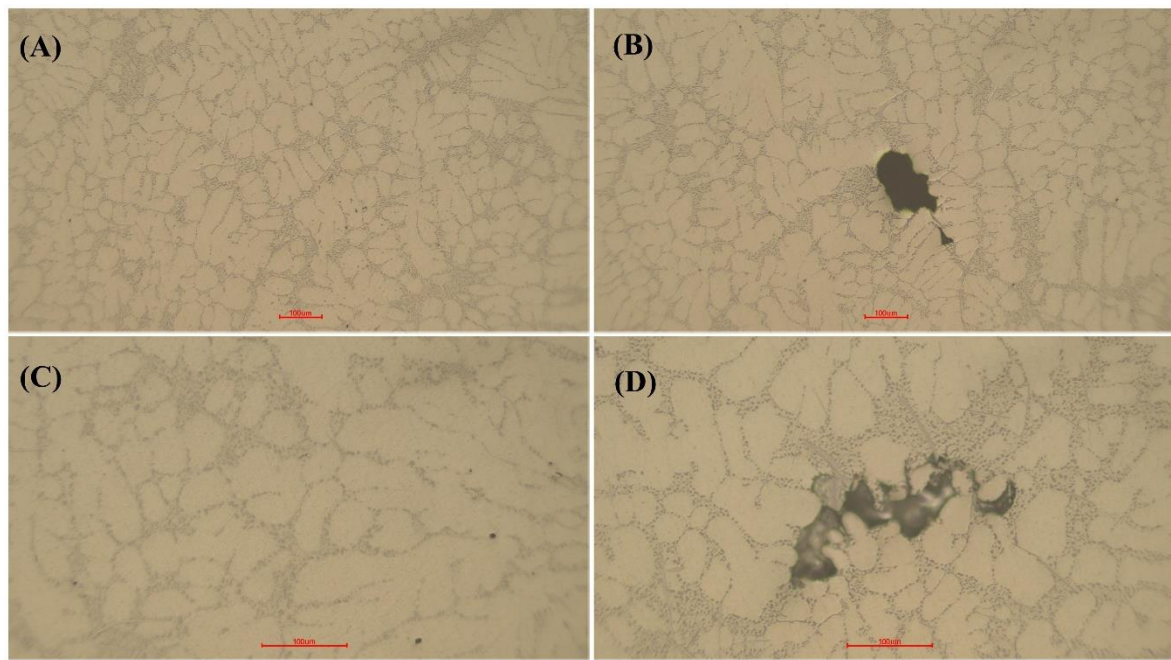


Figure 5.1.1.7 0.65 Fe level microstructure microscope results (a)x10, (b)x10 with porosity, (c)x20 (d)x20 with porosity; magnification at horizontal surface

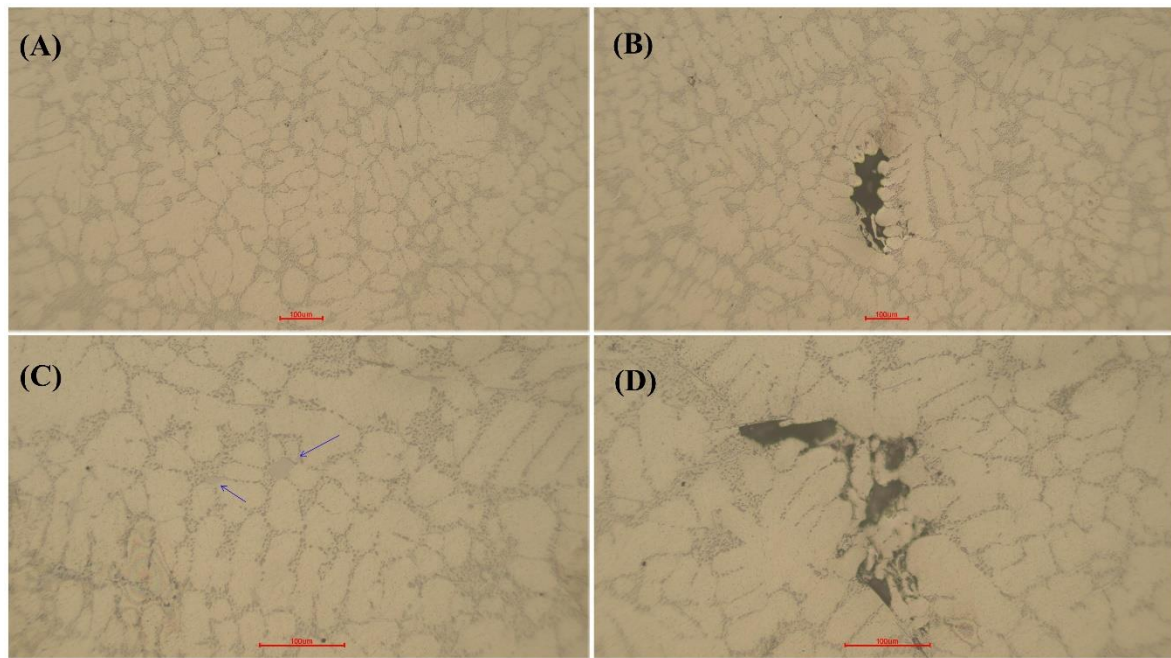


Figure 5.1.1.8 0.65 Fe level microstructure microscope results (a)x10, (b)x10 with porosity, (c)x20 (d)x20 with porosity; magnification at vertical surface

From the results we have observed the ductility of the aluminum alloy decreases as the Fe content increases. When more Fe added into the alloy results that the brittleness of the alloy to increase.

5.2 Optical Examination of Fracture Surface

The environment in which metallic materials are employed in various products causes them to break. Only after carefully inspecting the material and evaluating the shattered surface can the reason for breakage be determined. We'll look at the samples that passed the Charpy and tensile tests and comment on how brittle they are.

In the automotive and aerospace industries, new high-performance materials are continually being studied. Because of the requirement to minimize product size and weight while boosting rigidity and performance, research has become vital. Solid material selection and safety design based on strength calculations are necessary for fields such as autos, airplanes, ships, railcars, and human-crewed spaceships, as the fracture of metallic materials can put human life in danger [16].

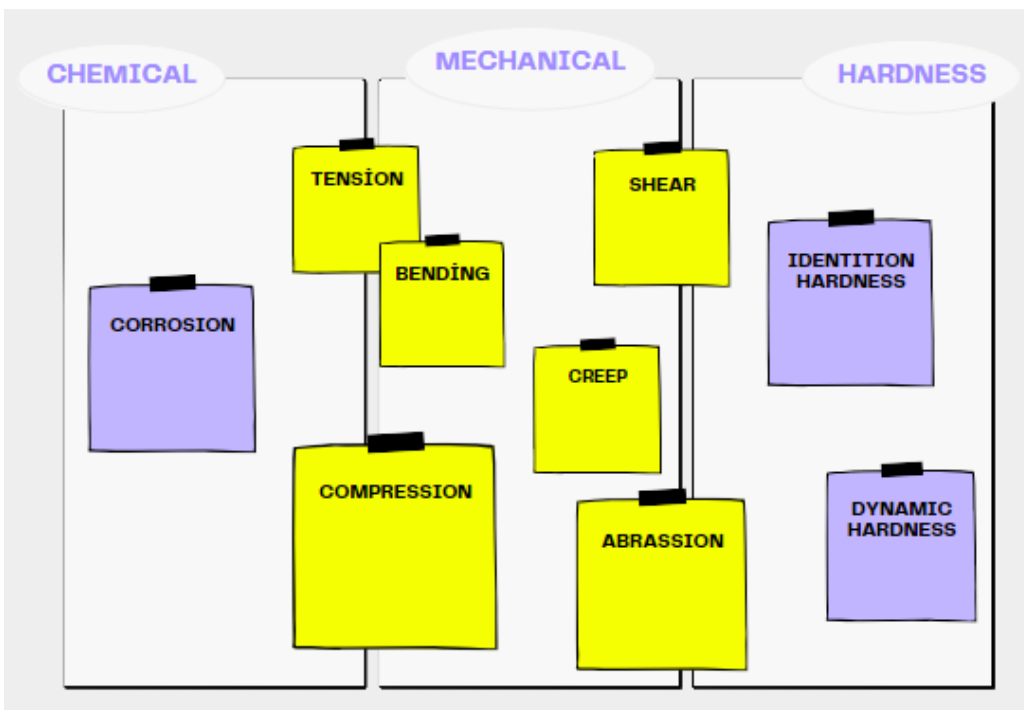


Figure 5.1.1.1 classification of mechanical test

Various material tests addressing the stress of metallic materials are performed while selecting these materials. Fracture causes and material attributes are investigated using material testing and fractography in order to select or improve materials. You can see above some tests in Figure 5.1.1.1.

Macroscopic observation is a type of analysis that uses the naked eye, low-magnification magnifiers, and stereoscopic microscopes, among other tools. This observation is simple to make at the site of a fracture and is dependent on the type of fracture, the presence of beach marks, and other factors. However, macroscopic observation alone cannot investigate how a fracture happens in depth.



Figure 5.1.1.2 Charpy fracture surface visual comparison between samples with different Fe level

The figure 5.2.1.2, above depicts the breakage of our four samples after the charpy test. The amount of overflow caused by a flat cut surface as a result of the impact may be seen in this photo. When viewed with the naked eye, the four samples give a rough notion of their fragility.

The quantity of overflow reduces as the iron level in the sample increases, resulting in a flatter surface. This indicates that the iron ratio causes the sample to become more brittle. In the shot, we can see this more clearly. To prove this and conduct a thorough investigation, inspections were conducted using an optical microscope and a scanning electron microscope, and photographs were obtained and put to the results section.

5.2.1 Sampling

Our tensile and Charpy-tested samples will be examined under a microscope to determine their brittleness following these treatments.

5.2.2 Optical Results

Our samples were examined under a microscope to see how fragile they were. It is an alloy that reacts to ductile due to its aluminum structure. The photos below show the findings of this investigation on the different reactions of the iron ratio in the structure of this alloy.

Below you can see the individual images of the samples subjected to Charpy and tensile tests.

5.2.2.1 Charpy Fracture Surface Results



**Figure 5.2.2.1 0.11 Fe level Charpy test fracture surface optical microscope results
(a)x10, (b)x80, (c)x10; magnification of fracture surface**



Figure 5.2.2.2 0.25 Fe level Charpy test fracture surface optical microscope results
(a)x10, (b)x50, (c)x10; magnification of fracture surface



Figure 5.2.2.3 0.42 Fe level Charpy test fracture surface optical microscope results
(a)x10, (b)x30, (c)x10; magnification of fracture surface



Figure 5.2.2.4 0.65 Fe level Charpy test fracture surface optical microscope results
(a)x10, (b)x50, (c)x10; magnification of fracture surface

When the samples' brittleness is analyzed, it is clear that the first sample reacts to the ductile substance, whereas the fourth sample reacts to the brittle. The wavy, indented, and projecting look of the first sample, the ductile structure, contrasts with the smoother appearance of the fourth sample. This signifies that the structure is highly vulnerable.

5.2.2.2 Tensile Fracture Surface Results



Figure 5.2.2.5 0.11 Fe level tensile test fracture surface optical microscope results
(a)x15, (b)x30, (c)x10; magnification of fracture surface



Figure 5.2.2.6 0.25 Fe level tensile test fracture surface optical microscope results
(a)x15, (b)x30, (c)x10; magnification of fracture surface



Figure 5.2.2.7 0.42 Fe level tensile test fracture surface optical microscope results
(a)x15, (b)x30, (c)x10; magnification of fracture surface



**Figure 5.2.2.8 0.65 Fe level tensile test fracture surface optical microscope results
(a)x15, (b)x30, (c)x10; magnification of fracture surface**

When we examined our samples, we discovered that samples with varied iron ratios broke in tensile and Charpy tests in different ways. The appearance of low-iron samples was more complicated and wavier. We were able to achieve a smoother surface by raising the iron ratio. Due to iron rise, we discovered that our samples were on the verge of becoming brittle.

Intermetallics were also found as a result of the increased iron content in the material's structure. In our samples with low iron content, intermetallics were less noticeable. It started off as little structures, but by the fourth sample, it had grown fairly large.

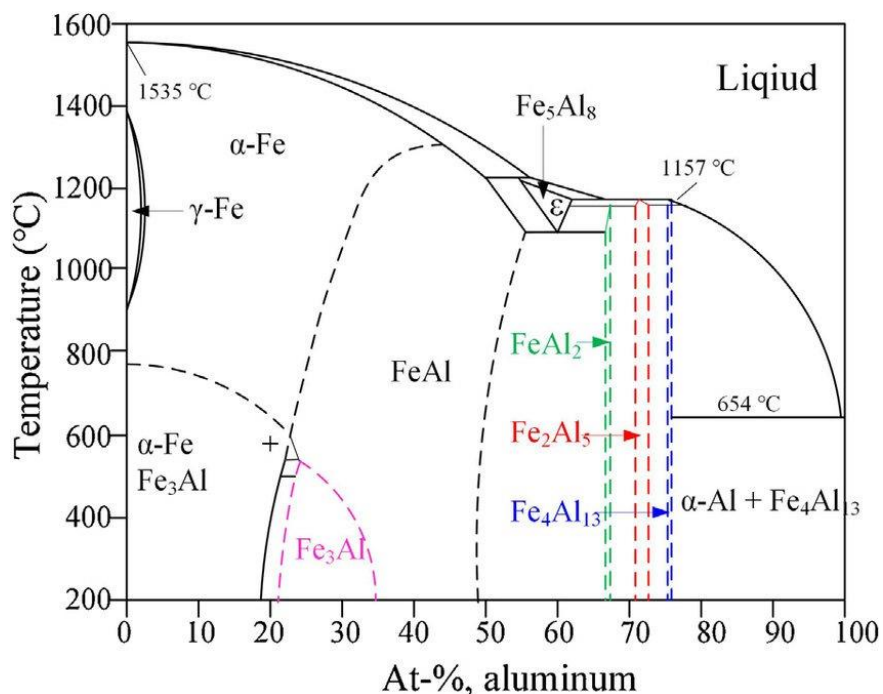


Figure 5.2.2.9 Iron Aluminum Phase Diagram

The phases are depicted in the diagram above. We tested our samples as a proportion of aluminum because Fe is the percentage of iron (0-20). They have an iron content of 0.11-0.65. As a result, we anticipate seeing Alpha-Fe iron and Fe₃Al intermetallic in this area of the phase diagram. In addition, as more Fe iron is added, we may face numerous intermetallic FeAl₂, FeAl₂, Fe₂Al₅, etc. forms. As a result, the larger the iron's ability to react, and thus the bigger the intermetallic formation, the more iron is added, that is, the higher the iron content in our samples.

5.3 SEM and EDX Examination of Fracture Surface

A scanning electron microscope (SEM) is a type of electron microscope that uses a focussed beam of electrons to scan the sample surface and produce images. Electrons interact with atoms in the sample to produce a variety of signals that carry information about the sample's topography and composition. After doing microscopic exams, we used this electron microscope to discuss the refraction results of our materials in order to acquire a more complete result. These tests were performed with a Zeiss EVO Ma10 device.



Figure 5.2.2.1 SEM - ZEISS Evo MA10

The engraved samples are put on the plate and affixed to the chamber under normal circumstances. We fixed and positioned our samples on the carousel because etching is not required in our samples and we can acquire a uniform microstructure this way. We proceeded to the vacuuming step after ensuring that our samples were well-settled. When the vacuuming was finished, the guns began to emit electrons from the device's hot bulbs, and we were ready to shoot our pictures.

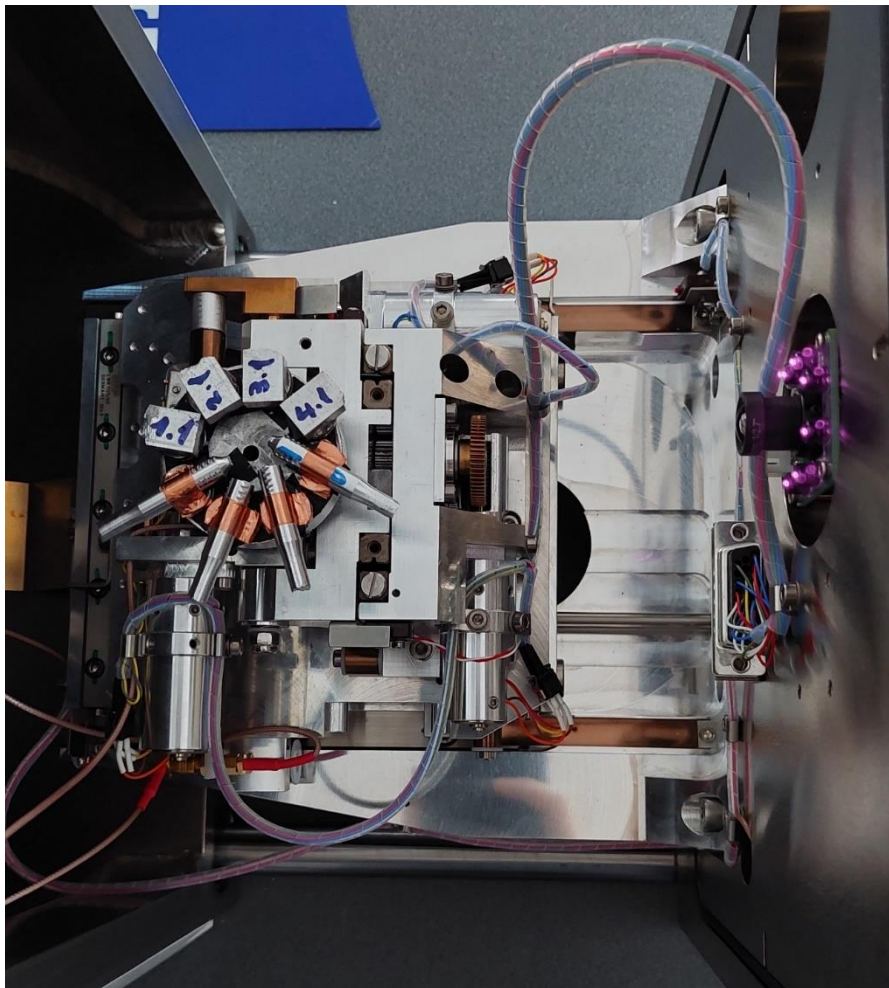


Figure 5.2.2.2 Placement of samples into SEM

The samples placed inside the gadget can be seen in the figure 5.2.2.2.

5.3.1 SEM and EDX Results

Iron has an atomic weight of 55 and aluminum has an atomic weight of 27. As a result, the impact energies differ. The number of electrons increases as the number of atoms increases. As a result, the impact energy is higher.

The greater the impact energy, the brighter the appearance. Iron will seem brighter white in this situation, while aluminum will appear darker. The outcomes can be seen in greater detail below.

The variance in these colors and contrasts informs us about the material's homogeneity. Photos shot in BSE mode will provide us with some insight. Comments on the structure of the samples were made using these contrast differences if the iron precipitated as iron or formed intermetallic and boosted the material's strength. Our technology has been subjected to X-Ray Mapping, allowing us to see intermetallic more clearly. The increase in the iron ratio is precisely proportionate to this circumstance.

Fractures were also seen and addressed in this context. We have two fundamental breaks, as is well recognized.

5.3.1.1 What is the Difference between Intergranular & Transgranular Fracture?

When a crack propagates along the grain boundaries of a material, intergranular fracture, intergranular cracking, or intergranular embrittlement occurs, usually when these grain borders are weakened. When a crack grows through the material grains, it is known as a transgranular fracture. The propagation of cracks along the grain boundaries of a metal or alloy is known as intergranular fracture. It's a fracture that follows the material's grains. Cracks spread quickly in this fracture, with little or no plastic deformation. [17]

A trans granular fracture is one that follows the grain pattern in the material's individual lattices. One sort of brittle fracture is this one. Transcrysalline fractures are another name for trans granular fractures. Intergranular fracture occurs when the crack follows the grain boundaries, whereas trans granular fracture occurs when the crack passes from one grain boundary to the next.

Our samples were subjected to tensile and impact testing and were subjected to SEM and EDX analyses. You can see below microstructural and fractural analysis of our samples.

5.3.1.2 Charpy Fracture Surface Results with SEM

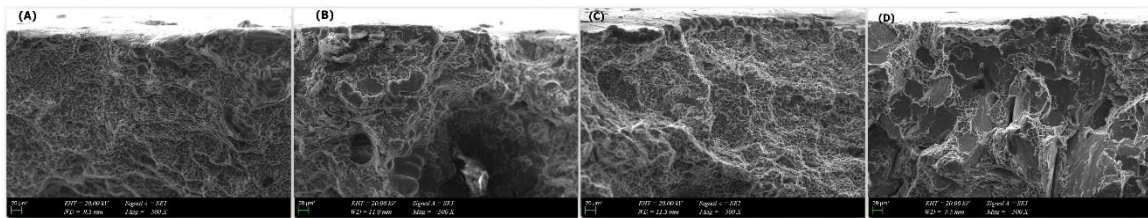


Figure 5.3.1.1 Charpy Impact Test SEM Micrographs at 500X magnification (A) 0.11 Fe, (B) 0.25 Fe, (C) 0.42 Fe, (D) 0.65 Fe.

The 500 magnification SEM pictures of the samples containing four distinct iron ratios may be seen in the figure 5.3.1.1.

We can see how much of the above-mentioned sample has overflowed to the surface throughout the breaking process. The surface gets increasingly flat, as may be seen with the naked eye. Below are photographs of our samples at various magnifications so that you may inspect them structurally and get a better concept of what they look like.

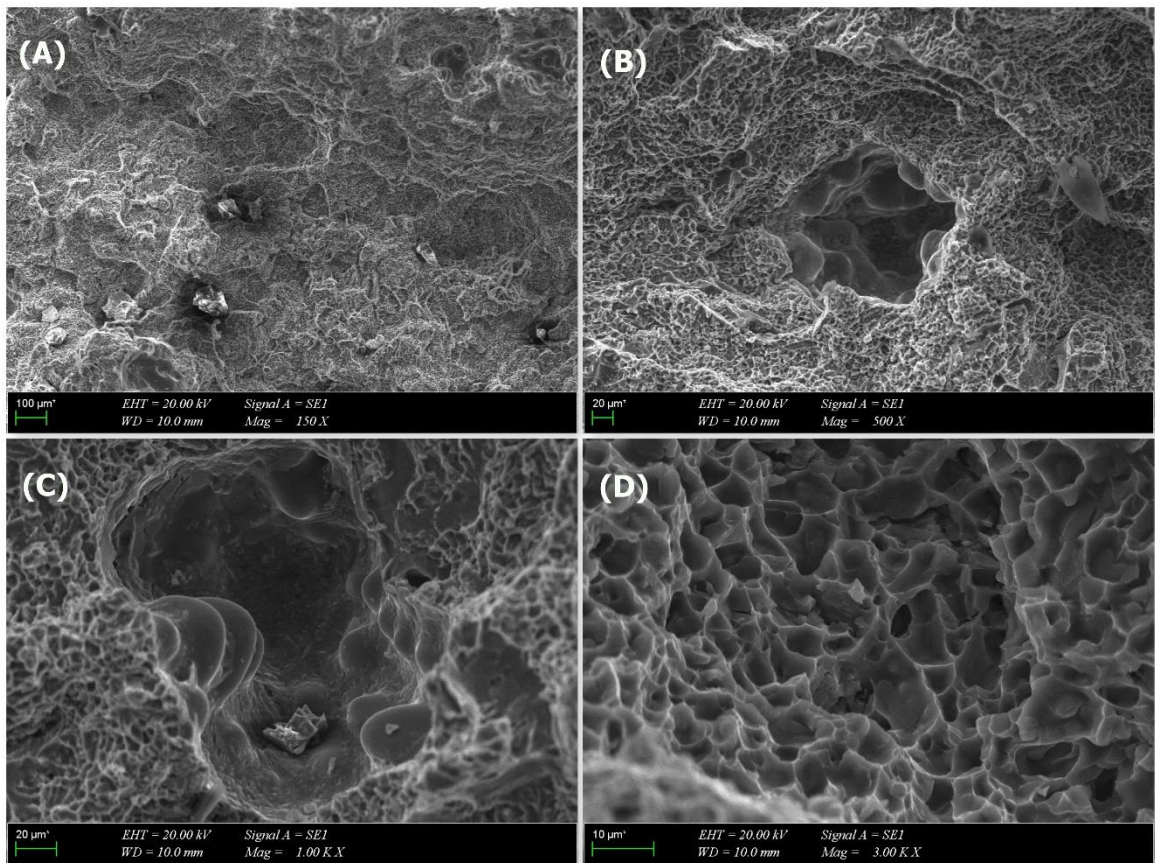


Figure 5.3.1.2 Charpy Impact Test SEM Micrographs with 0.11 Fe level (A)150X magnification, (B) 500X magnification, (C) 1.0kX magnification (D) 3.0kX magnification

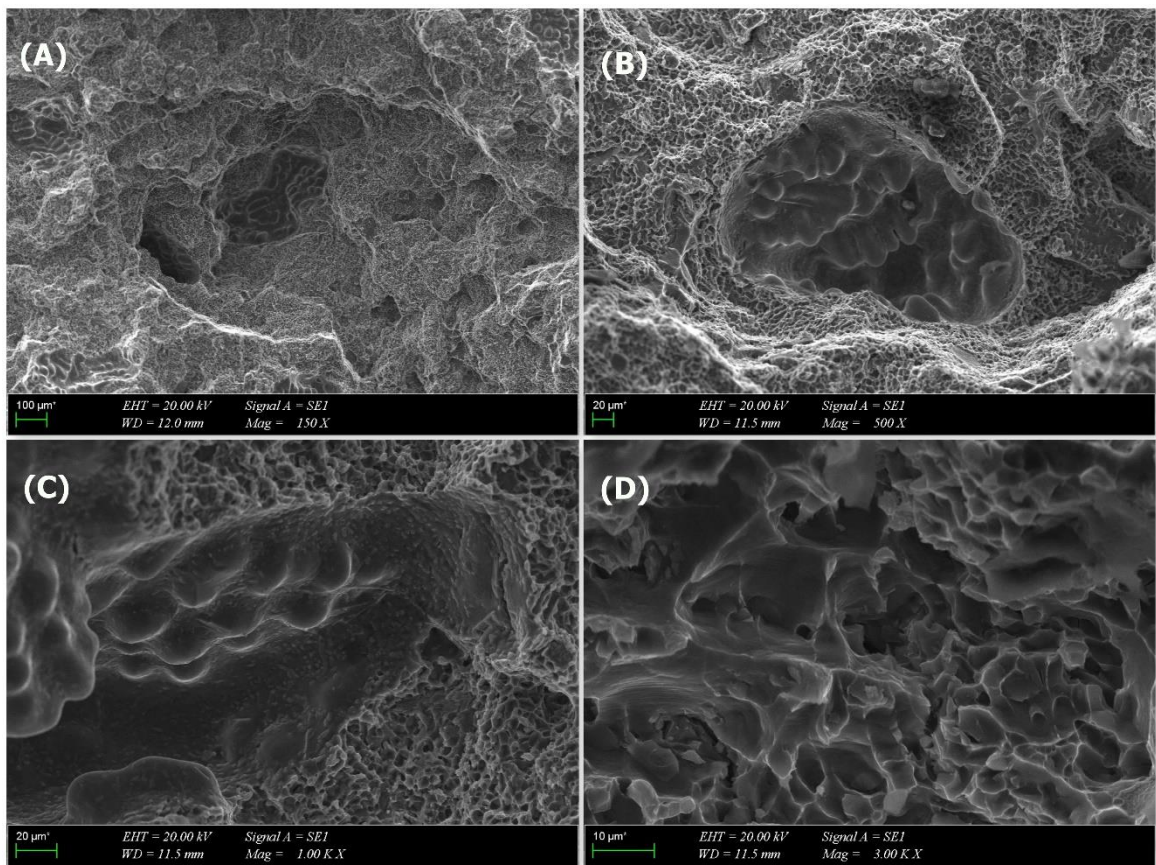


Figure 5.3.1.3 Charpy Impact Test SEM Micrographs with 0.25 Fe level (A)150X magnification, (B) 500X magnification, (C) 1.0kX magnification (D) 3.0kX magnification

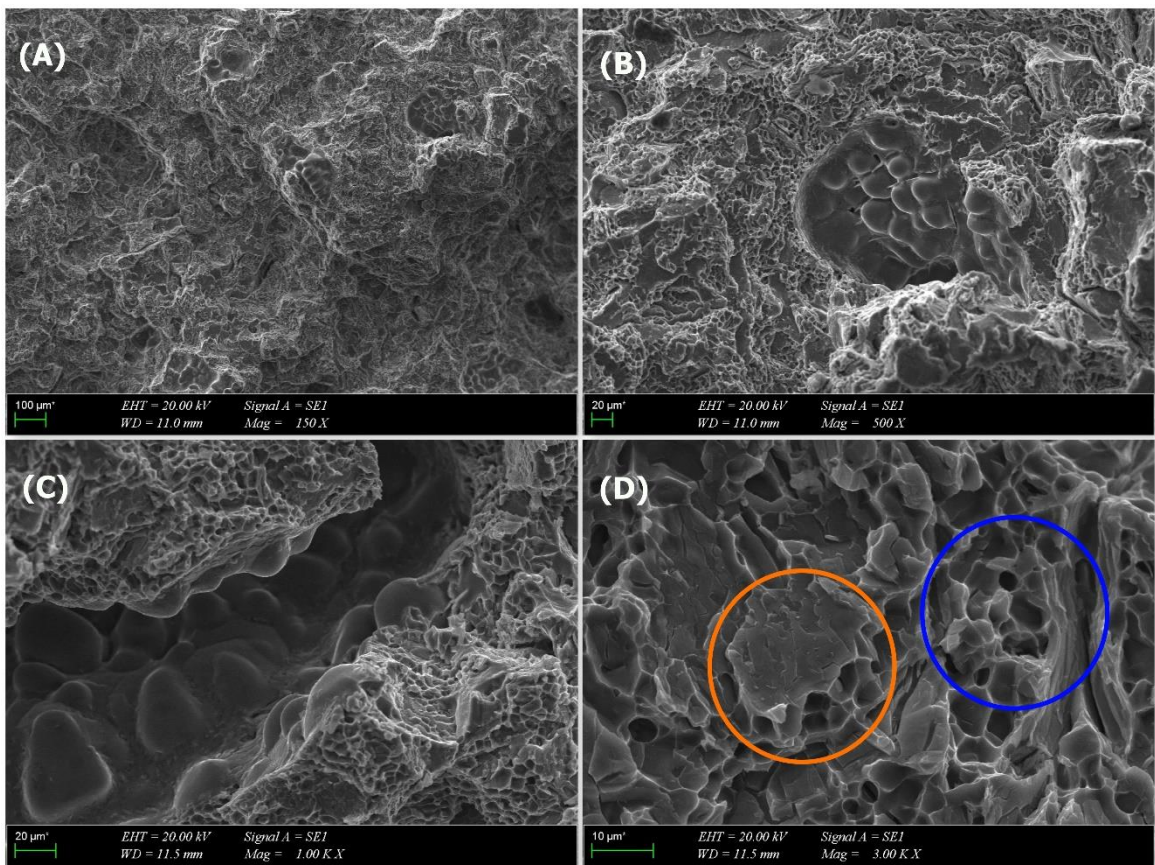


Figure 5.3.1.4 Charpy Impact Test SEM Micrographs with 0.42 Fe level (A)150X magnification, (B) 500X magnification, (C) 1.0kX magnification (D) 3.0kX magnification

At 3000 magnifications, the transgranular and intergranular fracture patterns may be seen clearly in the image above. The transgranular fracture is represented by the orange zone, whereas the intergranular fracture is represented by the blue zone.

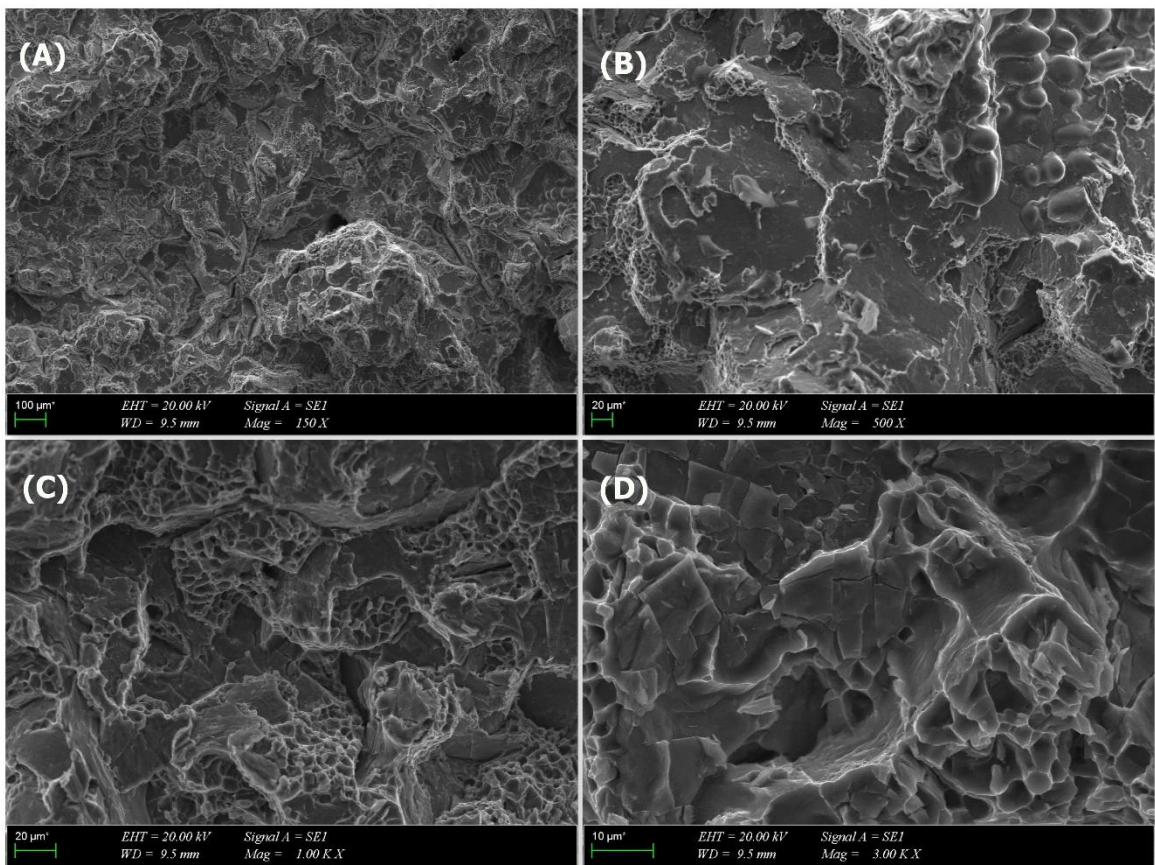


Figure 5.3.1.5 Charpy Impact Test SEM Micrographs with 0.65 Fe level (A)150X magnification, (B) 500X magnification, (C) 1.0kX magnification (D) 3.0kX magnification

When we looked at our last sample, we discovered flat fractures. Because the iron level in this sample was larger than in the others, we saw more transgranular fractures.

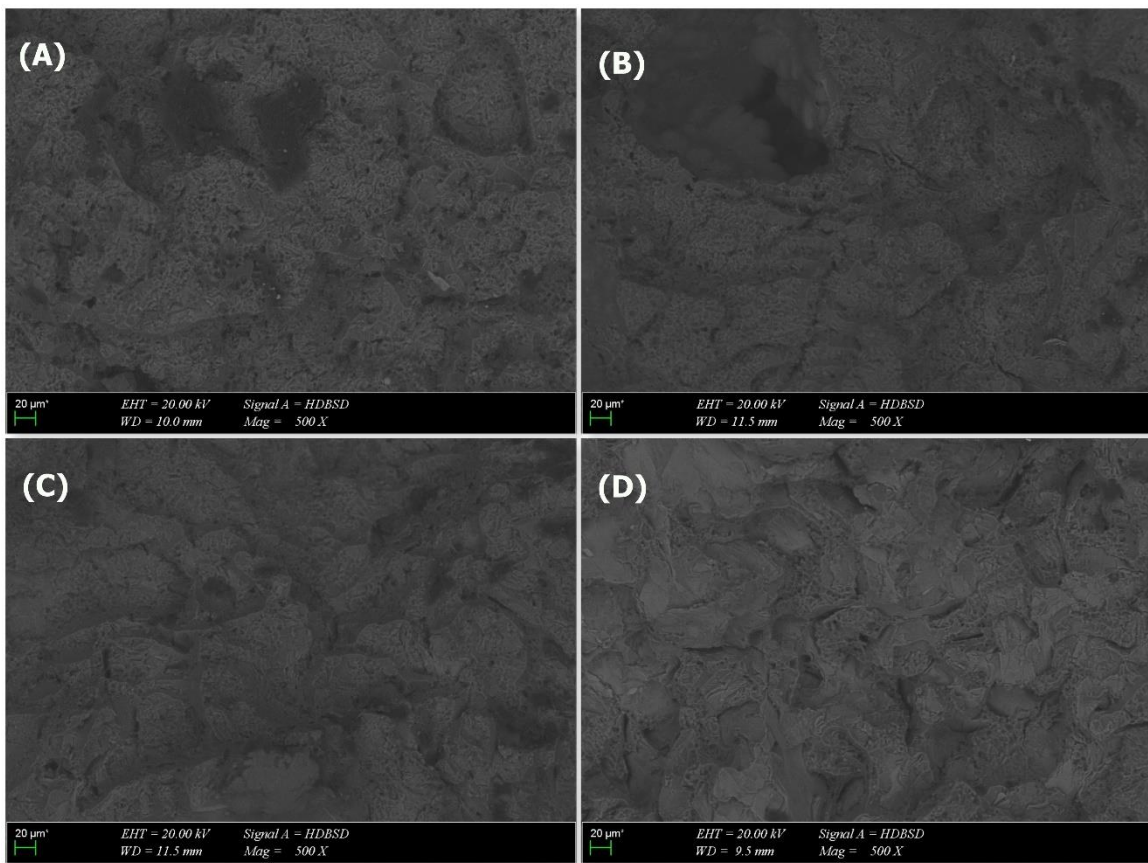


Figure 5.3.1.6 Charpy Impact Test SEM micrographs in BSD mode (A) 0.11 Fe, (B) 0.25 Fe, (C) 0.42 Fe, (D) 0.65 Fe

The contrast disparities in the images taken in BSD mode can be used to comment on the material's homogeneity. The photos of all four samples obtained in BSD mode are shown above.

It has been noticed that dark colors fade over time, resulting in a brighter appearance. It's possible that this is due to the high iron concentration.

EDX is used to provide a more complete investigation of the material's homogeneity.

5.3.1.3 Tensile Fracture Surface Results with SEM

Our tensile samples were also subjected to SEM analysis, just like our Charpy samples. You can take a look at the list below.

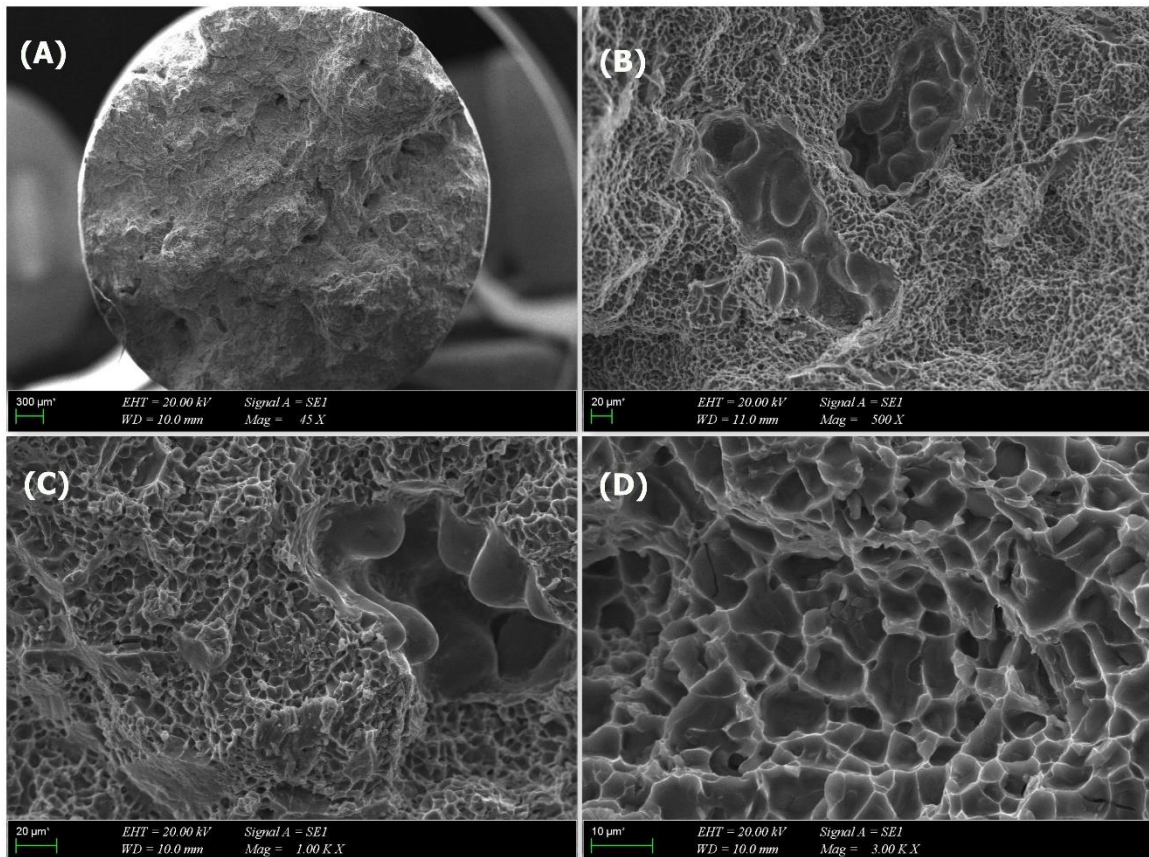


Figure 5.3.1.7 Tensile Test SEM Micrographs with 0.11 Fe level (A)150X magnification, (B) 500X magnification, (C) 1.0kX magnification (D) 3.0kX magnification

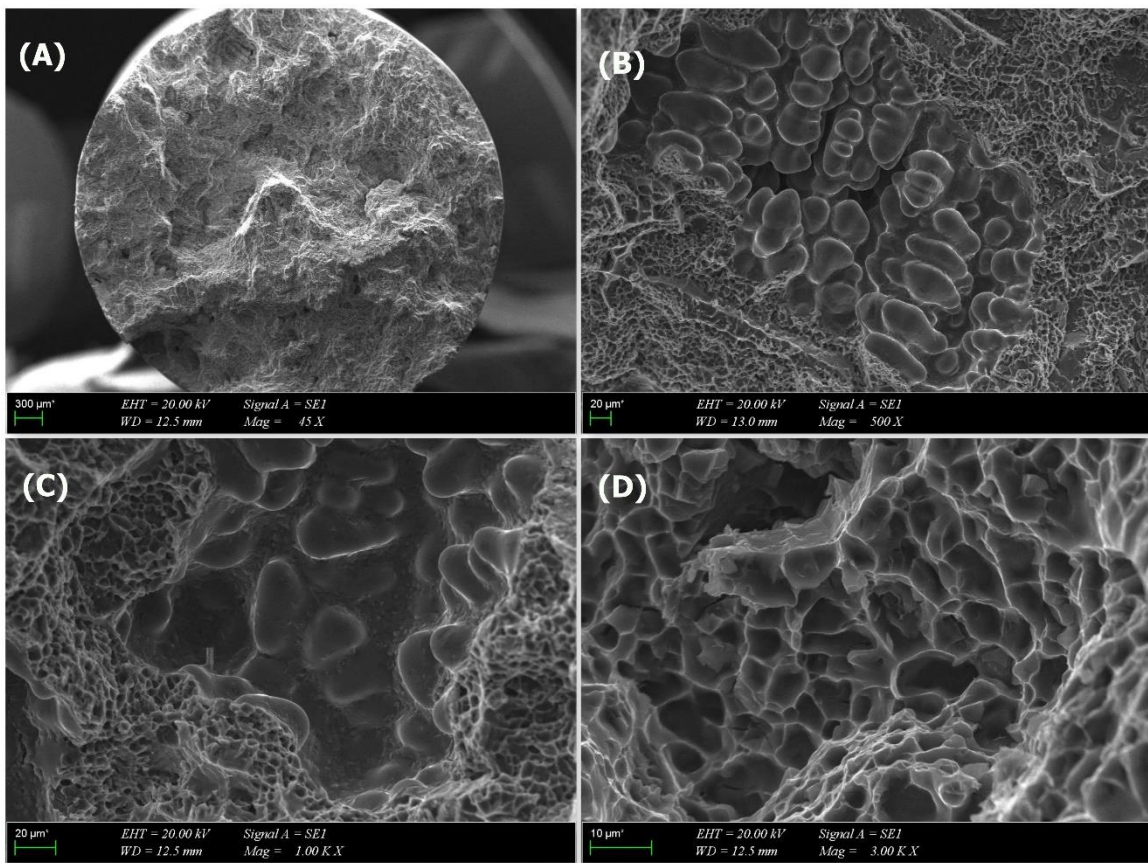


Figure 5.3.1.8 Tensile Test SEM Micrographs with 0.25 Fe level (A)150X magnification, (B) 500X magnification, (C) 1.0kX magnification (D) 3.0kX magnification

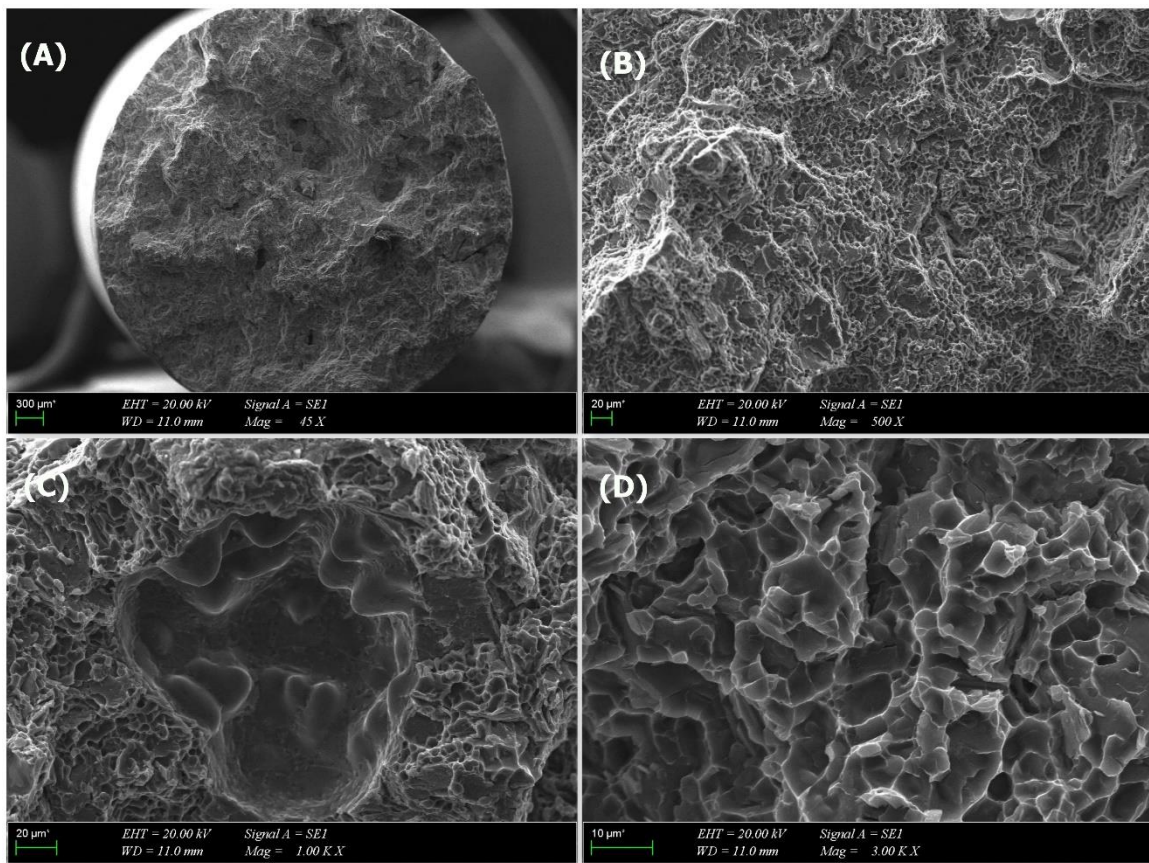


Figure 5.3.1.9 Tensile Test SEM Micrographs with 0.42 Fe level (A)150X magnification, (B) 500X magnification, (C) 1.0kX magnification (D) 3.0kX magnification

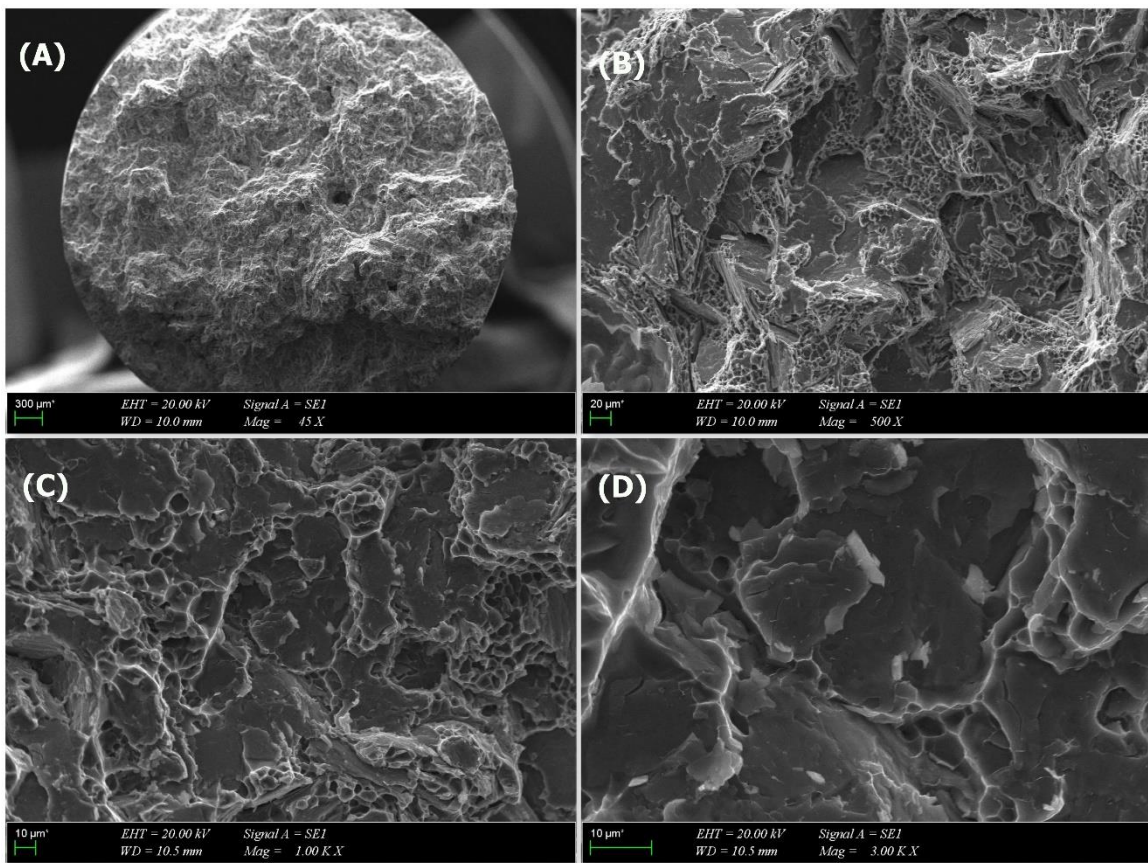


Figure 5.3.1.10 Tensile Test SEM Micrographs with 0.65 Fe level (A)150X magnification, (B) 500X magnification, (C) 1.0kX magnification (D) 3.0kX magnification

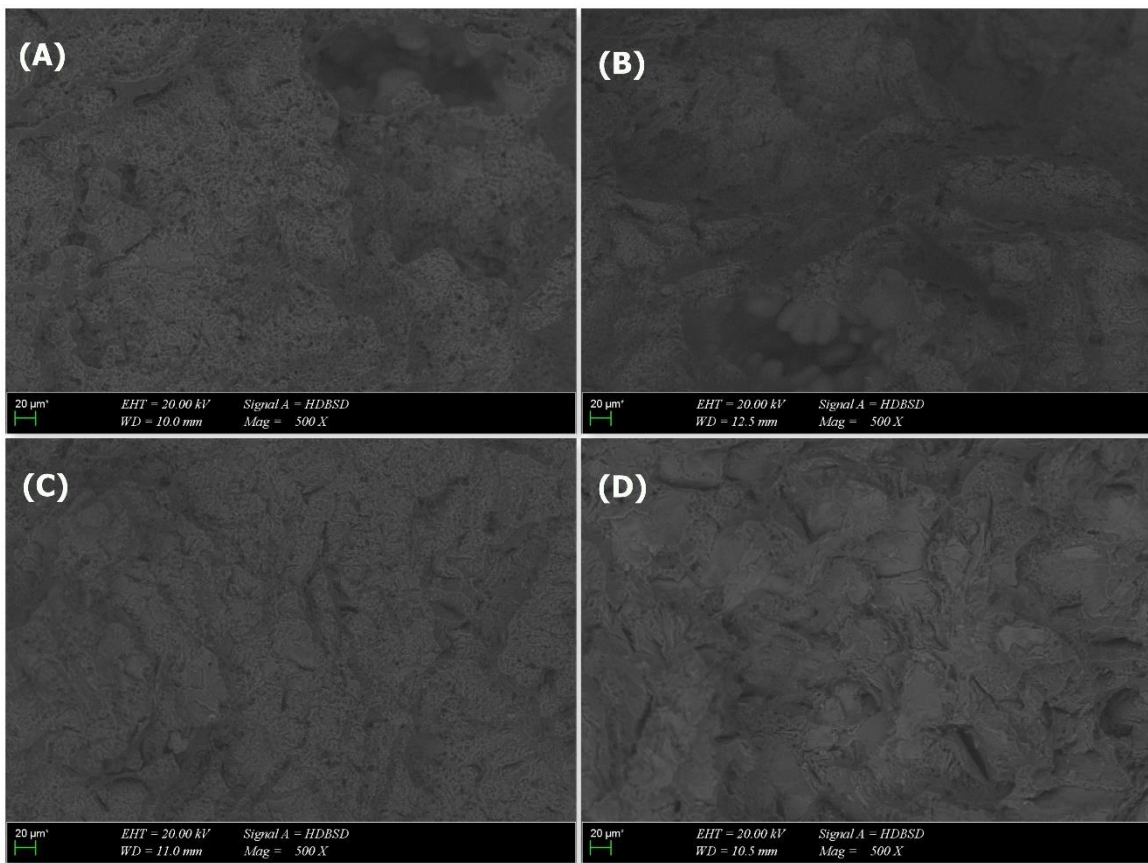
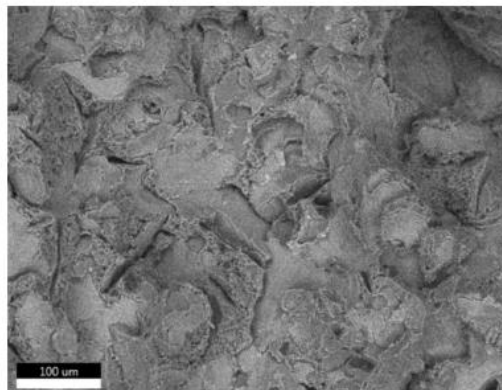


Figure 5.3.1.11 Tensile Test SEM micrographs in BSD mode (A) 0.11 Fe, (B) 0.25 Fe, (C) 0.42 Fe, (D) 0.65 Fe

Our materials, which were put through tensile tests, were also inspected in BSE mode.

Our samples were mapped and their homogeneity status was investigated in order to make a more precise judgment regarding their homogeneity.

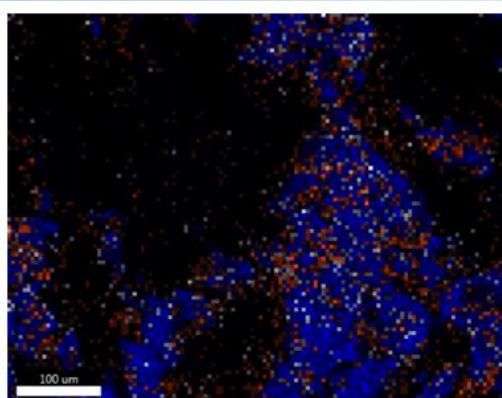
The microstructure of our charpy sample with the highest iron concentration can be observed more clearly in the mapping mode of homogeneity and intermetallic distribution below. The red and blue hues assigned in the mapping approach represent iron and aluminum. Intermetallicity has been proven in the fourth or most ferrous sample, despite sections closer to purple between the two colors being difficult to see.



Image

Live Map 1

ElementOverlay



EDAX APEX

Page 3

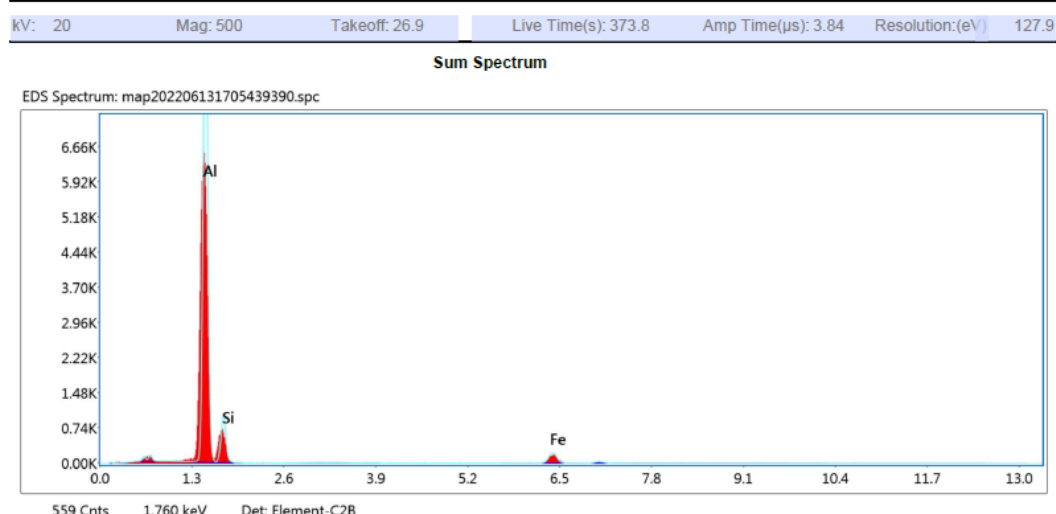


Figure 5.3.1.12 XRD Mapping of 0.65 Fe level 4th specimen

When we evaluated our SEM photos, we discovered two different types of refraction. When the intergranule was present, rupture was noticed between the dendrites in the fracture patterns that changed as the iron ratio increased.

The broken sample in this structure takes the simplest path and breaks after impact. In our first sample, we saw more spherical ruptures, but in our fourth sample, we saw a flatter fracture profile. 4. The general structure of the sample, with more intermetallic than the others; inter granule turned it into a transgranule structure. As a result, the brittle refraction pattern appears more frequently in 4.

5.3.1.4 Charpy Microstructural Results with EDX

The elements found in samples with four different iron ratios are depicted in the figures below. The broad diagrams for each sample were looked at first. This diagram is not exhibited if the iron ratio is less than 0.02 or not at all in the general view, because there is no homogeneous appearance. We do know, however, that iron precipitates in a bright white color, so when we looked at our photos, we especially looked at the white colored spots and evaluated our ratios.

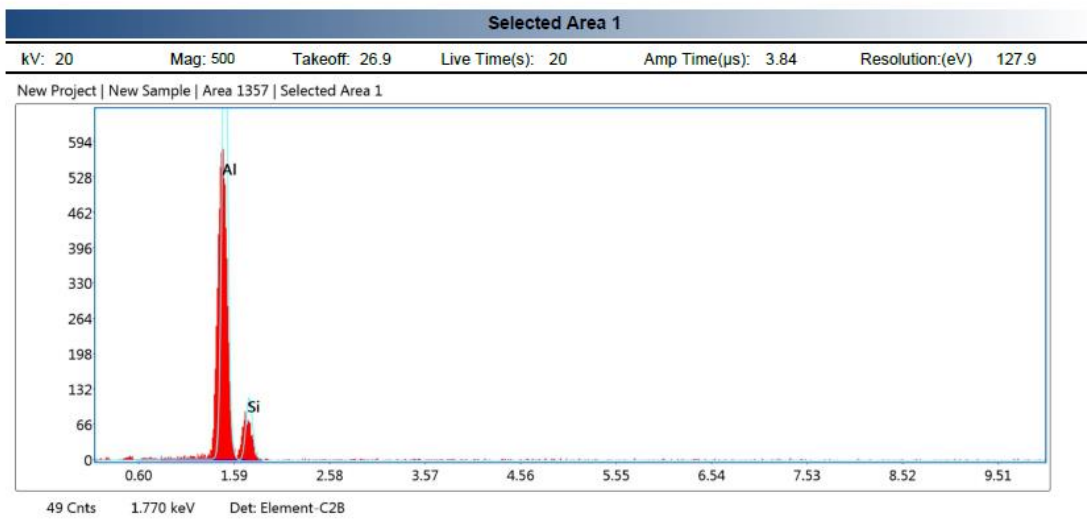
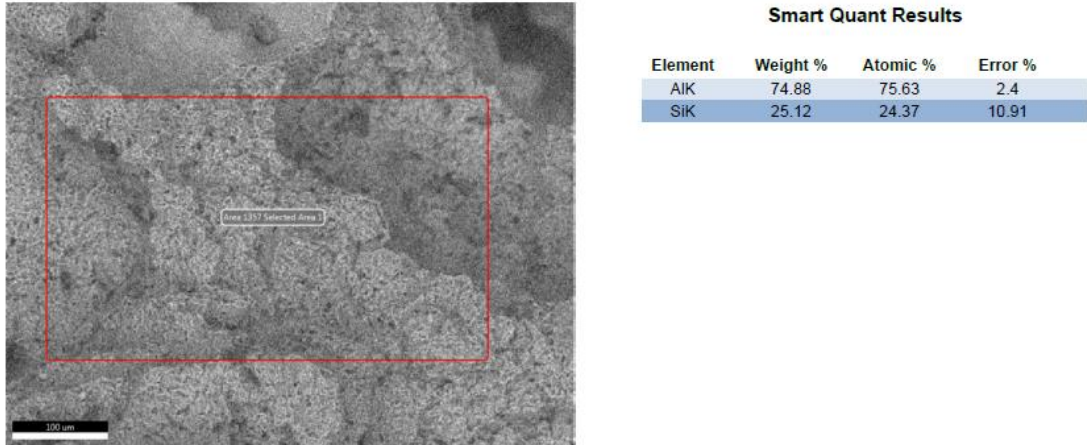


Figure 5.3.1.13 Charpy Impact Test sample with 0.11 Fe level, fracture surface EDX analysis at general area

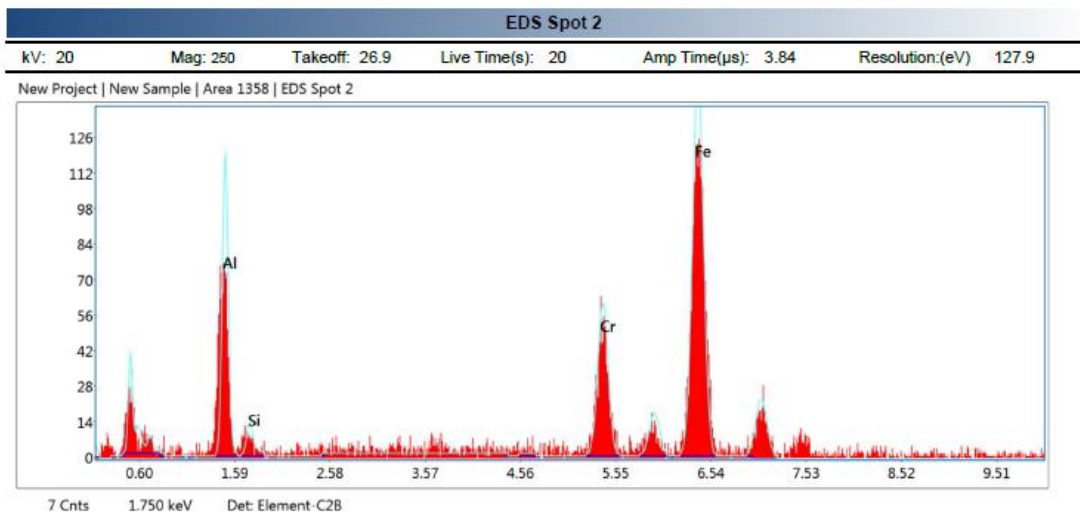
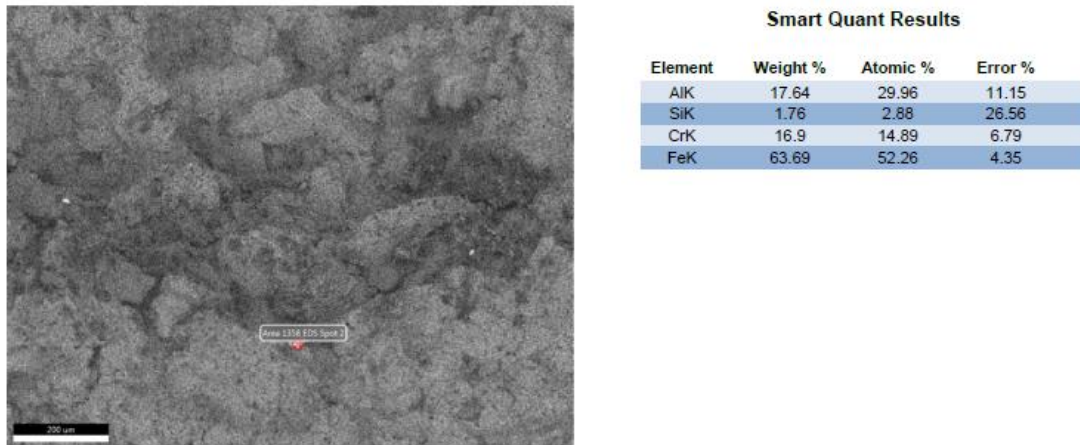


Figure 5.3.1.14 Charpy Impact Test sample with 0.11 Fe level, fracture surface EDX analysis at point 2

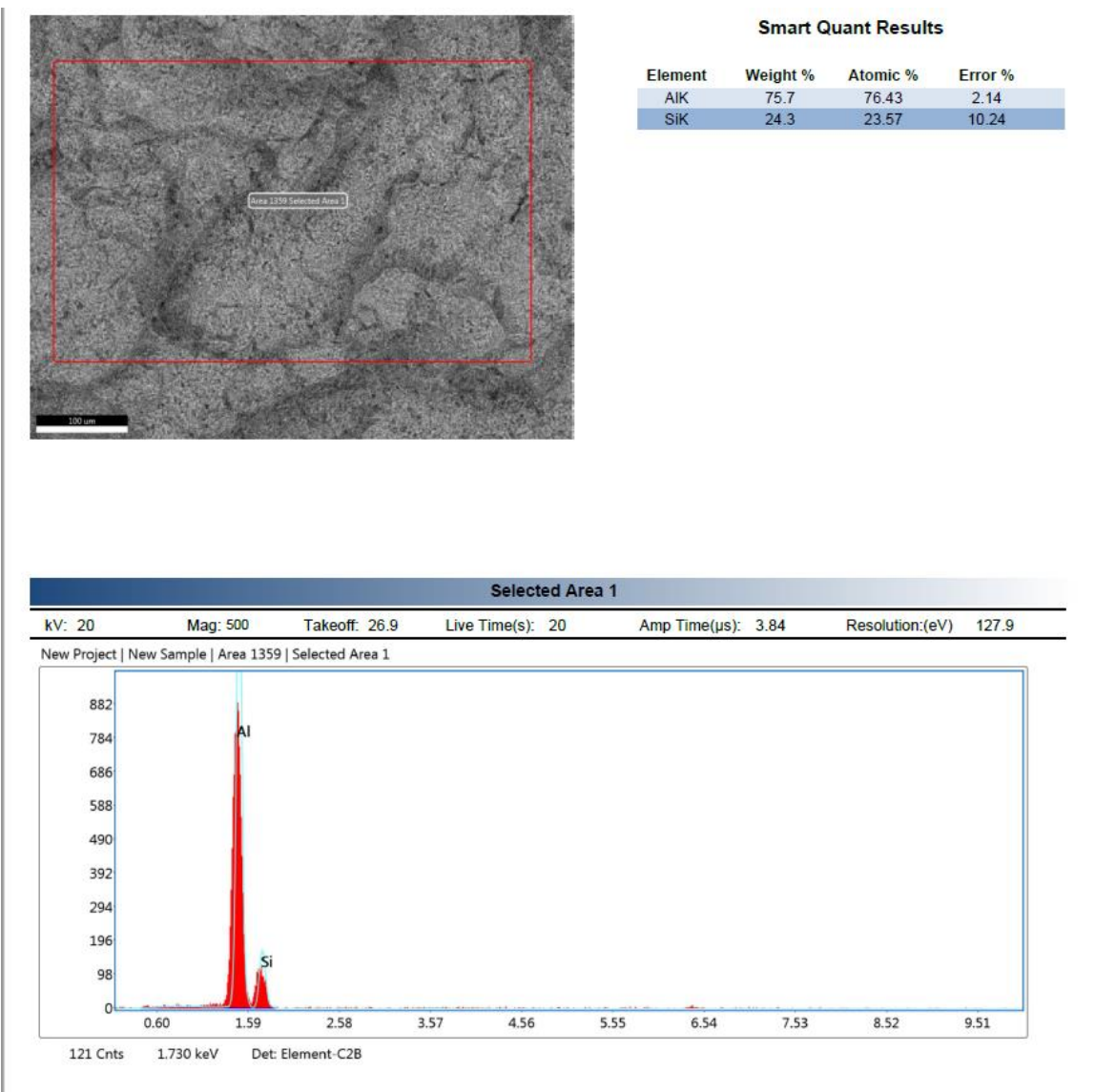


Figure 5.3.1.15 Charpy Impact Test sample with 0.25 Fe level, fracture surface EDX analysis at general area

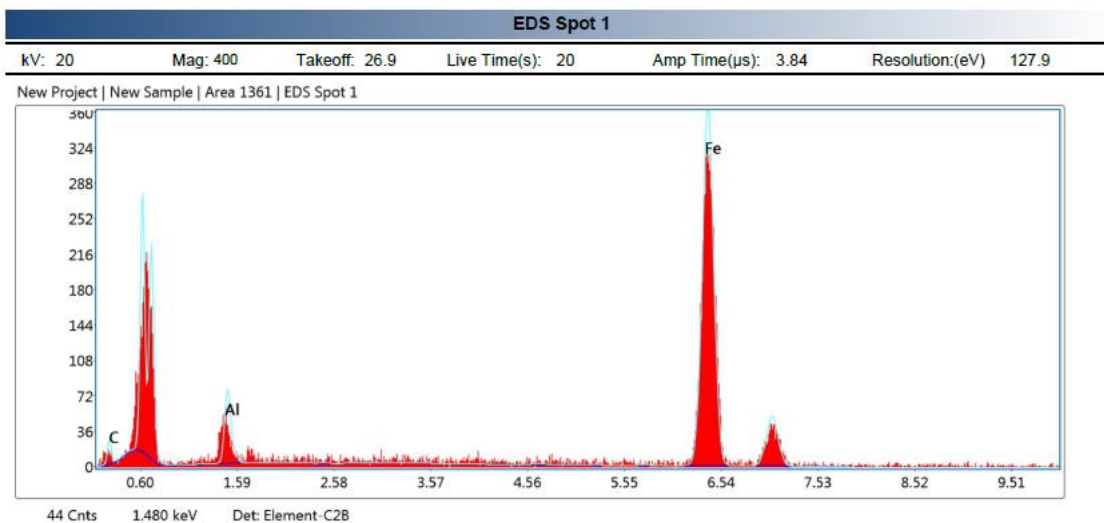
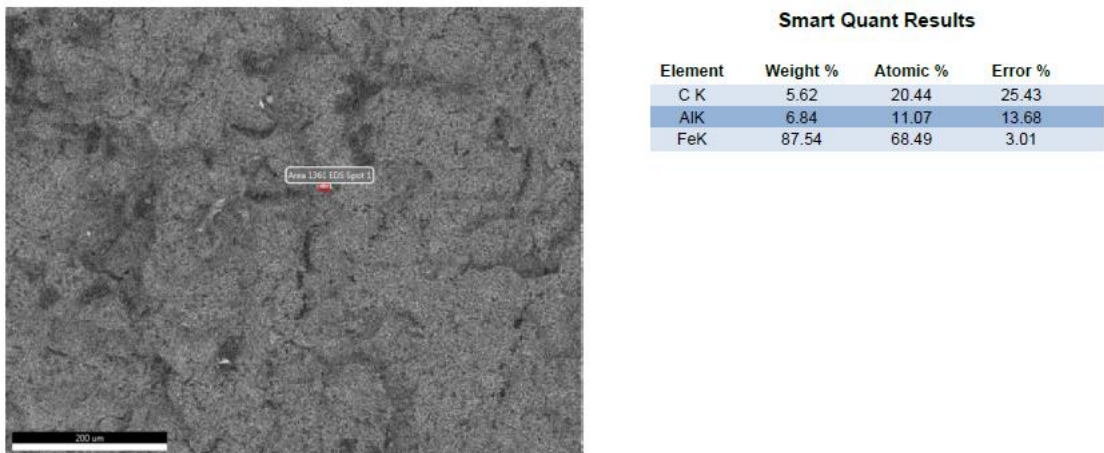


Figure 5.3.1.16 Charpy Impact Test sample with 0.25 Fe level, fracture surface EDX analysis at point 2

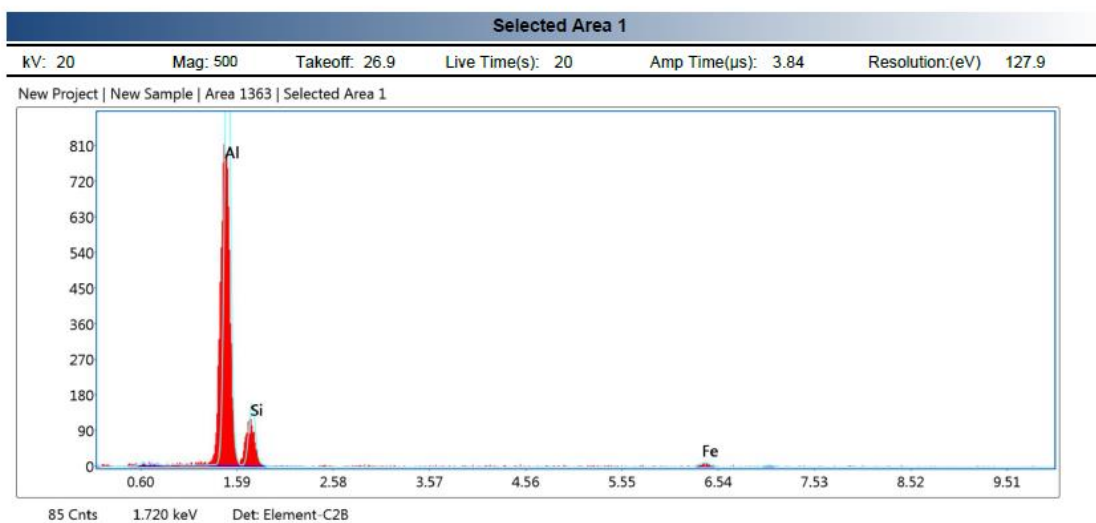
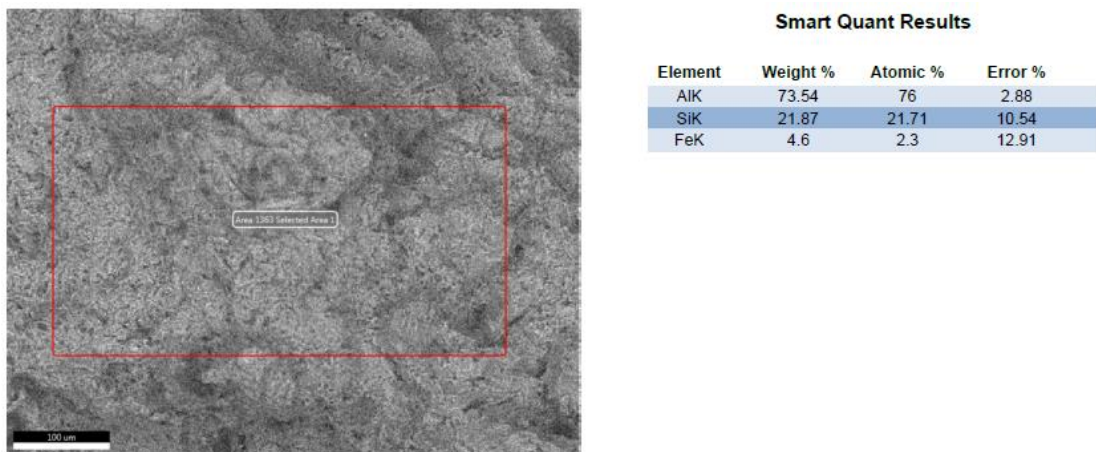


Figure 5.3.1.17 Charpy Impact Test sample with 0.42 Fe level, fracture surface EDX analysis at general area

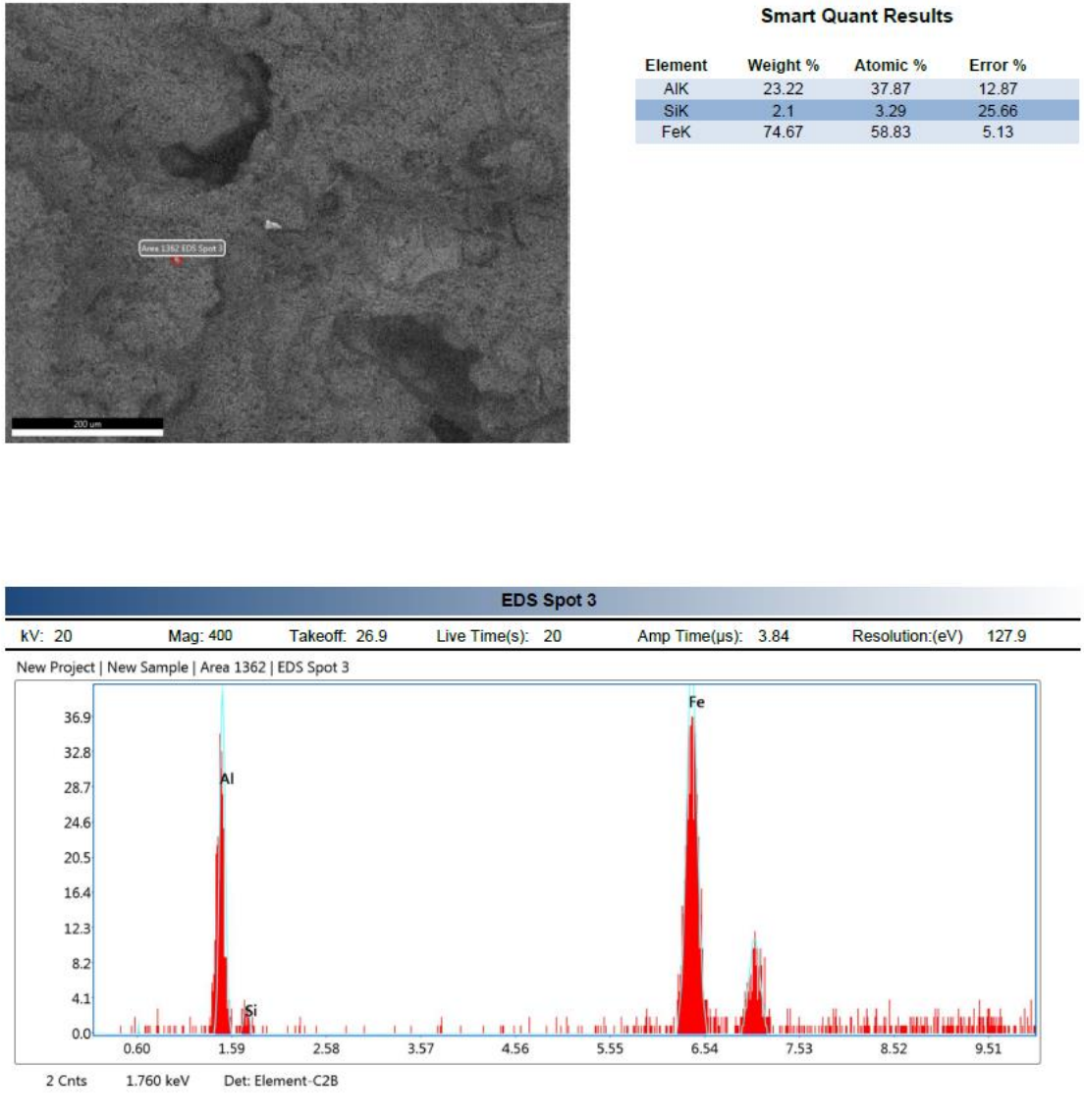
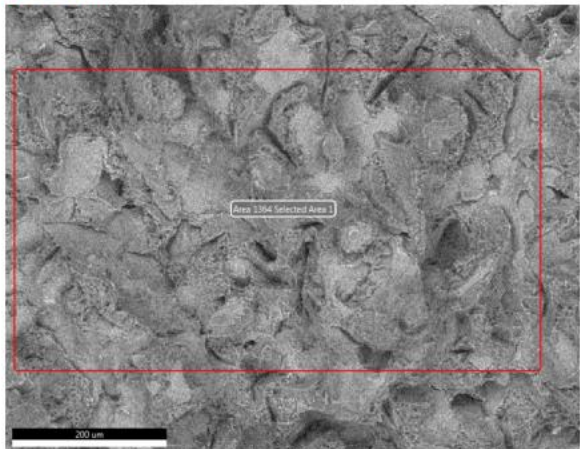


Figure 5.3.1.18 Charpy Impact Test sample with 0.42 Fe level, fracture surface EDX analysis at point 3

Area 1364



Smart Quant Results

Element	Weight %	Atomic %	Error %
AlK	72.68	77.14	3.87
SiK	17.45	17.8	11.69
FeK	9.87	5.06	9.68

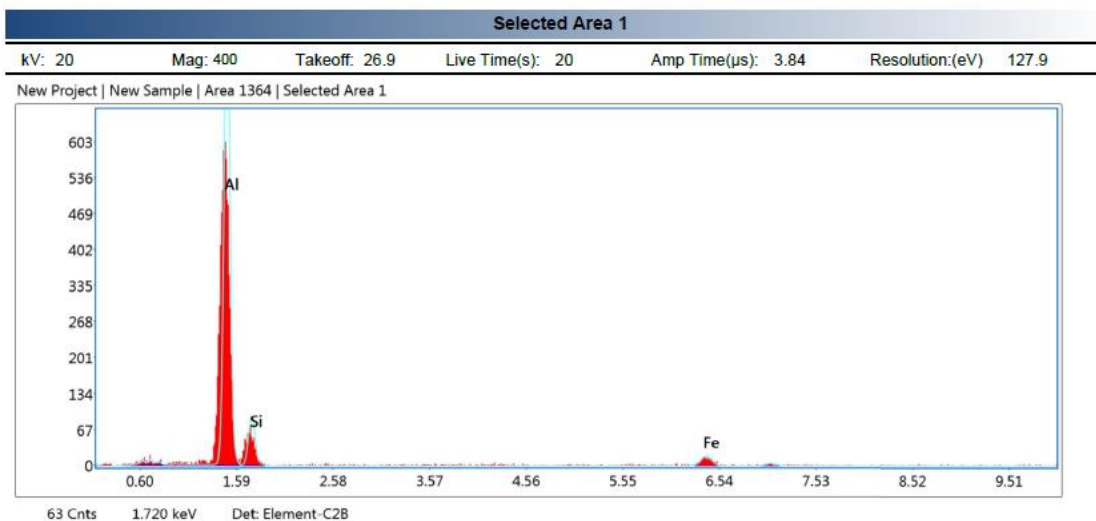


Figure 5.3.1.19 Charpy Impact Test sample with 0.65 Fe level, fracture surface EDX analysis at general area

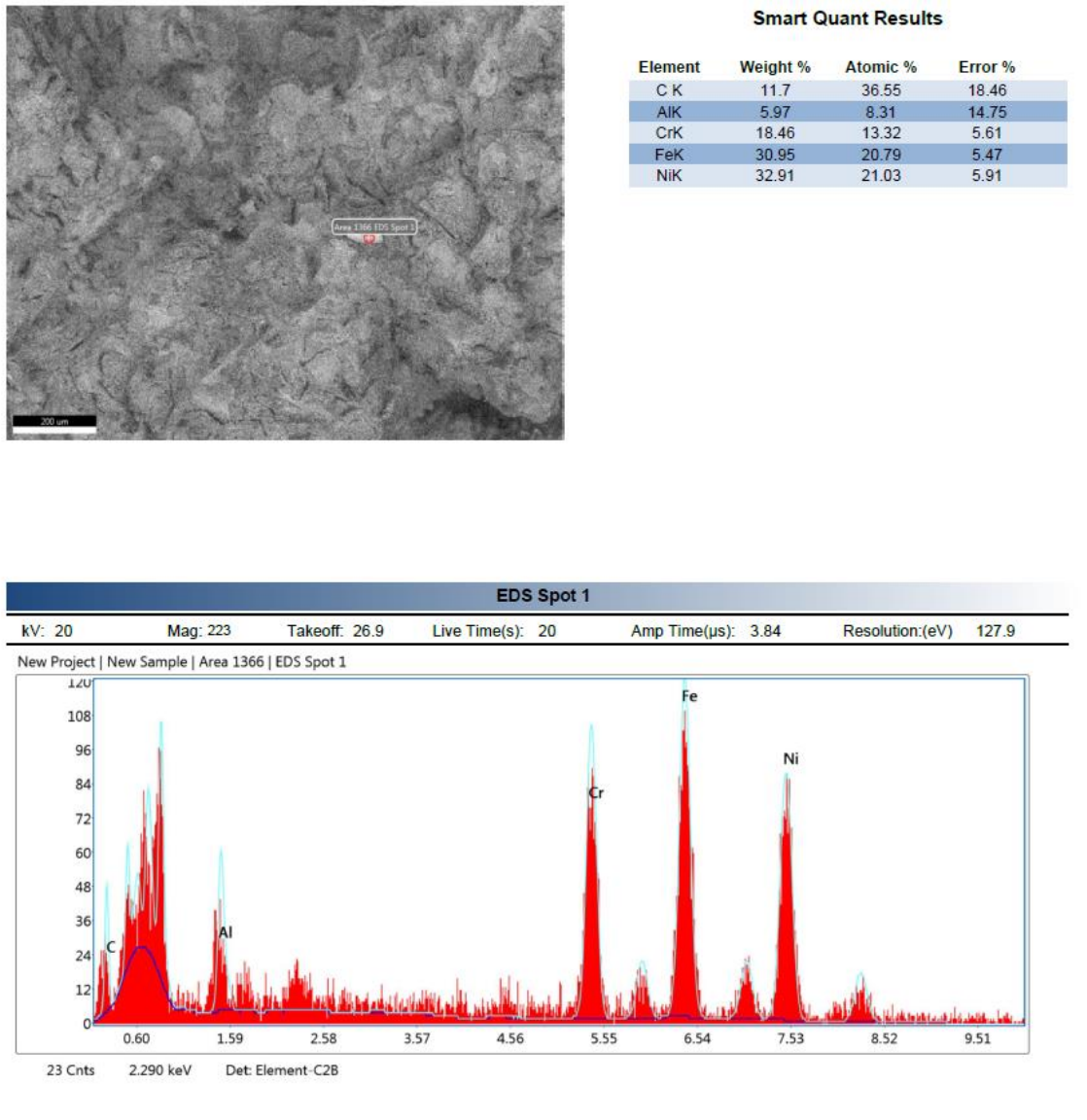


Figure 5.3.1.20 Charpy Impact Test sample with 0.65 Fe level, fracture surface EDX analysis at point 2

When the EDX results compared between are figures (figure 5.3.1.13, figure 5.3.1.15, figure 5.3.1.17, figure 5.3.1.19), it can be observed that general area's Fe level increases.

When the EDX results compared and examined between are figures (figure 5.3.1.14, figure 5.3.1.16, figure 5.3.1.18, figure 5.3.1.20), it can be said there are some non-homogenous distributions is present in each sample of alloy. Also, more detailed EDX results can be seen in Appendix Figure A, B, C, D, E, F, G, H.

6 CONCLUSIONS

6.1 Main Conclusions

The mechanical properties of an aluminum alloy were predicted when the Fe concentration changed in this research effort. Charpy V-notch impact and tensile tests with aluminum alloys containing various Fe levels are used for this. The tests are carried out in the same way every time.

Fe values in the samples were 0.11, 0.25, 0.42, and 0.65. We chose these percentages because they were the most homogeneous we could find. The structure's shift from ductility to brittleness can be determined in this way. The four types of fracture patterns are ductile, brittle, fatigue, and circumferential fractures. To pinpoint the source of the fracture, macroscopic and microscopic examinations are done on each model. The next sections overview each fracture pattern and a synopsis of the fracture surface. Depending on the amount of iron in the substance, the structure becomes more or less brittle. The material becomes increasingly brittle as the iron content rises.

The optical analysis of the fracture surface revealed the ductility and brittleness of the structure in both our Charpy V-notch impact test and tensile test specimens. The findings of Charpy V-notch impact tests reveal that as the Fe component of the alloy changes, the AlSi7Mg (A356) alloy transitions from ductile to brittle. Macroscopic and microscopic analyses were used to investigate the fractured samples.

In the figures, we can also see a hollow structure. This indicates the creation of porosity. Residues are apparent because of a casting issue. Porosity is hypothesized to arise as due to a casting flaw or the compression and conversion of hydrogen/oxygen gas into gas balloons. The sensitivity of hydrogen absorption accounts for the porosity. Mechanical qualities like as elongation suffer as a result.

The microstructure of aluminum alloys is investigated from two angles. The effects of production and casting quality, as well as the effects of elements in the aluminum alloy, may be observed in this manner. Rapid solidification, also known as dendritic solidification, was also observed in the material. The combination of Iron and Aluminum creates intermetallic.

Intermetallic is distinguished by its hue. Iron appears as a sparkling white substance as it precipitates out as iron. The little gray ones in between are intermetallic. Intermetallic boosts the object's strength and rigidity. In our samples, it is equally distributed and supports the microstructure. Intermetallic alters the material's fracture structure, resulting in a steady improvement in strength as the iron ratio rises. As a result of the increased iron content, we were able to create samples that were both stronger and more delicate.

The SEM investigation yielded more detailed images from the microscope. It was possible to get a sense of the sample's fragility structure. The formation of a more and more flat fracture profile has been seen. In other words, the intergranular structure evolved into a trans granular structure through time. The increase in the creation of intermetallic is thought to be the reason for this. The contrast contrasts in images recorded in BSE mode provide information about the homogeneity of the material. It's visible in the photographs in the results section. Furthermore, the mapping work we've done has allowed us to see the intermetallic, even if they aren't visible. The purple color that resulted from combining blue and red colors was found to be intermetallic.

As a result, we observed a significant change between aluminium alloys with different Fe content, in ways of energy and tensile strength. These significant changes can be explained by our examined microstructure.

6.2 Recommendation for Further Work

With more expansion, the number of samples and range with the Fe content can cause a better result. In addition, to expand the data of the experiments and conditions tests can also be repeated in different working conditions.

6.3 Evaluation of the Work from MUDEK Perspective

6.3.1 Economic Analysis

Primary purpose of this study is the provide results for the recycled aluminum alloy. Recycling can reduce the carbon footprint as well as the cost of the production. At different level of Fe content safety ratio and strength of the material does change.

With results of this study design and use of the recycled aluminum alloy can be determined. Which can also be used to optimize production costs.

6.3.2 Real-Life Conditions

In this study samples, were a variation of the already existing aluminum alloy used in wheels. In the tests, international standards were used. The conditions of this study were done in real-life conditions.

6.3.3 Productibility

Manufacturability is a crucial to a product's research and development, design, and analysis. With the results of this study manufacturers can decide on a design and operating conditions of a product.

6.3.4 Constraints

In this study, four different Fe levels were examined. Because of the small number of samples, it constraints us on the range which worked. Also, used instruments and measurement devices show some tolerance level which can affect the accuracy of the results.

REFERENCES

- [1] A.Y. Kaya, O. Özaydın, T. Yağcı, A. Korkmaz, E. Armakan and O. Çulha, Effect of Chip Amount on Microstructural and Mechanical Properties of A356 Aluminum Casting Alloy, Archives of Foundry Engineering, 21(3), pp. 19-26, 2021.
- [2] R. Cobden, Alcan and Banbury, "Aluminium: Physical Properties, Characteristics and Alloys," 1994.
- [3] N. Açıcı, "A356 Ve A380 Alaşımlarının Eğimli Soğutucu İle Dökümü Ve Yarı Katı Dövme İşlemi," Yıldız Teknik Üniversitesi, 2018.
- [4] I. Polmear, D. StJohn, J.-F. Nie and M. Qian, Light Alloys: Metallurgy of the Light Metals.
- [5] M. Yıldırım and D. Özyürek, "The effects of Mg amount on the microstructure and mechanical," Materials and Design, 2013.
- [6] H. Demirpolat, S. Akdı and B. Balkan, "The Effect of Homogenization and Chemical Compositions of 6005 and 6082 Aluminium Alloys on The Cold Forming Process," Avrupa Bilim ve Teknoloji Dergisi, vol. 28, no. 16-20, 2021.
- [7] "Notch Test with Charpy Impact Tester," Presto Group, [Online]. Available: <https://www.prestogroup.com/articles/notch-test-with-charpy-impact-tester/>.
- [8] "Çekme Deneyi," [Online]. Available: <https://mekatronikmuhendisligi.com/cekme-deneyi/>.
- [9] "Çekme Testi Nasıl Yapılır," [Online]. Available: <https://makelektronik.com.tr/bbk/9/Cekme-Testi-Nas%C4%B1l-Yap%C4%B1r.html>.
- [10] "Strength at Break (Tensile)," [Online]. Available: <http://omnexus.specialchem.com/polymer-properties/properties/strength-at-break-tensile>.

- [11] "Evaluation of materials using scanning electron microscope (SEM)," [Online]. Available: <https://www.thinkymixer.com/en-gl/library/report/evaluation-of-materials-using-scanning-electron-microscope-sem/>.
- [12] L. Kuchariková, E. Tillová, M. Chalupová, M. Mazur, A. Herčko and Č. R., "Analysis of microstructure in AlSi7Mg0. 3 cast alloy with different content of Fe," Transportation Research Procedia, pp. 59-67, 2019.
- [13] D. McMullan, "Scanning electron microscopy," Scanning, pp. 175-185, 1995.
- [14] W. Callister and D.G. Rethwisch, Materials Science and Engineering,, 8 ed., Wiley, 2011.
- [15] "METALOGRAFİK NUMUNE HAZIRLAMA YÖNTEMLERİ," [Online]. Available: http://www.bulutmak.com/uploads/2/0/0/3/20037867/metalografik_numune_hazirlama_yontemleri.pdf.
- [16] M. F. Ashby, Materials Selection in Mechanical Design, 2 ed., Butterworth-Heinemann, 1999.
- [17] N. E.Dowling, Mechanical Behavior of Materials, 4 ed., Pearson Education Limited.
- [18] b. X. Z. H. W. Z. L. J. D. Xiaobing Caoa, "Microstructures and mechanical properties of laser offset welded 5052 aluminum to press-hardenedsteel," Journal of Materials Research and Technology, 2020.
- [19] J. R. Davis, Tensile testing, 2 ed., ASM International, 2004.
- [20] K. Grjotheim, C. Krohn, M. Malinovsky, K. Matiasovsky and J. Thonstad, Aluminium electrolysis: Fundamentals of the Hall-Heroult Process, 2 ed., California: University of California, 1982.
- [21] Q. Li, Y. Zhu, S. Zhao, Y. Lan, D. Liu, G. Jian and H. Zhou, "nfluences of Fe, Mn and Y additions on microstructure and mechanical properties of hypoeutectic Al–7% Si alloy.," Intermetallics, p. 120, 2020.
- [22] R. Whan, Ed."Materials Characterizations," ASM Handbook,, vol. 10, pp. 299-308.

- [23] K. Vernon-Parry, "Scanning electron microscopy: an introduction," III-Vs Review, vol. 13, no. 4, pp. 40-44, 2000.
- [24] D. Tabor, The Hardness of Metals, Oxford university press, 2000.
- [25] M. Warmuzek, Aluminum-Silicon Casting Alloys: Atlas of Microfractographs, ASM International, 2004.
- [26] [Online]. Available: <https://www.prestogroup.com/articles/notch-test-with-charpy-impact-tester/>.
- [27] Metallic materials Charpy pendulum impact test Part 1: Test method, ISO, 2016.
- [28] "Automotive and Aerospace Industries Metallurgical Failure Analysis and Fracture Patterns," [Online]. Available: <http://keyence.co.uk/ss/products/microscope/vhx-casestudy/automobile/fracture-surface.jsp>.
- [29] "Grinding process," [Online]. Available: <https://www.summaryplanet.com/engineering/Grinding-process.html>.
- [30] "METALOGRAFİ DENEYİ LABORATUVAR FÖYÜ," [Online]. Available: <https://cdn.bartin.edu.tr/metalurji/d7ee7cd9-f063-4669-8e1c-393503ed6ffb/metalografdeneyfoyu.pdf>.
- [31] A. Kavukcu, "Çekme testi nedir? Neden uygulanır? Nasıl yapılır?," [Online]. Available: <https://malzemebilimi.net/cekme-testi-nedir-neden-uygulanir-nasil-yapilir.html>.
- [32] [Online]. Available: <http://www.steeltest.net/>.
- [33] [Online]. Available: <https://www.keyence.co.uk/ss/products/microscope/vhx-casestudy/automobile/fracture-surface.jsp>.

APPENDICES

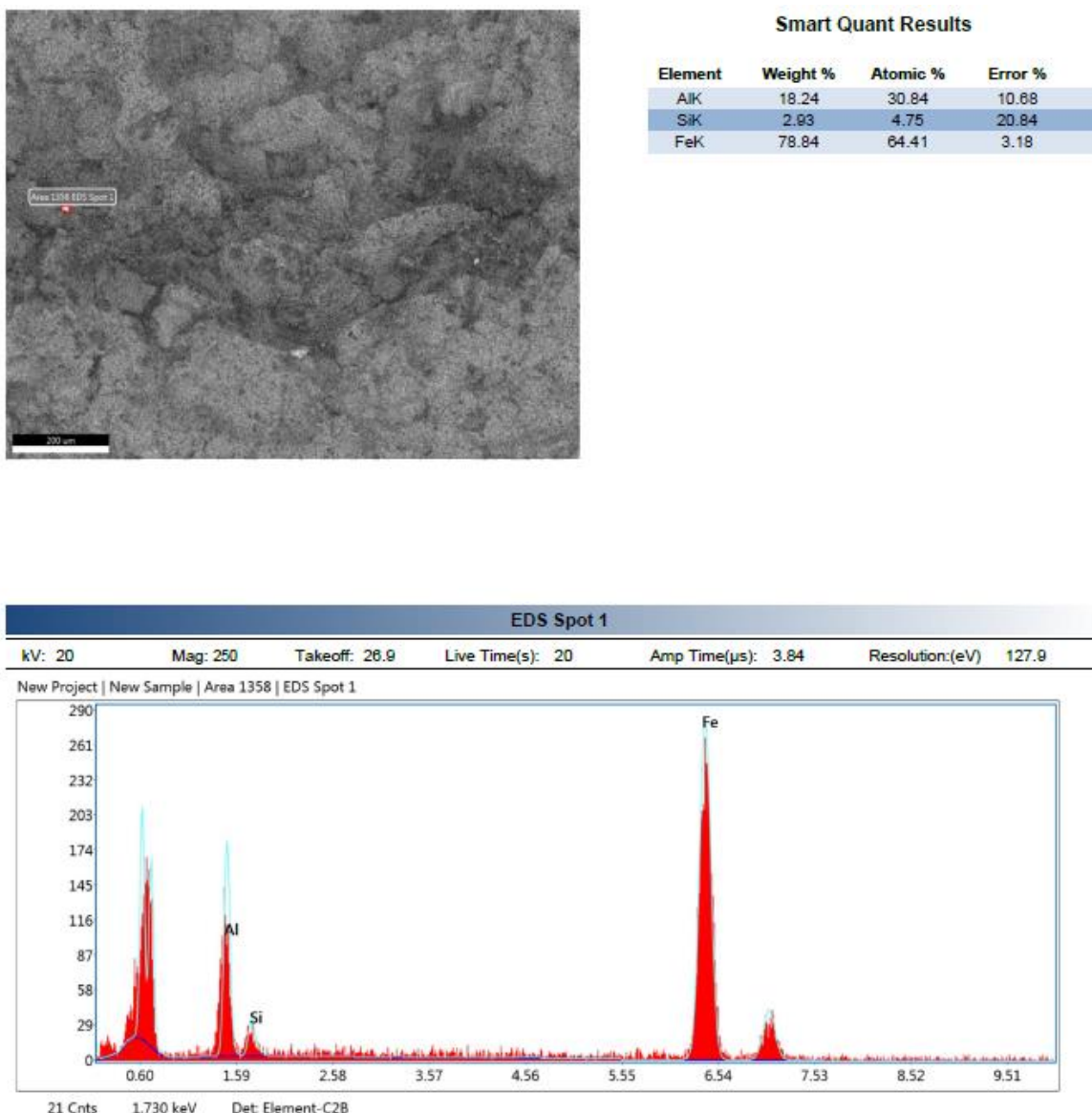


Figure. A 0.11 Fe level sample point EDX analysis point 1

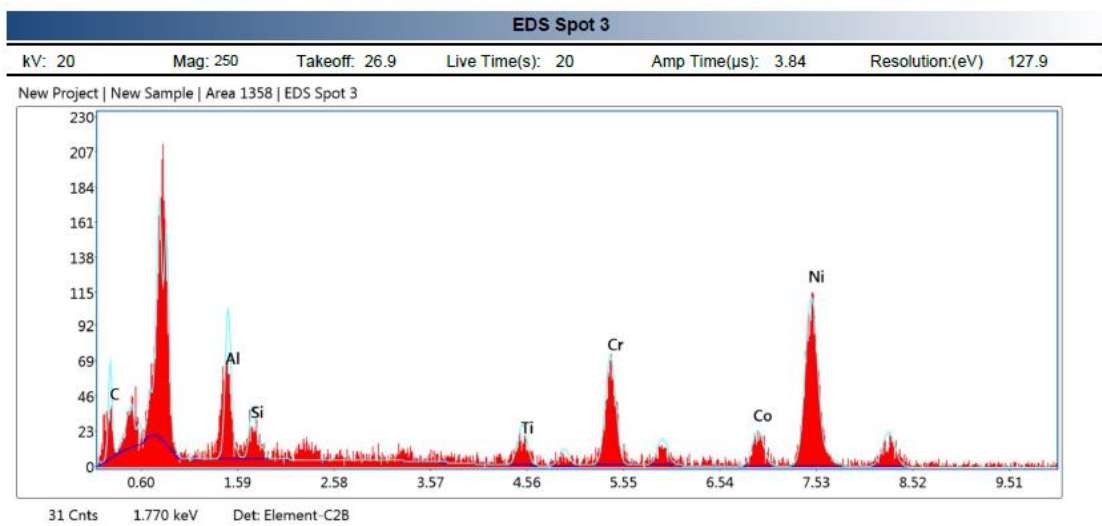
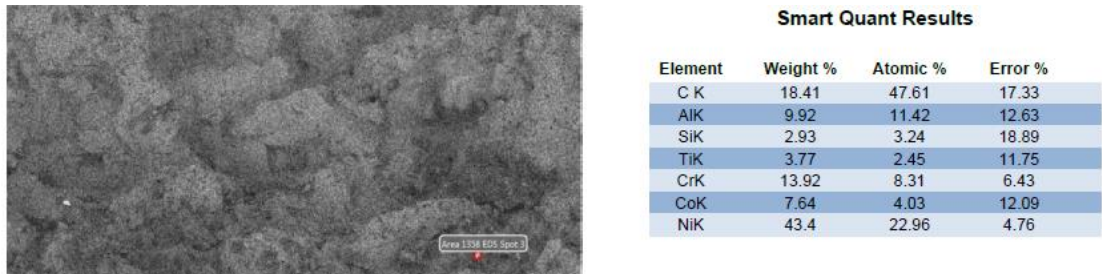


Figure. B 0.11 Fe level sample point EDX analysis point 3

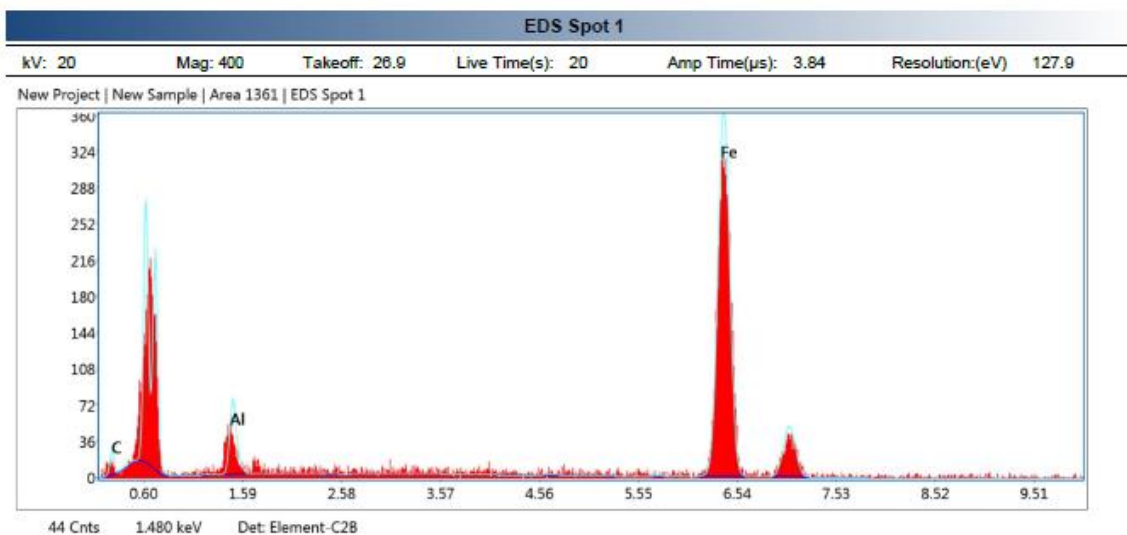
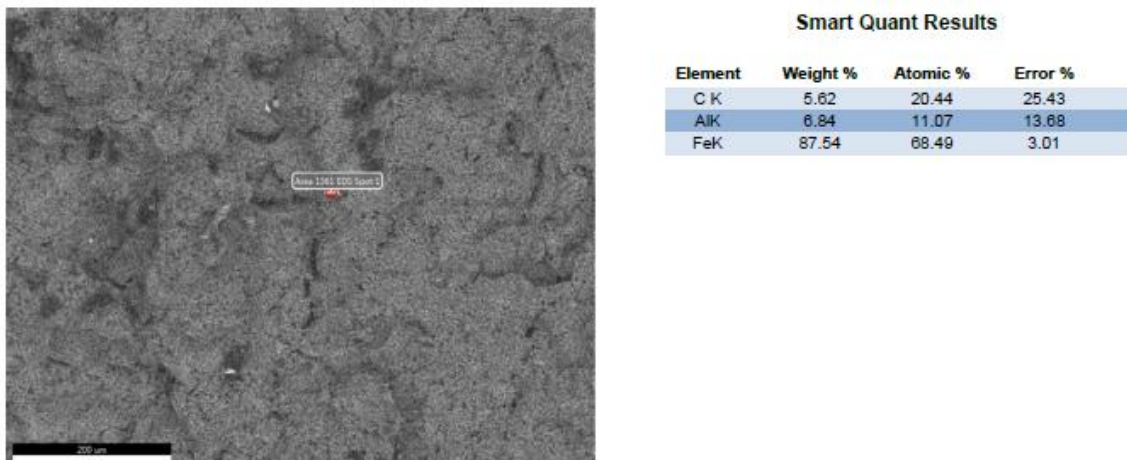


Figure. C 0.25 Fe level sample point EDX analysis point 1

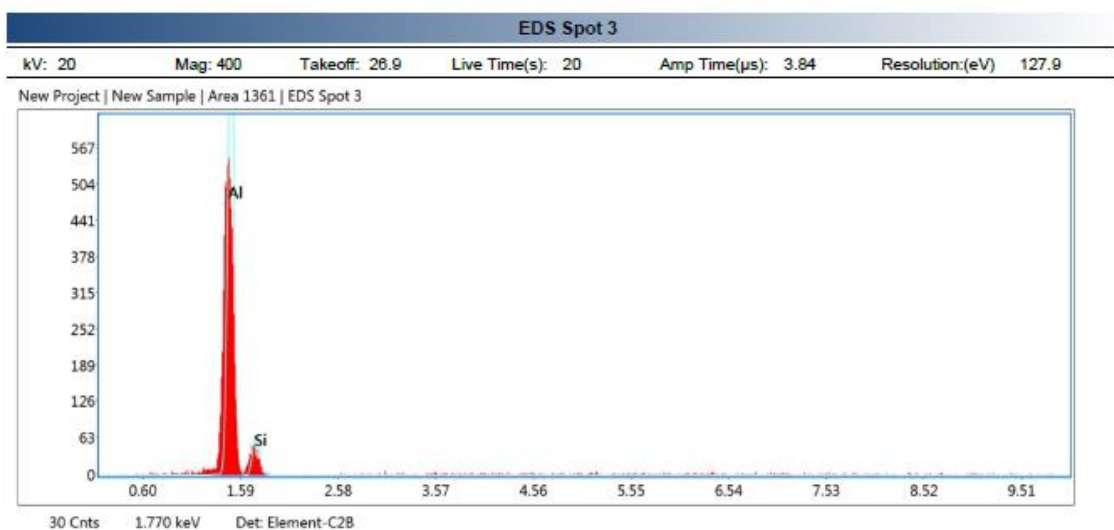
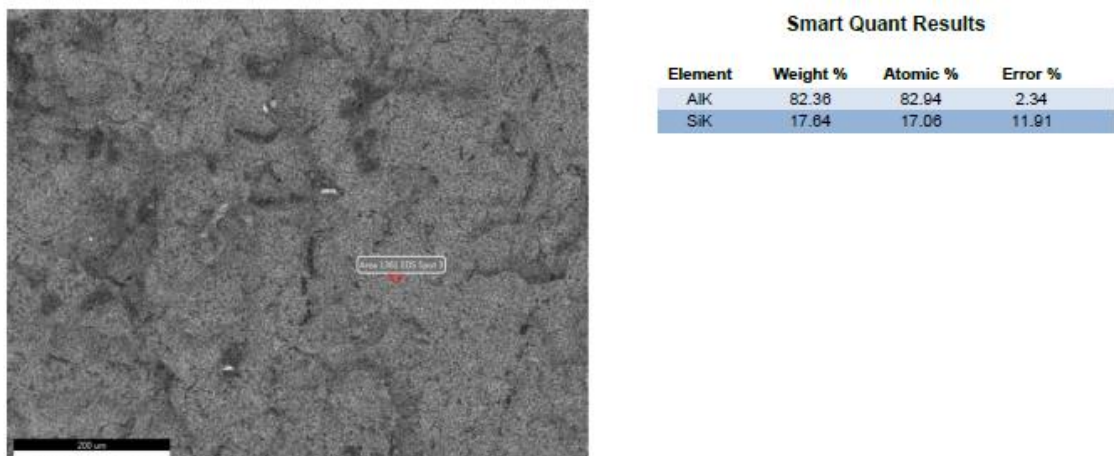
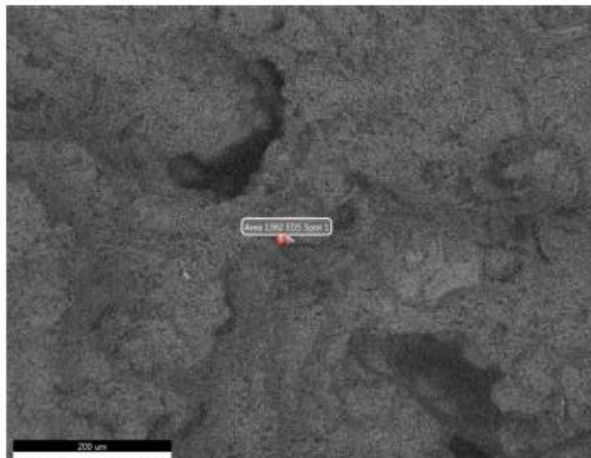


Figure. D 0.25 Fe level sample point EDX analysis point 3



Smart Quant Results

Element	Weight %	Atomic %	Error %
C K	12.86	36.93	17.83
O K	8.63	14.29	18.06
AlK	21.55	27.54	5.99
SiK	8.12	9.97	9.51
CoK	4.35	2.54	18.53
W L	46.48	8.72	12.36

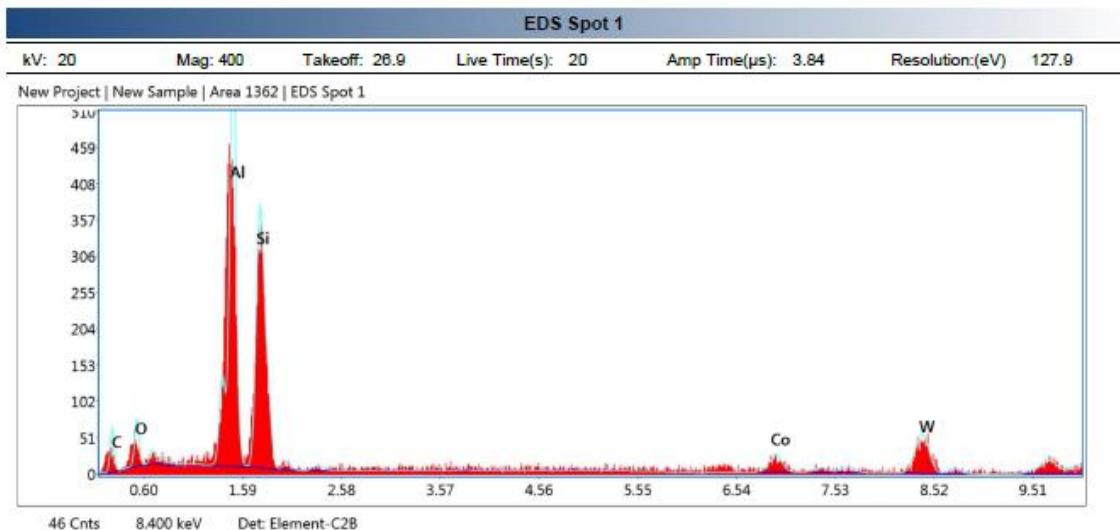


Figure. E 0.42 Fe level sample point EDX analysis point 1

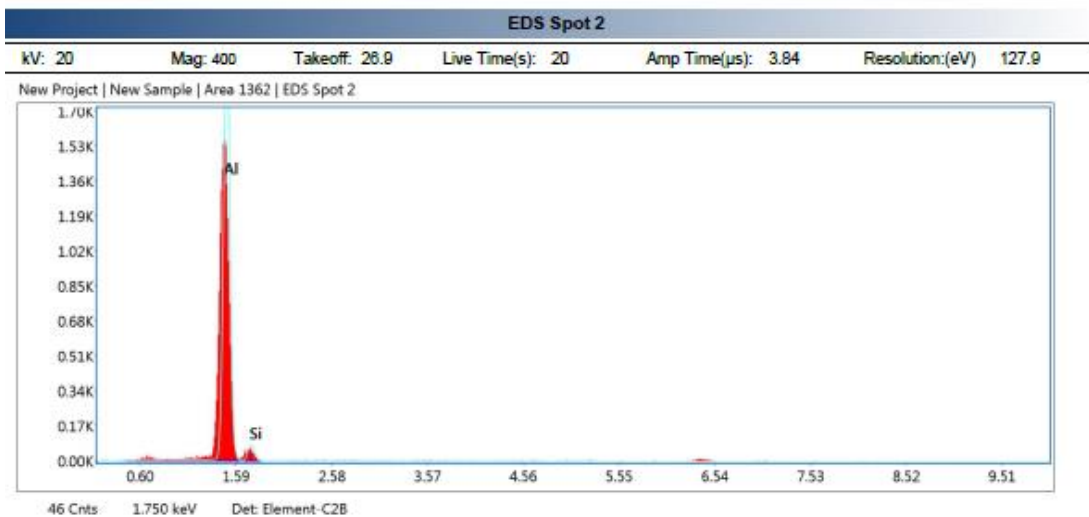
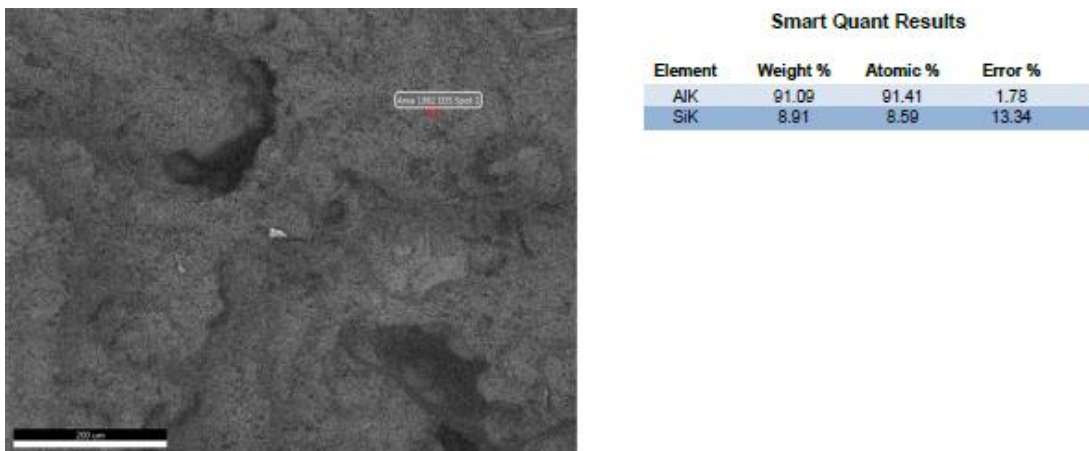


Figure. F 0.42 Fe level sample point EDX analysis point 2

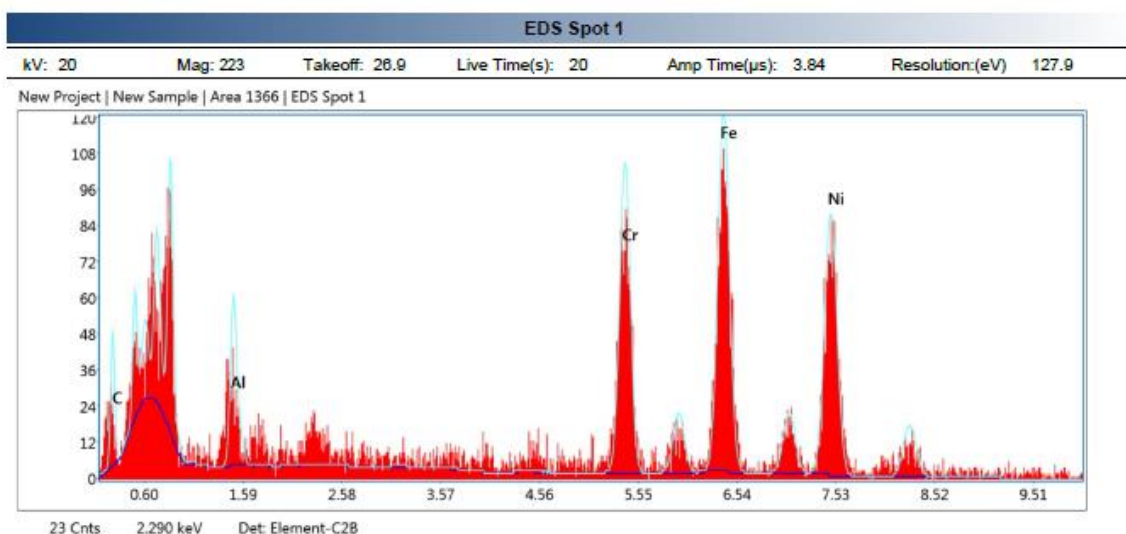


Figure. G 0.65 Fe level sample point EDX analysis point 1

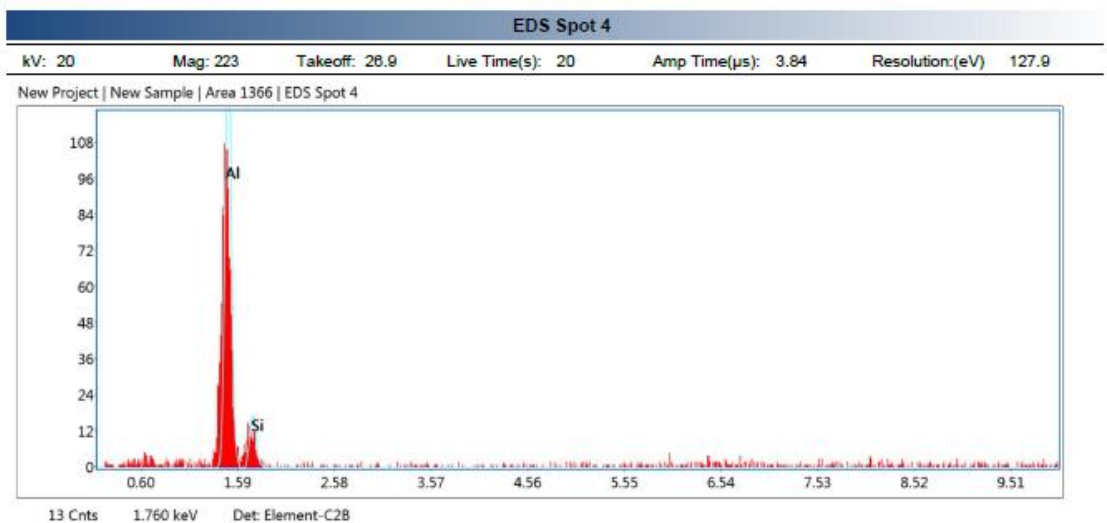
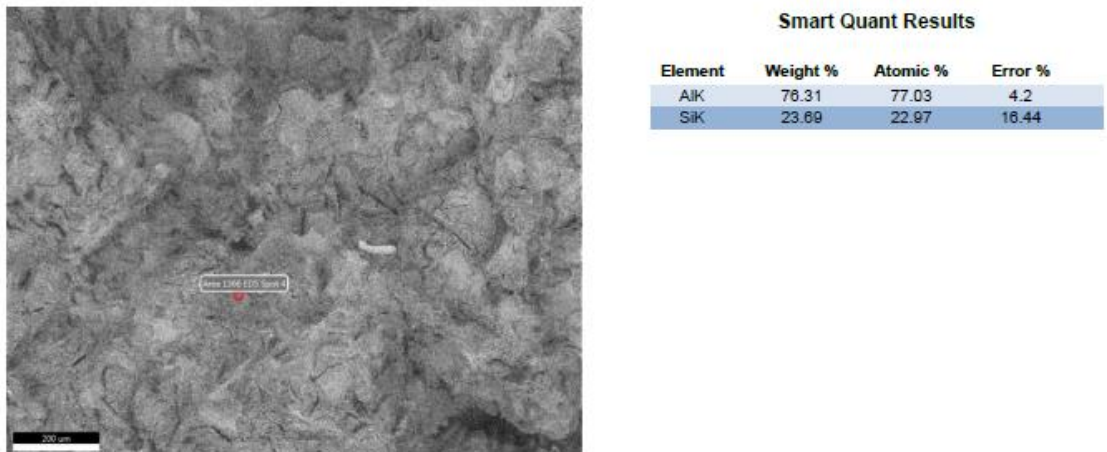


Figure. H 0.65 Fe level sample point EDX analysis point 3